POLITECNICO DI TORINO

Master's Degree in Energy and Nuclear Engineering

Renewable Energy Systems



Industrial Waste Heat Recovery Systems

Dynamic Modelling and Advanced Control Strategies for Real Industrial Facilities

Supervisors

Prof. Marco BADAMI

Candidate

Edoardo GASTALDI

Company Tutor

Doct. Fabio PEANO

Academic Year 2025/2026

September 2026

Abstract

Most energy losses in energy conversion and industrial processes take the form of waste heat that is often disposed of or released into the environment. Consequently, Waste Heat Recovery (WHR) systems are essential to capture and exploit this waste heat, offering significant environmental and economic benefits. This thesis aims to investigate the dynamic performance of two real industrial WHR facilities designed by Trigenia s.r.l.. Specifically, the core objective is the dynamic validation and optimization of tailored PID control strategies aimed at maximizing thermal energy recovery while minimizing the electrical power absorption of the fans. Furthermore, the energetic, economic and environmental benefits provided by these systems are analyzed. The study has been conducted using MATLAB-Simulink, a graphical program that enables to dynamically simulate multidomain systems, coupled with Simscape, which is an add-on product that extends Simulink with support for modeling of different physical domains.

The work focuses on two distinct WHR case studies. The first system, featuring a nominal heat recovery capacity of 1.4 MW, exploits heat from the steam boiler flue gas of an automotive plant to heat water used by a heat pump during the winter season and by a deaerator during the summer season. The second case study, a larger recovery system featuring a nominal capacity of 3.5 MW, is designed for a hot rolling mill reheating furnace. Here, hot flue gas is captured and utilized to heat a water circuit serving both industrial processes and a district heating network.

The results indicate that for both case studies, implementing a dual PID control architecture on the fan is essential to maximize heat recovery while minimizing electrical absorption: one controller regulates the extraction speed capacity, while the second modulates the actual fan speed. Furthermore, the analysis on the second case study demonstrates that the modulating damper strategy is less energetically efficient than a variable fan speed configuration. Despite its lower initial cost, the variable speed configuration is a better long-term investment, reaching the break-even point in about one year.

From an economic and environmental perspective, the analyzed WHR systems yield significant average savings compared to a baseline scenario: the first case study achieves average savings of 29.26 €/h and 225 $kgCO_2$/h of avoided emissions, while the second case study delivers an average of 170.74 €/h and 750.3 $kgCO_2$/h.

It is clear that to properly and effectively manage these complex WHR systems, control strategies are needed. In particular, PID controllers are used because they are still the most widely applied in industrial fields, with the ability to compensate for many practical operations, simplicity and high reliability.

Additionally, an alternative and innovative control strategy based on Deep Reinforcement Learning (DRL) is evaluated on the first case study. However, the results reveal that further studies and optimizations are required for its effective implementation.

Table of Contents

1 Introduction **1**
- 1.1 Context and Motivation . . . 1
- 1.2 Objective of the Thesis . . . 2
- 1.3 Thesis Outline . . . 2

2 Theoretical Background **4**
- 2.1 Industrial Energy Efficiency . . . 4
- 2.2 Waste Heat Recovery (WHR) . . . 6
- 2.3 Importance of Control Strategies . . . 8
  - 2.3.1 PID Controllers . . . 8

3 Methodology and Modelling Approach **11**
- 3.1 Dynamic Simulation Approach . . . 11
- 3.2 Energetic, Economic and Environmental Assessment . . . 12

I First case study: WHR system from Steam Boiler Flue Gas **15**

4 WHR System Description **17**
- 4.1 Plant Design Specifications . . . 18
  - 4.1.1 Heat exchanger specifications . . . 18
  - 4.1.2 Fan and motor technical data . . . 19
  - 4.1.3 Flue Gas Composition and Operating Conditions . . . 21
  - 4.1.4 Water operating conditions . . . 25
- 4.2 Control Strategy . . . 25

5 Dynamic Modelling in Simulink **29**
- 5.1 Simulink Model . . . 29
- 5.2 Detailed Subsystem Modelling . . . 30
  - 5.2.1 Moist Air Properties . . . 30
  - 5.2.2 Stack 1 and Stack 2 . . . 32

5.2.3 Fan . . . 34
5.2.4 Heat Exchanger . . . 36
5.2.5 Minor and Major Losses: Finding the Operating Point . . . 37
5.2.6 TIC-01 and TIC-02 . . . 38
5.2.7 TIC-03 and YIC-01 . . . 41
5.2.8 Thermal Liquid Loop . . . 42
5.3 Analysed Scenarios . . . 43

6 Simulation Results **46**
6.1 System Response to Piecewise Linear Flue Gas Profiles . . . 46
6.1.1 Impact of YIC-01 Lower Limit on Electrical Power . . . 49
6.2 System Response to Fluctuating Flue Gas Profiles . . . 52
6.3 Failure Analysis . . . 54
6.3.1 Failure of Damper 1 . . . 54
6.3.2 Failure of Damper 2 . . . 54
6.4 Energetic, Economic and Environmental Evaluation . . . 57
6.5 Summary of Main Findings . . . 58

II Second Case Study: WHR system from Hot Rolling Mill Reheating Furnace **59**

7 WHR System Description **61**
7.1 Plant Design Specifications . . . 62
7.1.1 Main Exhaust Fan Specifications . . . 62
7.1.2 Air Pre-Heater Specifications . . . 63
7.1.3 Heat Exchanger Characteristics . . . 64
7.1.4 Heat Recovery Fan Specifications . . . 64
7.1.5 Flue Gas Composition and Operating Conditions . . . 65
7.1.6 Water Circuit Operating Conditions . . . 66
7.2 Control Strategy . . . 67
7.2.1 Variable Fan Speed Control . . . 67
7.2.2 Modulating Damper Control . . . 67

8 Dynamic Modelling in Simulink **69**
8.1 Simulink Model . . . 69
8.2 Detailed Subsystem Modelling . . . 70
8.2.1 Flue Gases Properties Configuration . . . 70
8.2.2 Water Circuit Configuration . . . 72
8.2.3 Equivalent Flue Gas Source . . . 72
8.2.4 Furnace . . . 72
8.2.5 Air Circuit . . . 73

8.2.6 Air Pre-Heater . . . 73
8.2.7 Furnace Damper Control . . . 74
8.2.8 Main Exhaust Fan . . . 75
8.2.9 Flue Gas-Water Heat Exchanger . . . 76
8.2.10 Stack Draught . . . 77
8.2.11 Heat Recovery Fan . . . 78
8.2.12 Variable Fan Speed Control Implementation . . . 79
8.2.13 Modulating Damper Control Implementation . . . 79
8.3 Analysed Scenario . . . 81

9 Simulation Results **82**
9.1 Variable Fan Speed Control Configuration . . . 82
9.1.1 Shut-off Damper Full Stroke Time Impact . . . 85
9.1.2 Impact of TIC-01 Absence on System Performance . . . 87
9.2 Modulating Damper Control Configuration . . . 89
9.3 Energetic, Economic and Environmental Evaluation . . . 90
9.3.1 Performance of the Variable Fan Speed Configuration . . . 90
9.3.2 Comparative Analysis . . . 91
9.4 Summary of Main Findings . . . 93

10 Conclusions and Future Perspectives **94**
10.1 Exploratory Study on Deep Reinforcement Learning Control . . . 94
10.2 Conclusions . . . 98

Bibliography **100**

List of Tables

3.1 Reference parameters for the economic, energetic and environmental analysis 12

4.1 Heat exchanger specifications [17] 18
4.2 Volumetric composition, molecular weight and mass composition of the dry combustion air. 22
4.3 Volumetric and mass composition of the wet combustion air. 24
4.4 Wet flue gas volume composition 25
4.5 Nomenclature of the control variables. 27

5.1 Flow resistance parameters for the WHR system 38
5.2 Final tuned PID gains for TIC-01 and TIC-02 controllers. 40
5.3 Final tuned PID gains for TIC-03 and YIC-01 controllers. 42

6.1 Hourly primary energy savings 57

7.1 Nominal operating parameters of the air pre-heater [34] 63
7.2 Nominal operating parameters of the flue gas-water heat exchanger [35] 64
7.3 Flue gas composition 66

9.1 Hourly primary energy savings 91

List of Figures

2.1 Cost savings and payback periods of 3300 efficiency measures in SMEs, United States, 2002-2024 [6] 5
2.2 Categorization of WHR technologies [8] 7
2.3 PID block diagram [10] 9

4.1 P&ID of the WHR system from steam boiler flue gas [16] 18
4.2 Fan characteristic curve [18] 19
4.3 Efficiency map [20] 21
4.4 Block diagram of the process control strategy [22] 28

5.1 WHR system modelled on Simulink 29
5.2 Dry flue gas enthalpy vector 31
5.3 Simulink Model of the two Stacks 32
5.4 Simulink parameter dialog box for the fan configuration 35
5.5 Fan characteristic curve constructed by Simulink 35
5.6 Simulink parameter dialog box for the heat exchanger configuration 37
5.7 Plant resistance curve and Fan characteristic curve: Operating point 38
5.8 Simulink scheme for TIC-01 and TIC-02 controllers 39
5.9 Simulink scheme for YIC-01 and TIC-03 controllers 41
5.10 Flue gas mass flow rates represented by piecewise linear functions . 44
5.11 Flue gas mass flow rates represented by fluctuating functions 44

6.1 System response with piecewise linear flue gas profiles and $n_{\text{cap,min}} =$ 1900 rpm 48
6.2 Comparison of the mechanical power absorbed in two cases with different lower limit of YIC-01 operating range 49
6.3 System response with piecewise linear flue gas profiles and $n_{\text{cap,min}} =$ 1400 rpm 51
6.4 System response with fluctuating flue gas profiles and $n_{\text{cap,min}} = 1400$ rpm 53
6.5 System response during a failure of damper 1. 55
6.6 System response during a failure of damper 2. 56
6.7 Economic and environmental benefits 57

7.1 P&ID of the WHR system from hot rolling mill reheating furnace [32] 62
7.2 Main fan characteristic curve [33] 63
7.3 Heat recovery fan characteristic curve [36] 65
7.4 Motor efficiency map [37] 66

8.1 Simulink model of WHR system from hot rolling mill reheating furnace 70
8.2 Simulink parameter dialog box for the fan configuration 73
8.3 Simulink Scheme for the air circuit 74
8.4 Simulink parameter dialog box for the air pre-heater configuration . 74
8.5 Simulink scheme for PID-SR controller 75
8.6 Simulink parameter dialog box for the main exhaust fan configuration 76
8.7 Main exhaust fan characteristic curve constructed by Simulink . . . 76
8.8 Simulink parameter dialog box for the flue gas-water heat exchanger configuration 77
8.9 Stack draught implementation 78
8.10 Simulink parameter dialog box for the heat recovery fan configuration 78
8.11 Heat recovery fan curve constructed by Simulink 79
8.12 TIC-01 and TIC-02 implementation for the variable fan speed control strategy 80
8.13 TIC-01 and TIC-02 implementation for the modulating damper control strategy 80

9.1 Stack mass flow rate balance 82
9.2 PID-SR response 83
9.3 PID-SR response during critical moments 84
9.4 TIC-01 and TIC-02 response 85
9.5 Furnace pressure response to shut-off damper FST 86
9.6 Overall comparison of system performance 88
9.7 TIC-01 and TIC-02 response for the modulating damper control configuration 89
9.8 PID-SR response for the modulating damper control configuration . 90
9.9 Electrical energy absorption and heat recovery comparison 90
9.10 Economic and environmental benefits 91
9.11 Economic and environmental benefit comparison between the configurations with and without TIC-01 controller 92

10.1 Schematic representation of the DRL framework applied for the WHR system from steam boiler flue gas 96
10.2 Outlet water temperature comparison between DRL and PID configurations 97
10.3 Energy and RMSE comparison between DRL and PID configurations 97

Chapter 1

Introduction

1.1 Context and Motivation

About 52 % of all global primary energy is lost as waste heat after conversion. This means that a significant amount of energy that is potentially exploitable is wasted. Most of this unused energy comes from the electricity generation, transportation and industrial sectors [1]. Increasing attention to electricity prices and environmental aspects has led to the investigation of solutions for recovering waste heat and increasing energy efficiency. There is a range of waste heat recovery methods and applications that can be installed on-site or integrated into district heating networks. The installation of Waste Heat Recovery (WHR) systems can help decarbonise hard-to-abate industries and cities by transforming excess heat into one of the main sources of clean heat and power generation, thus playing a key role in the global decarbonisation path. As established in the Paris Agreement in 2015, and reiterated during COP30 in 2025, emissions must be reduced in order to keep the 1.5 °C global warming limit within reach and one of the strategies highlighted to accomplish the target is doubling the rate of energy efficiency improvements by 2030 [2]. WHR systems can represent an important tool to reduce emissions and increase energy efficiency, by capturing and reusing waste heat to prevent environmental dissipation.

Since WHR systems exploit waste heat that is a by-product of another process, the fluctuations of that heat source cannot be adjusted for heat recovery purposes. As a consequence, proper control strategies are the only way to decouple the recovery cycle from these fluctuations. Control strategies optimize thermal energy recovery by tracking fixed or dynamic setpoints, ensuring efficiency and safety. For example, by controlling the flue gas temperature in a branch by adjusting the damper aperture, the system can maximize heat recovery. Control strategies relying on Proportional-Integral-Derivative (PID) controllers are the industry standard for these tasks.

In this context, dynamic modeling environments like MATLAB's Simulink and Simscape are fundamental for studying these plants and are perfectly suitable for developing and analysing control strategies. Unlike steady-state models that do not allow the evaluation of transient behaviour, dynamic models solve differential equations over time, allowing for the observation of realistic and variable thermal profiles and system responses.

1.2 Objective of the Thesis

The main objective of the thesis is to analyse, through dynamically modelling, WHR systems equipped with PID controllers. Specifically, the purpose is to validate and optimize the control strategies designed by Trigenia S.r.l., an Italian certified Energy Service Company (ESCo), where this study was conducted as part of a curricular internship. Additionally, economic and environmental benefits are analysed for both the systems. This work investigates two specific WHR systems designed by Trigenia s.r.l.:

- **First Case Study:** WHR system from Steam Boiler Flue Gas, designed for an automotive company.
- **Second Case Study:** WHR system from a Hot Rolling Mill Reheating Furnace, designed for a steel manufacturing company.

The dynamic simulations and the validation of the control systems are performed using the MATLAB Simulink-Simscape environment.

1.3 Thesis Outline

Before detailing the specific case studies, this work presents a preliminary part dedicated to the theoretical background, which outlines the fundamental concepts of industrial efficiency, Waste Heat Recovery (WHR) systems and the importance of control strategies. Then, the methodology and modelling approach are described. Following this foundation, the thesis is structurally divided into two main parts, each dedicated to the analysis of a specific WHR system. In particular, **Part I** regards the case study of a WHR system exploiting heat from the steam boiler flue gas of an automotive company, while **Part II** focuses on a second case study regarding a WHR system capturing heat from the flue gas of a hot rolling mill reheating furnace in a steel manufacturing plant. A symmetrical internal structure is maintained across both parts to provide a consistent and rigorous methodological approach. More precisely, each part begins with the system description, which provides all the technical details, such as the specifications from the data sheet of

the main components, and outlines the adopted control strategies. Following this, a chapter is dedicated to the dynamic modelling detailing both the Simulink-Simscape model and the analysed scenarios. Finally, the simulation results are presented and discussed in the concluding chapter of each case study. To conclude the work, Section 10.1 introduces an exploratory study of an advanced control strategy, based on Deep Reinforcement Learning, applied to the first case study.

Chapter 2

Theoretical Background

2.1 Industrial Energy Efficiency

Energy efficiency is defined as the ratio of output of performance, service, goods or energy to input of energy. It involves the practice of using less energy to provide the same amount of useful output from a service [3]. In particular, in the industrial sector, the increase in energy efficiency is becoming an increasingly important concern. According to the IEA, industrial sector accounts for nearly 40 % of total final energy consumption[1], meaning that any progress in industry has a significant impact on the world's ability to meet its energy targets. However, while industry consumes the most energy, its rate of efficiency improvement has slowed sharply. In particular, between 2010 and 2019, industrial energy intensity[2] improved by nearly 2 % annually, but since 2019, that rate has dropped to under 0.5 % [4].

The industrial sector is the second-highest source of emissions, after the energy sector, responsible for nearly a quarter of global net greenhouse gas (GHG) emissions. There are several options to reduce industrial emissions, such as demand management, energy and materials efficiency, circular material flows, as well as abatement technologies and transformational changes in production processes. In particular, energy efficiency improvements are a primary and cost-effective strategy for mitigating GHG emissions [5].

The main strategies to improve energy efficiency in the industrial sector include:

- **Electrification of low-temperature heat**: due to its large share in energy

[1]Total final consumption (TFC) is the sum of consumption by the different end-use sectors. TFC is broken down into energy demand in the following sectors: industry (including manufacturing and mining), transport, buildings (including residential and services) and other (including agriculture and non-energy use).

[2]Energy intensity is defined as the amount of primary energy required per unit of economic output. It is the main metric the world uses to track the energy efficiency of the economy

use and the efficiency gains enabled by heat pumps, this strategy can be an important lever to accelerate efficiency progress.

- **Upgrading industrial motor systems**: this includes implementing more stringent standards for new motors driving equipment such as fans, pumps and compressors. In addition, promoting the use of variable speed drives, coupled with proper control strategies, can increase savings in variable-load applications.

- **Material efficiency**: optimising design, increasing scrap use and enhancing recycling are examples of strategies that contribute to reduce material needs and improve efficiency.

- **Process optimisation**: the reduction of waste heat, coupled with waste heat recovery systems, is a key measure for accelerating industrial efficiency.

Energy efficiency improvements also bring benefits from an economic point of view. To this end, the IEA developed a study analysing over 3300 efficiency measures implemented in small and medium-sized enterprises (SMEs) in the United States. The analysis demonstrates that energy savings account for 41 % of total cost savings, while the remaining part consists of indirect multiple benefits, like higher productivity (18 %), improved resource use (39 %) and reduced waste production (2 %) as depicted in Figure 2.1. When these multiple benefits are fully accounted for, the total cost savings more than double. Consequently, this comprehensive valuation drastically accelerates the return on investment, reducing the average payback period from three years (when considering only energy savings) to approximately 1.7 years [6].

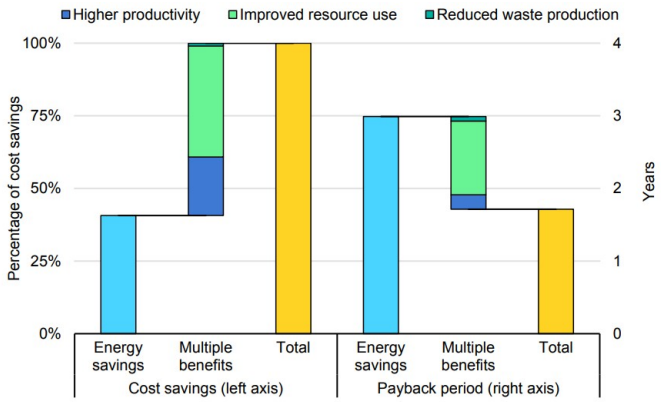


Figure 2.1: Cost savings and payback periods of 3300 efficiency measures in SMEs, United States, 2002-2024 [6]

2.2 Waste Heat Recovery (WHR)

Waste heat recovery (WHR) refers to the process of capturing and reusing heat that is generated as a by-product of various industrial processes. This heat is typically released into the environment through exhaust gases, fluids or hot surfaces, and represents a significant loss of energy. Waste heat is generated across a wide range of industrial sectors, such as the steel industry, that is one of the most energy-intensive sectors, cement production, food processing and automotive industry.

Waste heat recovery technologies can be categorized in different ways, but the primary classification criteria are based on temperature grade and operational principle [7],[8].

Temperature Grade Categorization WHR systems can be categorized into three main types based on the waste heat temperature as follows:

- **High-temperature waste heat**: it involves waste heat at temperature above 300 °C and is often found in processes such as metal smelting and glass manufacturing.
- **Medium-temperature waste heat**: this type of system deals with waste heat at a temperature ranging from 100 °C to 300 °C; it is often found in processes like cement production and food processing.
- **Low-temperature waste heat**: this type is generally below 100 °C and is often found in process like refrigeration and air conditioning; it is the most difficult type of waste heat to recover, but it can still be utilized for heating applications or preheating feedwater.

Operational Principle Categorization WHR technologies are broadly classified into active and passive systems based on whether the heat is being used directly at the same or at lower temperature level or whether it is transformed to another form of energy or to a higher temperature. In Figure 2.2 the WHR categorization is depicted.

- **Active technology**: In active waste heat recovery systems, waste heat is transformed into a different energy vector or upgraded to a higher thermal potential, often requiring auxiliary energy input or specialized thermodynamic cycles. They are further divided into three categories according to the final form of energy delivered:
  - Waste Heat to Heat (WHTH): upgrading heat to a higher temperature level (sorption heat pump or mechanical vapour compressor);

  - Waste Heat to Cold (WHTC): converting heat into cooling capacity (absorption or adsorption chillers);
  - Waste Heat to Power (WHTP): converting thermal energy into electricity or mechanical work (Organic or Steam Rankine Cycles and Kaline Cycles).

- **Passive Technology**: In passive waste heat recovery systems, heat is directly transferred from the waste stream to a secondary process fluid without changing the energy form or raising the thermal level through external work. Heat exchangers and thermal energy storages are the main passive waste heat recovery systems.

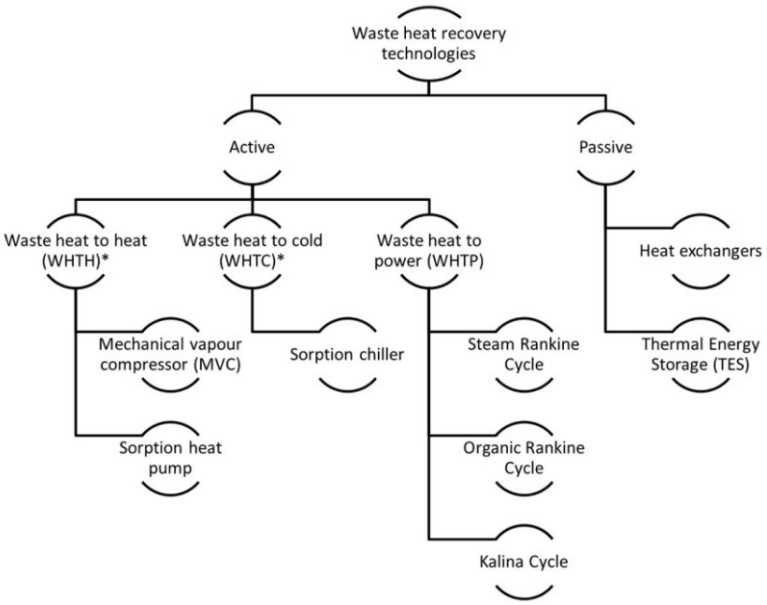


Figure 2.2: Categorization of WHR technologies [8]

On one hand, WHR systems bring numerous advantages because they generate cost savings, help to reduce GHG emissions and contribute to circular economy principles. Moreover, WHR systems directly contribute to the United Nations Sustainable Development Goals (SDGs), notably SDG 7 (Affordable and Clean Energy) and SDG 13 (Climate Action).

On the other hand, WHR systems can face with technical and non-technical barriers. Technical barriers are represented by the variability in waste heat availability and space constraints in existing industrial setups; non-technical barriers are represented by the high upfront cost and the policy challenges, in particular on lack of regulation, information and incentives for WHR investments.

2.3 Importance of Control Strategies

Control systems are essential in WHR plants to ensure safety, eliminate the need for constant human attention and maintain economical operation, as well as to allow the maximization of heat recovery. Implementing robust control strategies, such as PID controllers, brings several advantages. Particularly, a well-designed control system can:

- continuously regulate the heat recovery rate to balance fluctuating thermal demands with source availability.
- optimize the operational cycles of system components to maximize overall efficiency and extend equipment lifespan.
- trigger alarms when fluid parameters deviate from critical setpoints or when equipment malfunctions.
- facilitate the real-time monitoring of the plant's thermodynamic and fluid dynamic performance.

Clearly, properly designed control strategies also bring financial and operational benefits. Specifically, they help optimize operating efficiency and generate cost savings (for example, reducing the fan speed when the waste heat decreases allow to reduce electrical consumption)[9].

2.3.1 PID Controllers

Among the various methods explored in the literature, Proportional-Integral-Derivative (PID) controllers stand out as one of the most effective and widely adopted solutions, thanks to their simplicity and reliability. From a mathematical perspective, a PID controller generates a control signal $u(t)$ that is the sum of three distinct terms based on the control error $e(t)$. The control error is defined as the difference between the set point (y_{SP}) and the measured process variable ($y(t)$):

$$e(t) = y_{SP} - y(t) \tag{2.1}$$

These three terms are the following:

- **Proportional term**: it computes the control signal in proportion to the control error, with the formula:

  $$K_p \cdot e(t) \tag{2.2}$$

  where K_p is the proportional gain.

- **Integral term**: it acts on the history of the error by accumulating (integrating) the error over time, with the formula:

$$K_i \cdot \int_0^t e(\tau)d\tau \tag{2.3}$$

  where K_i is the integral gain.

- **Derivative term**: it calculates the rate of change of the error. By determining how fast the error is growing or shrinking, it extrapolates the error along its tangent line to predict future behavior, with the following formula:

$$K_d \cdot \frac{de(t)}{dt} \tag{2.4}$$

  where K_d is the derivative gain.

Therefore, summing the three terms, the control signal sent to the actuator is defined by the following expression:

$$u(t) = K_p \cdot e(t) + K_i \cdot \int_0^t e(\tau)d\tau + K_d \cdot \frac{de(t)}{dt} \tag{2.5}$$

A schematic representation of a PID controller is depicted in Figure 2.3. In

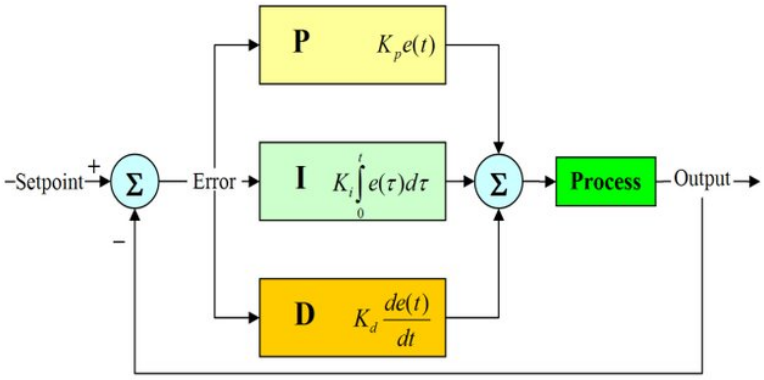


Figure 2.3: PID block diagram [10]

engineering applications and control system analysis, the PID controller is frequently represented in the Laplace domain. By applying the Laplace transform to the time-domain equation, the transfer function $C(s)$ of the controller, which relates the control signal $u(s)$ to the error $e(s)$, is obtained:

$$C(s) = \frac{u(s)}{e(s)} = K_p + \frac{K_i}{s} + K_d s \tag{2.6}$$

An important aspect is the tuning phase. It is defined as the process of adjusting the proportional, integral and derivative gains of the PID controller to make the system stable and accurate. Although there are different tuning methods, such as the Ziegler-Nichols or the Cohen-Coon method, in this thesis a manual tuning was performed: the gains were iteratively adjusted based on the system's response until a stable and accurate condition was reached. The rules followed for manual tuning are the following:

- **Proportional Gain (K_p)**: increasing it speeds up the controller's initial reaction, but decreases stability by making the response more oscillatory.
- **Integral Gain (K_i)**: increasing it causes the error to decay more rapidly, but decreases overall stability.
- **Derivative Gain (K_d)**: it acts as a predictive brake, which generally improves stability and helps damp out oscillations.

However, in real world applications, ideal PID controllers must be modified to address physical limitations and signal imperfections. In particular, they must include an anti-windup mechanism. It is necessary because physical actuators (such as valves or motors) have realistic constraints; for instance, a valve cannot be opened more than 100 % or closed beyond 0 %. When a large disturbance or setpoint change forces the actuator to its physical limit, it saturates, and the feedback loop is temporarily broken. The controller's integral term will continue to accumulate the remaining error over time, causing the integral term to grow excessively large (to "wind up"). This results in massive overshoots and prolonged oscillations. Therefore, PID controllers employ anti-windup algorithms (such as clamping or back-calculation) to dynamically reset or clamp the integrator during actuator saturation [11].

Chapter 3

Methodology and Modelling Approach

3.1 Dynamic Simulation Approach

The dynamic simulation was performed using MATLAB and Simulink (release R2024b), in particular relying on the Simscape environment. With Simscape, unlike Simulink models which rely on causal signal-flow representations, it is possible to create complex physical networks by simply assembling physical components (such as fans, heat exchangers, pipes) represented as interconnected blocks. All the equations are inherently implemented inside these blocks and by connecting them, the software automatically formulates and solves the differential equations of the entire system. In particular, the WHR models developed in this work use components from four physical domains: the Gas domain, the Thermal Liquid domain, the Moist Air domain and the Mechanical domain. All the implementation details concerning the two WHR systems are provided in Section 5 and Section 8, respectively.

The virtual models for the two case studies were built to accurately replicate the real physical systems based on the Piping and Instrumentation Diagrams (P&ID) and technical specifications provided by Trigenia s.r.l. The primary components, such as heat exchangers and fans, were parametrised using the manufacturers' nominal datasheets. Where specific component data was unavailable, reasonable engineering assumptions, consistent with the underlying thermodynamic and fluid dynamic principles, were made to complete the models. For each case study, multiple scenarios were developed by varying the total flue gas mass flow rate, aiming to test the plant and the control strategy under different operating conditions. Additionally, further analyses specific to each case study were performed, as detailed in Sections 5.3 and 8.3 for the first and second case studies, respectively.

3.2 Energetic, Economic and Environmental Assessment

The evaluation of the energetic, economic and environmental benefits of the WHR systems is based on comparing the heat recovery system against a baseline scenario where the same thermal energy is produced by a reference natural gas boiler. Grid electricity consumption for the WHR systems is evaluated considering the average Italian thermoelectric generation mix. Table 3.1 reports the reference constants used across the equations. The conversion and emission factors used in the evaluation are sourced from official institutional publications. Any parameters not covered by these references are directly based on internal operational data and technical specifications provided by the company. The calculation steps for both

Table 3.1: Reference parameters for the economic, energetic and environmental analysis

Parameter	**Symbol**	**Reference Value**	**Description**
Boiler efficiency	η_{th}	0.9	Efficiency of the replaced methane boiler
Grid electrical efficiency	η_{el}	0.46	IT thermoelectric generation fleet [12]
Lower Heating Value	$\mathrm{LHV}_{\mathrm{CH_4}}$	9.8 kWh/Sm^3	Energy content [13]
Emission factor	$e_{\mathrm{CH_4}}$	2.004 $\mathrm{kgCO_2/Sm^3}$	CO_2 released per unit volume of methane burned [14]
Grid emission factor	e_{el}	0.37 $\mathrm{kgCO_2}$/kWh	Average carbon emissions of the Italian electrical grid considering only fossil fuel generation[15]
Gas unit cost	C_{gas}	0.46 €/Sm^3	Overall cost including system charges and distribution
Electricity unit cost	$C_{el,unit}$	0.1402 €/kWh	Overall cost including excise and system fees

systems are identical in structure, but they differ in how the average useful thermal power P_{th} (kW) and the average electrical power consumption P_{el} (kW) are defined:

- **First case study**: the water is heated by the WHR system and sent to a water-source heat pump during the winter season. Therefore the calculation must account for the thermodynamic and electrical performance of the heat pump.

  - Average thermal power P_{th} (kW): Represents the thermal power delivered by the water-source heat pump's condenser to the thermal users, calculated as:

$$P_{th} = P_{th,WHR} \cdot \frac{COP}{COP - 1} \tag{3.1}$$

    where the Coefficient of Performance of the heat pump (COP) is considered constant.

  - Average electrical power P_{el} (kW): Includes both the compressor of the heat pump ($P_{el,HP}$) and the WHR fan (P_{fan}):

$$P_{el} = P_{el,HP} + P_{fan} \tag{3.2}$$

    where the heat pump's electrical consumption is derived from its thermodynamic balance:

$$P_{el,HP} = \frac{P_{th,WHR}}{COP - 1} \tag{3.3}$$

- **Second case study**: the recovered thermal energy from the flue gases is directly supplied to thermal users and the local district heating network.

  - Average thermal power P_{th} (kW): Represents the thermal power directly recovered from the flue gases and delivered to the local district heating network and thermal users. Therefore, $P_{th} = P_{th,WHR}$.
  - Average electrical power P_{el} (kW): Consists of the fan absorption (P_{fan}) required to overcome the pressure drops of the recovery system. Therefore, $P_{el} = P_{fan}$.

Using the definitions above, the energetic, economic and environmental benefits are calculated using the following equations:

1. **Energetic benefit** ($\mathrm{kWh_p/h}$): it represents the net primary energy saved E_{saved} calculated as the difference between the primary energy avoided from not operating the gas boiler $E_{p,th}$ and primary electrical energy consumed by the WHR system $E_{p,el}$:

$$E_{saved} = E_{p,th} - E_{p,el} \tag{3.4}$$

   where

$$\begin{aligned} E_{p,th} &= \frac{P_{th}}{\eta_{th}} \\ E_{p,el} &= \frac{P_{el}}{\eta_{el}} \end{aligned} \tag{3.5}$$

2. **Economic benefit** (€/h): it represents the net economic benefit B_{eco} evaluated as the difference between the operating cost of the electricity consumed C_{el} and the equivalent fuel savings R_{th}:

$$B_{eco} = R_{th} - C_{el} \tag{3.6}$$

where

$$\begin{aligned} R_{th} &= \frac{E_{p,th}}{LHV_{CH_4}} \cdot C_{CH_4} \\ C_{el} &= P_{el} \cdot C_{el,unit} \end{aligned} \tag{3.7}$$

3. **Environmental benefit** ($kgCO_2/h$): it represents the net reduction in hourly carbon emissions ΔCO_2 calculated as the difference between the emissions avoided from not burning methane $CO_{2,avoided}$ and those generated by grid electricity consumption $CO_{2,emitted}$:

$$\Delta CO_2 = CO_{2,avoided} - CO_{2,emitted} \tag{3.8}$$

where

$$\begin{aligned} CO_{2,avoided} &= \frac{E_{p,th}}{LHV_{CH_4}} \cdot e_{CH_4} = V_{CH_4} \cdot e_{CH_4} \\ CO_{2,emitted} &= P_{el} \cdot e_{el} \end{aligned} \tag{3.9}$$

Part I

First case study: WHR system from Steam Boiler Flue Gas

In this part, a particular control strategy for a WHR system is analysed. The plant consists of three steam generators fed by natural gas, that produce steam for the production lines of the company, that produces automotive's components. The WHR plant aims at exploiting the sensible and latent heat still present in the flue gases emitted by the steam generators, in order to heat up the water circulating in a closed loop. The water is used by a Heat Pump (as a heat source) during the winter season and directed to a deaerator during the summer season. Originally, the plant consisted of two steam generators connected to a shared chimney lacking heat recovery. The revamped configuration introduces an additional steam generator whose exhaust gas merges with the original stack network. This setup enables the combined collection of flue gases from all the boilers, feeding them into the newly implemented waste heat recovery plant. The control strategy for this application relies on four PID controllers aiming at maximize the exploitation of hot flue gas while minimizing electrical absorption of the fan.

Chapter 4

WHR System Description

The WHR plant under analysis is designed to exploit the thermal energy from the exhaust gases of three steam generators. Specifically, the system handles the flue gases produced by two boilers, which share a common exhaust stack, alongside the flue gases from a newly installed third boiler equipped with its own dedicated stack. The primary objective of this WHR system is to extract these gases prior to their atmospheric discharge and direct them through a heat recovery loop. By doing so, both the sensible and latent heat of the flue gases are transferred to a water circuit, recovering energy that would otherwise be lost. Figure 4.1 shows the P&ID[1] of the WHR plant. On the left side, the original stack serving two steam generators (not depicted) is shown. In the centre, the new steam generator and its dedicated stack are illustrated. Finally, on the right side, the heat exchanger and the fan are placed. The heat pump and the deaerator are not included in this representation. To regulate the mass flow rate of the extracted gases, a control damper is installed on each branch line (SR-01 and SR-02). The collected gases are then manifolded and directed to the flue gas-water heat exchanger (HE-01), located on the right side of the layout. At the heat exchanger outlet, the cooled and now-dry flue gases are drawn by an extraction fan (CF-01) and ultimately discharged into the atmosphere through a dedicated stack at a reduced energy level. The positions of both branch dampers and the speed of the extraction fan are dynamically managed by specific PID controllers, as detailed in Section 4.2.

[1] P&ID: Piping and Instrumentation Diagram

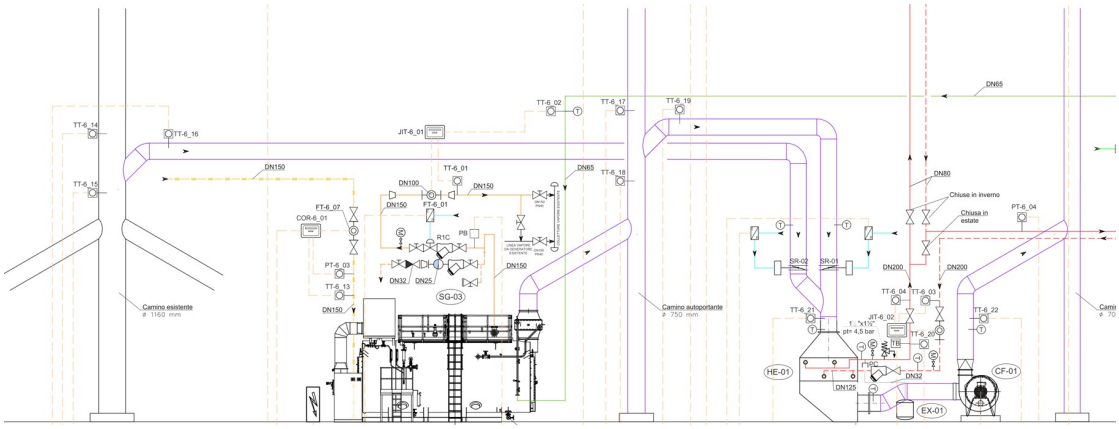


Figure 4.1: P&ID of the WHR system from steam boiler flue gas [16]

4.1 Plant Design Specifications

4.1.1 Heat exchanger specifications

The core component of the waste heat recovery system is undoubtedly the flue gas-water heat exchanger. It is a finned-tube heat exchanger constructed with an AISI 316 stainless steel frame and tubes, coupled with aluminum fins to maximize the heat transfer surface. Its task is to provide a nominal thermal power of 1400 kW; however, the manufacturer purposely oversized it by approximately 21%, allowing for an actual exchanged power of around 1694 kW split as follows:

- Latent thermal power: 1304.65 kW
- Sensible thermal power: 389.60 kW

The nominal operating conditions, including mass flow rates, temperature levels and pressure drops for both the tube and shell sides, along with the main geometric dimensions, are summarized in Table 4.1.

Table 4.1: Heat exchanger specifications [17]

Parameter	**Tube side**	**Shell side**
Fluid Description	Water	Flue Gas / Water Steam
Fluid flow (kg/h)	172306.7	11974.78 / 1550.22
Inlet temperature (°C)	18	125
Outlet temperature (°C)	31.69	37.9
Pressure Drops (kPa)	46.12	0.0421
Volume (L)	1633.4	1226.3

4.1.2 Fan and motor technical data

Another key component of the system is the fan, that is located downstream of the heat exchanger. The fan selected for this application is a direct drive, single inlet centrifugal fan. It is manufactured from steel sheet protected with cataforesis primer and polyurethane paint finish RAL 7045. Figure 4.2 depicts the fan characteristic curve provided by the manufacturer, which was obtained using a fluid at 15 °C and with a density of $1.226\,\mathrm{kg\,m^{-3}}$. In the same graph, as can be seen, also the plant resistance curve is represented.

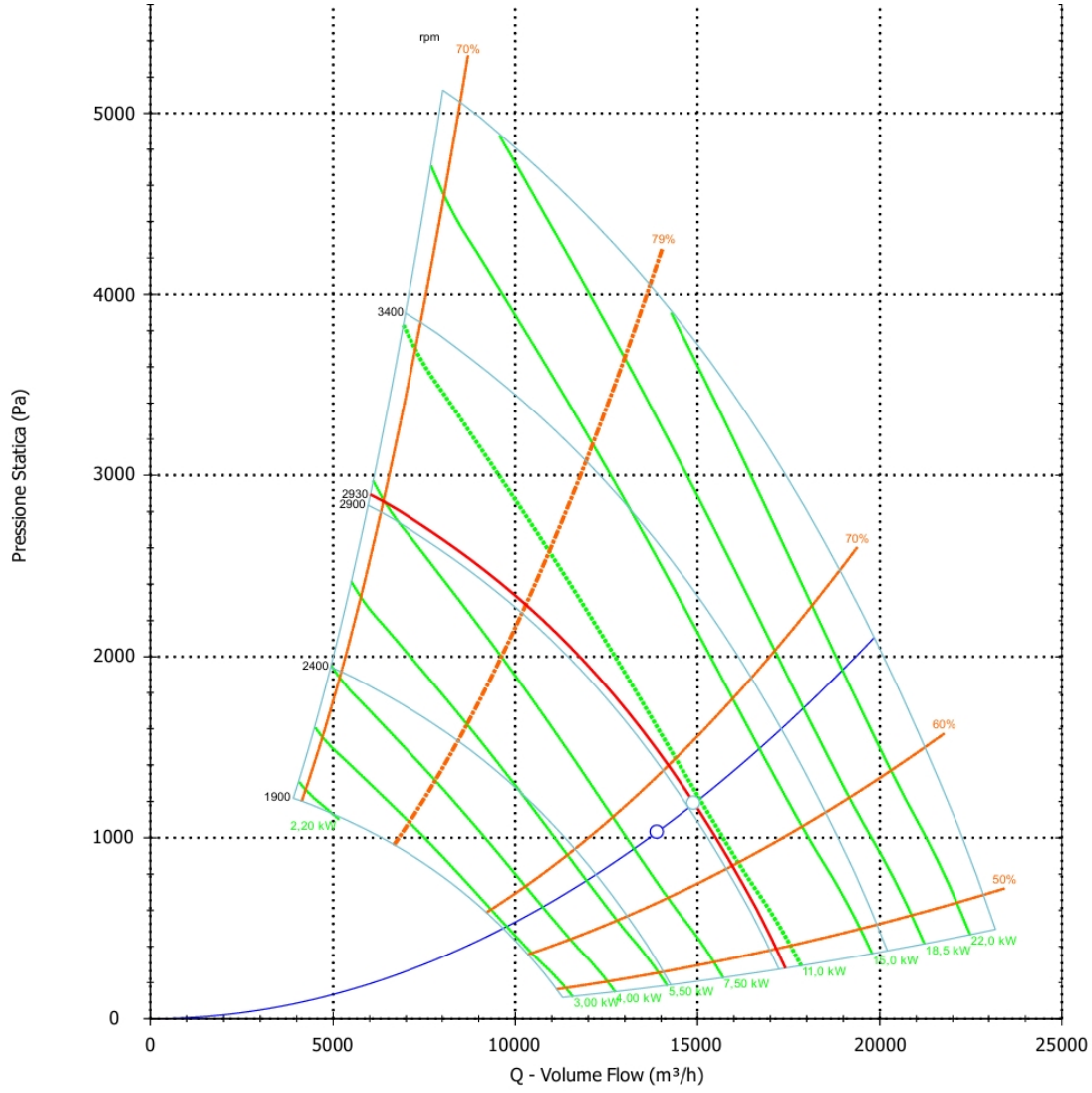


Figure 4.2: Fan characteristic curve [18]

The nominal design conditions of the fan are as follows:

- Nominal fan speed: $n = 2930\,\text{rpm}$
- Nominal volumetric flow rate: $\dot{V} = 14909\,\text{m}^3\,\text{h}^{-1}$
- Nominal static pressure drop: $\Delta P_{st} = 1188\,\text{Pa}$
- Nominal dynamic pressure drop: $\Delta P_d = 523\,\text{Pa}$
- Nominal mechanical power: $P = 10.7\,\text{kW}$
- Nominal static efficiency: $\eta_{st} = 46\,\%$
- Nominal total efficiency: $\eta_{tot} = 66\,\%$

The nominal operating point is at the intersection of the plant resistance curve (blue line) and the fan curve at nominal speed (red line). However, the fan is over-sized for this application, in fact the actual working point is along the plant resistance curve at $\dot{V} = 13900\,\text{m}^3\,\text{h}^{-1}$ and $\Delta P_{st} = 1033\,\text{Pa}$.

The extraction fan is driven by an integrated three-phase electric motor. According to the specifications provided by the fan manufacturer, the unit requires a mechanical shaft power of 10.7 kW at the nominal speed of 2930 rpm. The general specifications indicate the use of a high-efficiency motor with an IP55 protection degree and Class F insulation. Since the detailed datasheet of the motor was not explicitly provided by the fan manufacturer, it was necessary to identify an equivalent commercial unit to characterize its performance, particularly under partial load conditions. To this end, the official Innomotics (formerly Siemens) configurator [19] was used to select a motor compatible with the required nominal operating point. The identified model is the 2-pole 1AV3162A motor (Innomotics GP series, frame size 160 M, mounting type IM B3). According to the datasheet generated by the portal, the motor delivers a nominal power of 11 kW at 2945 rpm, with a nominal torque of 35.5 N m. These characteristics perfectly match the fan requirements. Furthermore, the motor belongs to the IE3 efficiency class, ensuring a nominal full-load efficiency of 91.2 %. Figure 4.3 presents the efficiency map extracted from the Innomotics configurator. This map allows the evaluation of mechanical efficiency at partial loads, enabling the calculation of the electrical power by dividing the mechanical power by the corresponding efficiency.

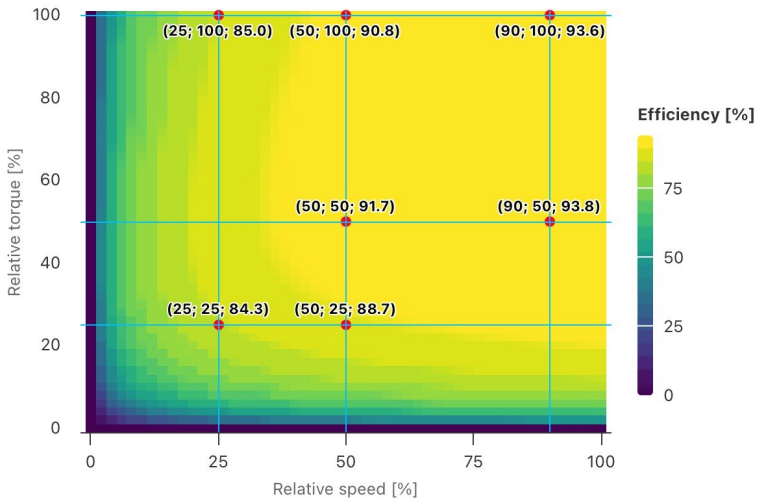


Figure 4.3: Efficiency map [20]

4.1.3 Flue Gas Composition and Operating Conditions

In this plant, the steam generators are fed by atmospheric air and natural gas (mainly modeled as methane, CH_4). The theoretical stoichiometric combustion reaction is the following:

$$CH_4 + 2O_2 \rightarrow CO_2 + 2H_2O \tag{4.1}$$

In order to evaluate the humidity of the flue gas, the following steps are performed:

- First, the **excess air** is evaluated taking into account the dry inlet air, using an oxygen probe that measures the dry flue gas.
- Second, using the calculated excess air, the measured inlet relative humidity, and the ambient temperature, the **absolute humidity** is evaluated by considering the actual wet inlet air.

Excess air evaluation

Combustion is not performed with pure oxygen but with ambient air, which is a gas mixture. Furthermore, in real industrial applications, such as this one, the reaction does not occur under perfectly stoichiometric conditions. A specific amount of excess air e is systematically introduced to ensure the complete oxidation of the fuel, thereby preventing the formation of unburned hydrocarbons and toxic carbon monoxide (CO), as well as to control the flame temperature. The total oxygen moles n_{O_2} for the combustion of one mole of CH_4 are:

$$n_{O_2} = 2 \cdot (1 + e) \tag{4.2}$$

Thanks to a stack probe, it is possible to measure the volumetric fraction of residual oxygen in the dry flue gases $c_{O_2} = 3\%$. The expression of c_{O_2} is defined as follows:

$$c_{O_2} = \frac{n_{O_2,out}}{n_{tot,out}} \tag{4.3}$$

where the moles of residual O_2 and the total moles as product (produced CO_2, residual O_2, and air inerts) are calculated by establishing the molar balance strictly for the dry exhaust gases:

$$\begin{aligned} n_{O_2,out} &= 2e \\ n_{tot,out} &= n_{CO_2} + n_{O_2} + n_{inerts} = \frac{2 + 2e}{y_{O2}} - 1 \end{aligned} \tag{4.4}$$

So, combining eq. 4.3 with eq. 4.4, it is possible to find the air excess:

$$e = \frac{c_{O_2} \cdot (2 - y_{O_2})}{2 \cdot (y_{O_2} - c_{O_2})} \tag{4.5}$$

where y_{O_2} is the oxygen concentration in the dry combustion air. Substituting the measured parameters yields an air excess of **e=14.96%**.

Finally, knowing the concentrations and the molecular weights of the gases present in the dry combustion air [21], it is possible to calculate the mass fraction m_i of each substance:

$$m_i = \frac{y_i \cdot MW_i}{\sum_{i}^{N=4} y_i \cdot MW_i} \tag{4.6}$$

Table 4.2 reports the volumetric composition, the molecular weight and mass composition of the dry combustion air.

Table 4.2: Volumetric composition, molecular weight and mass composition of the dry combustion air.

Property	**N_2**	**O_2**	**Ar**	**CO_2**
Volumetric fraction y_i (%)	78.08	20.95	0.93	0.04
Molecular weight MW_i $(kg/kmol)$	28.014	31.999	39.948	44.010
Mass fraction m_i (%)	75.51	23.14	1.29	0.06

Absolute humidity evaluation

Now, the actual humid air is taken into account. The absolute humidity of the inlet

combustion air (x_{in}), expressed in $g_{H_2O}/kg_{\text{dry air}}$, is determined using the measured relative humidity ($RH = 60\%$) and the ambient temperature ($T_{in} = 20°C$). The calculation requires the evaluation of the saturation pressure of water vapor (p_{sat}) at the given temperature:

$$x_{in} = 1000 \cdot \frac{\left(\frac{RH \cdot p_{sat}(T_{in})}{p_{atm}}\right) \cdot MW_{H_2O}}{\sum_i y_{i,\text{dry}} \cdot MW_i} \tag{4.7}$$

where:

- p_{atm} is the total atmospheric pressure.
- MW_{H_2O} is the molecular weight of water.
- $y_{i,\text{dry}}$ and MW_i are the volumetric fraction and the molecular weight of the i-th component of the dry air mixture (Table 4.2).

Substituting the measured ambient conditions, the calculated absolute humidity of the inlet air is $x_{in} = 8.718\ g_{H_2O}/kg_{\text{dry air}}$. Considering 1 kg of dry air, the addition of water vapor increases the total mass of the mixture to $(1 + x_{in}/1000)$ kg. The mass of each dry gas component remains constant, but its relative mass fraction in the wet mixture ($m_{i,\text{wet}}$) decreases due to the increased total mass. Therefore, the new mass fraction for each dry species (N_2, O_2, Ar, CO_2) is computed as follows:

$$m_{i,\text{wet}} = \frac{m_{i,\text{dry}}}{1 + \frac{x_{in}}{1000}} \tag{4.8}$$

where $m_{i,\text{dry}}$ is the mass fraction of the i-th component in the dry air mixture (Table 4.2).
Similarly, the mass fraction of the water vapor ($m_{H_2O,\text{wet}}$) in the inlet air stream is obtained by dividing the mass of water by the new total mass of the mixture:

$$m_{H_2O,\text{wet}} = \frac{\frac{x_{in}}{1000}}{1 + \frac{x_{in}}{1000}} \tag{4.9}$$

To evaluate the volumetric composition, the following expression is used:

$$y_i = \frac{\frac{m_i}{MW_i}}{\sum_i \frac{m_i}{MW_i}} \tag{4.10}$$

Now, it is possible to calculate the mass composition of the wet combustion air applying eq. 4.8 and eq. 4.9 and to calculate the volumetric composition with eq.

Table 4.3: Volumetric and mass composition of the wet combustion air.

Property	$\mathbf{N_2}$	$\mathbf{O_2}$	**Ar**	$\mathbf{CO_2}$	$\mathbf{H_2O}$
Volumetric fraction y_i (%)	77.00	20.66	0.92	0.04	1.38
Mass fraction $m_{i,wet}$ (%)	74.86	22.94	1.28	0.06	0.86

4.10, the results are summarized in Table 4.3.
Knowing the combustion reaction with excess air:

$$\begin{array}{ccccccccccccc} \mathrm{CH_4} & + & 2\mathrm{O_2} & + & \text{inerts} & \longrightarrow & 2\mathrm{H_2O} & + & \mathrm{CO_2} & + & \mathrm{O_2} & + & \text{inerts} \\ 1\,\text{mol} & + & 2(1+e)\,\text{mol} & + & n_{\text{inerts}} & \longrightarrow & 2\,\text{mol} & + & 1\,\text{mol} & + & 2e\,\text{mol} & + & n_{\text{inerts}} \end{array}$$

where:

$$n_{inerts} = n_{air} - 2(1+e) \tag{4.11}$$

$$n_{air} = \frac{2(1+e)}{y_{O_2}} \tag{4.12}$$

resulting in $n_{inerts} = 8.83\ mol$ and $n_{air} = 11.13\ mol$, it is possible to evaluate the moles and the volume composition of the humid flue gases. The molar amount of each species in the wet flue gas ($n_{i,f}$) is determined through the combustion stoichiometric balance. Inert gases like Nitrogen (N_2) and Argon (Ar) pass through the boiler unreacted. Therefore, their outgoing moles are simply the product of the total wet air moles and their respective inlet volumetric fractions:

$$n_{N_2,f} = n_{air} \cdot y_{N_2} \tag{4.13}$$

$$n_{Ar,f} = n_{air} \cdot y_{Ar} \tag{4.14}$$

For the reactive species, the balance accounts for the moles consumed and generated by the methane oxidation:

$$n_{O_2,f} = n_{air} \cdot y_{O_2,ac} - 2 \tag{4.15}$$

$$n_{CO_2,f} = n_{air} \cdot y_{CO_2,ac} + 1 \tag{4.16}$$

$$n_{H_2O,f} = n_{air} \cdot y_{H_2O,ac} + 2 \tag{4.17}$$

Then, the volumetric fraction of the i-th species in the flue gas is obtained by dividing the moles of the i-th species by the total moles:

$$y_{i,f} = \frac{n_{i,f}}{n_{tot}} = \frac{n_{i,f}}{1 + n_{air}} \tag{4.18}$$

The results are reported in Table 4.4.

Table 4.4: Wet flue gas volume composition

	N_2	O_2	Ar	$H_2O_{(g)}$	CO_2
Volumetric fraction $y_{i,f}$ (%)	70.65	2.47	0.85	17.76	8.28

Finally, it is possible to calculate the absolute humidity of the flue gases as follows:

$$x_f = \frac{y_{H2O,f}}{\sum\limits_{i \neq H_2O} y_{i,f} \cdot MW_i} \tag{4.19}$$

The calculation yields an absolute humidity of $x_f = 0.1302\ \mathrm{kg_{H_2O}/kg_{dry\ gas}}$, which corresponds to **13.02%**. This important result is used in the Simulink-Simscape simulation as will be discussed in 5.2.2.
Consequently, the actual exhaust stream leaving the boiler is a "wet" gas mixture, containing both the water vapor generated by the methane oxidation and the moisture originally present in the combustion air. The presence of water vapor in the flue gases increases the heat transfer in the heat exchanger: in fact during the cooling, once the dew point temperature[2] is reached, the water vapor starts to condensate, rejecting latent heat.
As regards the flue gas temperature, it is measured and corresponds to $T_{fg} = 125°C$.

4.1.4 Water operating conditions

The water loop is a closed circuit in which water is heated in the flue gas-water heat exchanger (HE-01) and subsequently cooled in the evaporator of the heat pump (HP-01) during the winter season or in a heat exchanger to pre-heat the make-up water for the deaerator during the summer season. In nominal operating condition, the water is heated to 25°C in the HE-01 and cooled to 18°C. A temperature probe, located at the outlet of HE-01 measures temperature variations and sends a signal to TIC-03 controller, as explained in Section 4.2.

4.2 Control Strategy

For this application, Trigenia s.r.l. designed a specific and tailored control strategy using PID controllers. The proposed control logic aims to ensure the optimal management of flue gas extraction across all possible combinations of thermal

[2]The dew point is the temperature at which air must be cooled to become completely saturated with water vapor

demand and steam generator loads. The primary goal is to continuously maximize the volume of extracted flue gas while minimizing the electrical power consumed by the fan. Specifically, the control strategy must prevent both the unwanted release of hot flue gases into the atmosphere (which represents a waste of recoverable thermal energy) and operating conditions characterized by excessive fan speeds that lead to an unnecessary throttling of both dampers (resulting in wasted electrical energy and improper fan operation). This objective is achieved through the coordinated action of the frequency converter and the two dampers, managed via cascaded PID control loops. The actuating devices utilized in this control strategy are:

- The centrifugal fan CF-01, driven by a dedicated frequency converter;
- The modulating damper SR-01, located on the stack intake of the new steam generator SG-03;
- The modulating damper SR-02, located on the stack intake of the existing steam generators SG-01 and SG-02.

In the following explanations, some variables will be used and their names with the associated definitions are reported in Table 4.5.
The implemented PID controllers are the following:

- **TIC-01**: Control of the $\texttt{TD} - \texttt{01}$ temperature difference by modulating the SR-01 damper. Its objective is to maximize the amount of flue gas extracted to the WHR system while minimizing the intake of ambient air from the top of the stack.
- **TIC-02**: Control of the $\texttt{TD} - \texttt{02}$ temperature difference by modulating the SR-02 damper position. Its objective is to maximize the amount of flue gas extracted to the WHR system while minimizing the intake of ambient air from the top of the stack.
- **TIC-03**: Control of the water temperature ($\texttt{TT} - \texttt{6_20}$) at the outlet of the flue gas-water heat exchanger (HE-01) by modulating the actual CF-01 fan speed relative to its extraction capacity. Its objective is to maintain the water temperature within the target operating range, adjusting to the thermal demand of the network.
- **YIC-01**: Control of the maximum damper opening value ($\texttt{SR_Y_MAX}$) by modulating the extraction capacity of the CF-01 fan ($\texttt{CF} - \texttt{01_CAP}$). Its objective is to minimize the electrical power consumption of the CF-01 fan and prevent improper operating conditions, such as high fan speeds coupled with restricted damper openings.

Table 4.5: Nomenclature of the control variables.

Variable	**Definition**
TT − 6_15	Flue gas temperature in stack 1, upstream of the WHR extraction point.
TT − 6_16	Flue gas temperature in the duct from stack 1 to the WHR system.
TT − 6_18	Flue gas temperature in stack 2, upstream of the WHR extraction point.
TT − 6_19	Flue gas temperature in the duct from stack 2 to the WHR system.
TT − 6_04	Water temperature at the outlet of the HE-01.
TD − 01	Temperature difference between TT − 6_15 and TT − 6_16 for the TIC-01 controller.
TD − 02	Temperature difference between TT − 6_18 and TT − 6_19 for the TIC-02 controller.
SR − 01_Y	SR-01 damper position feedback.
SR − 02_Y	SR-02 damper position feedback.
CF − 01_CAP	Maximum allowable inverter frequency (fan capacity) for TIC-03 controller.
CF − 01_COM	CF-01 fan inverter frequency.
SR − 01_COM	SR-01 damper opening command.
SR − 02_COM	SR-02 damper opening command.

In order to facilitate the comprehension of the operating mechanism of the implemented controllers, in Figure 4.4 a diagram of the process control is depicted. As can be observed, while the controllers TIC-01 and TIC-02 operate independently, the controllers TIC-03 and YIC-01 are strictly connected: YIC-01 provides the maximum fan speed to TIC-03 which in turn calculates the actual fan velocity.

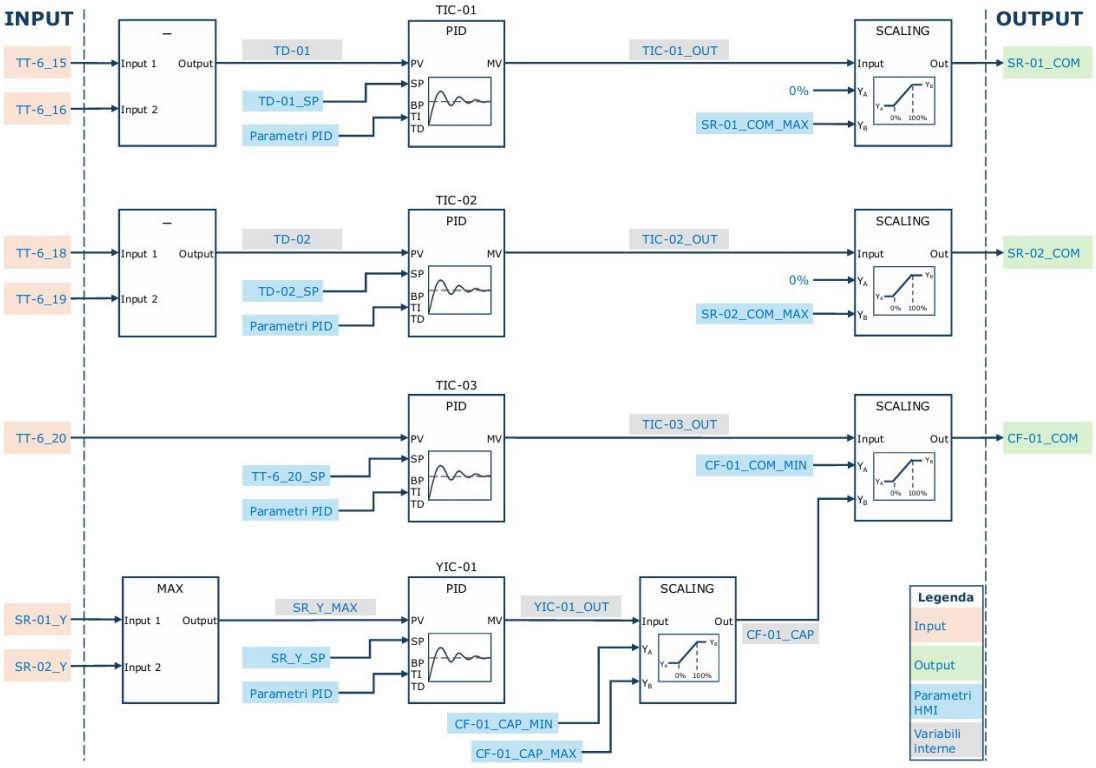


Figure 4.4: Block diagram of the process control strategy [22]

Chapter 5

Dynamic Modelling in Simulink

5.1 Simulink Model

The plant was modelled using Matlab-Simulink, in particular using the Simscape environment. The model is represented in Figure 5.1. The flue gas part is modelled using the Moist Air domain (represented in violet), while the water circuit is modelled using Thermal Liquid domain (represented in yellow). Moreover, a further domain is used to properly model the fan component, that is the Mechanical domain (represented in green). As can be observed, in addition to the self-explanatory

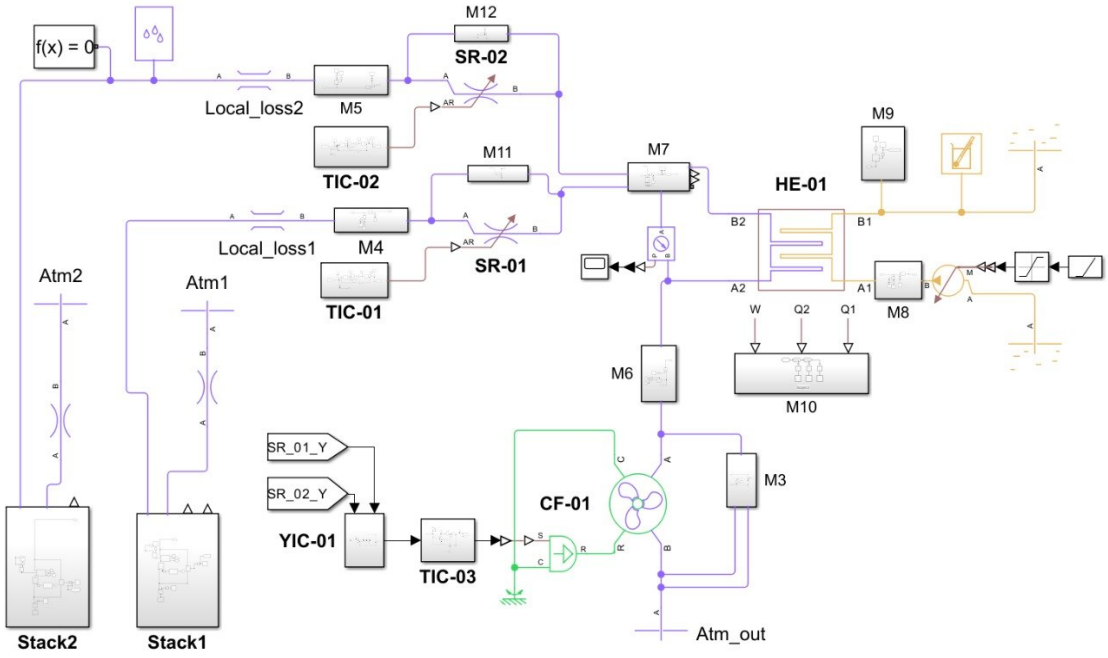


Figure 5.1: WHR system modelled on Simulink

components, there are some blocks called with letter M followed by a number and they represent measuring subsystems in which variables are measured and controlled (such as temperature, mass flow rate, pressure, ...). Clearly, the Simulink scheme is very similar to the P&ID scheme shown in Section 4 making it easy to trace the path of the streams. Starting from the two stacks, flue gas can go towards the atmosphere or towards the heat exchanger branch. Before reaching HE-01, the flue gases pass through the dampers, SR-01 and SR-02 respectively for flue gas from Stack 1 and flue gas from Stack 2, controlled by TIC-01 and TIC-02 controllers. Afterwards, they are collected and directed to the Heat Exchanger thanks to the block Fan CF-01 positioned downstream to the Heat Exchanger. The block Fan, as can be observed, is driven by YIC-01 and TIC-03 controllers. The water loop consists of a circuit where water is drawn from a primary reservoir, heated within the heat exchanger, and subsequently discharged into a secondary reservoir.

5.2 Detailed Subsystem Modelling

5.2.1 Moist Air Properties

The "Moist Air Properties" block defines all the thermodynamic properties of the fluid, that, in this model, is represented both by the flue gas and the ambient air. The flue gases are produced by the steam generators (modelled as Reservoir block) while the ambient air can be introduced from the top of the stack (modelled as Reservoir block). By default, the "Moist Air Properties" incorporates the properties of dry air and water vapor. In addition to these primary components, a "Trace Gas" can be defined using custom parameter. For this application, the Trace Gas is used to represent the dry flue gas and the block is configured to "Track mass fraction and gas properties". Exploiting the data derived in 4.1.3, the composition of the dry flue gas is known. To account for humidity, it is sufficient to set the correct moisture mass fraction directly within the Reservoir block (see section 5.2.2). To accurately model the dry flue gas, its specific enthalpy vector as a function of temperature must be determined. This was achieved by evaluating the enthalpy of each individual substance present in the mixture (N_2, CO_2, O_2, Ar). The calculation is based on an empirical hyperbolic function from [23], which computes the ideal gas heat capacity at constant pressure (C_p^0) expressed in J/(kmol K):

$$C_p^0 = C1 + C2\left[\frac{C3/T}{\sinh(C3/T)}\right]^2 + C4\left[\frac{C5/T}{\cosh(C5/T)}\right]^2 \tag{5.1}$$

To derive the enthalpy function required for the model, the heat capacity is integrated between a reference temperature ($T_{ref} = 273.15\ K$) and the fluid

temperature (T), resulting in the following expression:

$$h(T) = C1(T - T_{ref}) + C2 \cdot C3 \left[\coth\left(\frac{C3}{T}\right) - \coth\left(\frac{C3}{T_{ref}}\right)\right] - C4 \cdot C5 \left[\tanh\left(\frac{C5}{T}\right) - \tanh\left(\frac{C5}{T_{ref}}\right)\right] \tag{5.2}$$

Subsequently, the enthalpy for each substance was calculated across a temperature vector defined in Simulink. The overall specific enthalpy of the dry flue gas mixture was then computed using a mass-weighted average:

$$h_{\mathrm{f}} = \frac{\sum_i y_{\mathrm{dry},i} \cdot h_i}{\sum_i y_{\mathrm{dry},i} \cdot MW_i} \tag{5.3}$$

It is important to note that this calculated vector accounts only for the dry portion of the flue gas. The latent and sensible heat associated with the water content are managed internally by Simscape through the moisture parameters set in the Reservoir blocks, as will be detailed in Section 5.2.2. Figure 5.2 illustrates the resulting dry flue gas enthalpy as a function of temperature. Finally, to find

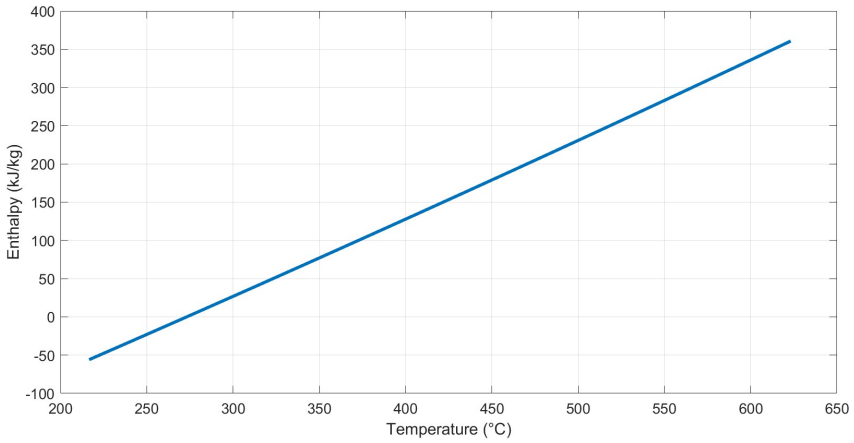


Figure 5.2: Dry flue gas enthalpy vector

the Trace Gas Specific Constant, the following calculation is performed using the universal gas constant ($R_u = 8314.46\ J/(kmol \cdot K)$) and the dry mixture's molar mass:

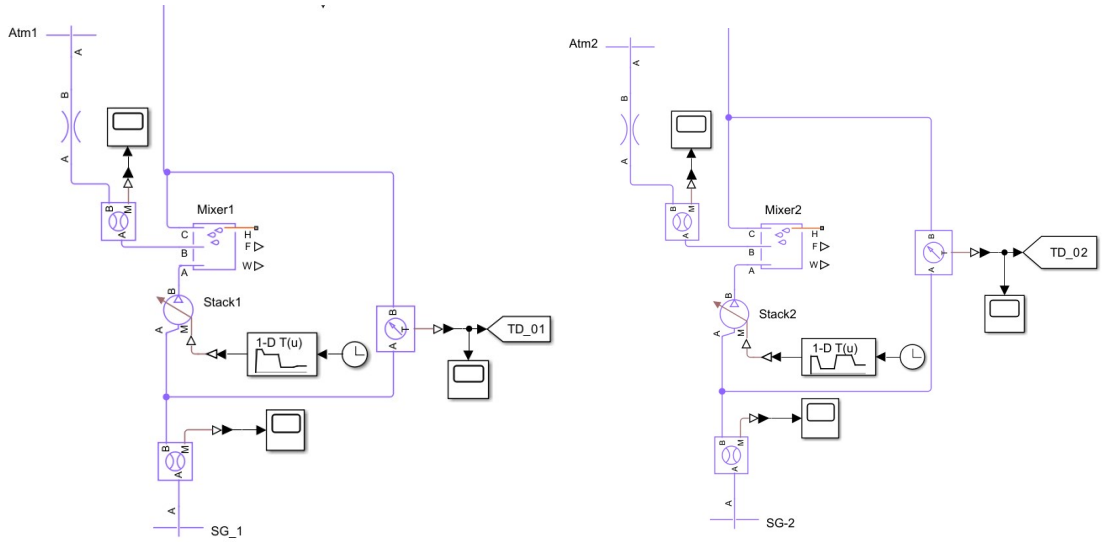
$$R_f = \frac{R_u}{\sum_i y_{\mathrm{dry},i} \cdot MW_i} \tag{5.4}$$

which evaluates to $278.38 J/(kg \cdot K)$.
Regarding the other transport properties required by the Trace Gas model, like

dynamic viscosity, thermal conductivity and diffusivity in air, the default values were maintained. In the context of this study, where the flue gases from a boiler are utilized to heat water for a heat pump at relatively low maximum temperatures (up to 125°C), the variation of these transport coefficients has a negligible impact on the macroscopic thermodynamic balances and the overall results of the simulation. Since the primary focus is on the energy recovery and temperature control rather than detailed fluid dynamic phenomena, a precise characterization of these specific parameters was deemed unnecessary.

5.2.2 Stack 1 and Stack 2

As detailed in Section 4, the plant features two distinct stacks: the first is coupled with two steam generators, whereas the second serves the new steam generator. The Stacks are modelled using the same Simscape blocks and a comparable architectural layout, as depicted in Figures 5.3a and 5.3b.



(a) Stack 1 **(b)** Stack 2

Figure 5.3: Simulink Model of the two Stacks

To model the Stacks, the following blocks were used:

- **Reservoir (MA)**: it models an infinite volume of moist air and sets constant boundary conditions [24]. Two Reservoir blocks were used, one to model the external environment and the other one to model the steam generator. The first Reservoir (external environment) is set as follows:
  - $p = 101325\ Pa$: this value represents the standard atmospheric pressure.

It is selected because the reservoir models an open-air intake, directly drawing air from the external surroundings.

- $T = 10°C$: this temperature is chosen as a representative mean value for the winter season. It provides a realistic environmental reference for evaluating the system's thermal performance under cold operating conditions.
- Specific humidity=0.005: this parameter defines the constant moisture content of the ambient air, representing a typical humidity value for a temperate climate during winter. In Simscape, this represents the mass of water vapor as a fraction of the total mass of the moist air mixture.

The second Reservoir (steam generator) is set as follows:

- $p = 101325\ Pa$: this value corresponds to the atmospheric pressure, which is assumed because the flue gases flow through a chimney that essentially vents directly into the atmosphere.
- $T = 125°C$: this is the actual flue gas temperature measured at the boiler outlet.
- Humidity Ratio: $x_f = 0.1302$. This value represents the moisture content of the flue gases and was previously calculated in Section 4.1.3.
- Reservoir Trace Gas Mass Fraction: $x_{trace} = 0.885$

To correctly implement the flue gas composition in the Reservoir (Trace Gas Mass Fraction), the mixture was modeled by assuming the absence of atmospheric air ($m_{dry_air} = 0$). Consequently, the dry fraction of the flue gas is entirely represented by the trace gas (m_{trace}), while the moisture is represented by the water vapor (m_{vapor}).

According to Simscape definitions, the Humidity Ratio (x_f) is the ratio of the water vapor mass to the dry gas mass:

$$x_f = \frac{m_{vapor}}{m_{trace}} = 0.1302 \tag{5.5}$$

Assuming a reference mass of 1 kg for the dry flue gas ($m_{trace} = 1\,\text{kg}$), the resulting water vapor mass is 0.1302 kg.

The Trace Gas Mass Fraction (x_{trace}) is defined as the ratio of the trace gas mass to the total mass of the mixture. Substituting the known values yields:

$$x_{trace} = \frac{m_{trace}}{m_{tot}} = \frac{m_{trace}}{m_{trace} + m_{vapor}} = \frac{1}{1 + 0.1302} = 0.885 \tag{5.6}$$

Consequently, the Trace Gas Mass Fraction is utilized to define solely the dry fraction of the combustion gases, ensuring that the moisture effects

are not duplicated and are correctly isolated within the humidity domain. This approach is consistent with the enthalpy vector provided for the trace gas, which was calculated exclusively for the dry flue gases, excluding the water vapor contribution. All remaining parameters were left at their default Simscape settings.

- **Flow Rate Source (MA)**: it models an ideal mass flow rate source regardless of the pressure differential [25]. For this application, it models the flue gas flow rate from the boilers. The mass flow rate signal is provided by a 1-D Lookup Table that models the desired flue gas mass flow rate for both the Stacks.

- **Constant Volume Chamber (MA)**: it models a constant volume of moist air, storing mass and energy, and exchanging them through its three ports [26]. For this application, it has a dual purpose: the first is to model the physical volume within the chimney and the second is related to computational reasons. Specifically, a single node would have been sufficient to model the intersection point (stream from the boiler, stream to the external environment and stream to the heat exchanger); however this approach forced Simulink to instantaneously calculate all the parameters at a crucial point, leading to heavy and time-consuming computations.

- **Local Restriction (MA)**: it models the pressure drop due to a localized reduction in flow area [27]. For this application, it is used to model the resistance along the chimney and to regulate the passage of the flue gas towards the external environment (and also to regulate the air from the external environment). The restriction area is set to $0.7\,\mathrm{m}^2$.

5.2.3 Fan

The fan is modelled with the block Fan (MA). The chosen parametrization is "Static pressure and flow rate at reference shaft speed". The block configuration is based on the reference fan characteristic curve and nominal operating condition reported in Section 4.1.2. The scaling between the reference fan curves and the actual flow rate and pressure gain is determined from affinity laws according to the official MathWorks documentation [28]. This block connects the Moist Air domain with the Mechanical domain. The mechanical part is represented by the Ideal Angular Velocity Source block that generates the velocity value proportional to the input signal that is provided by the output of the TIC-03. In Figure 5.4, the implemented fan parameters are shown.

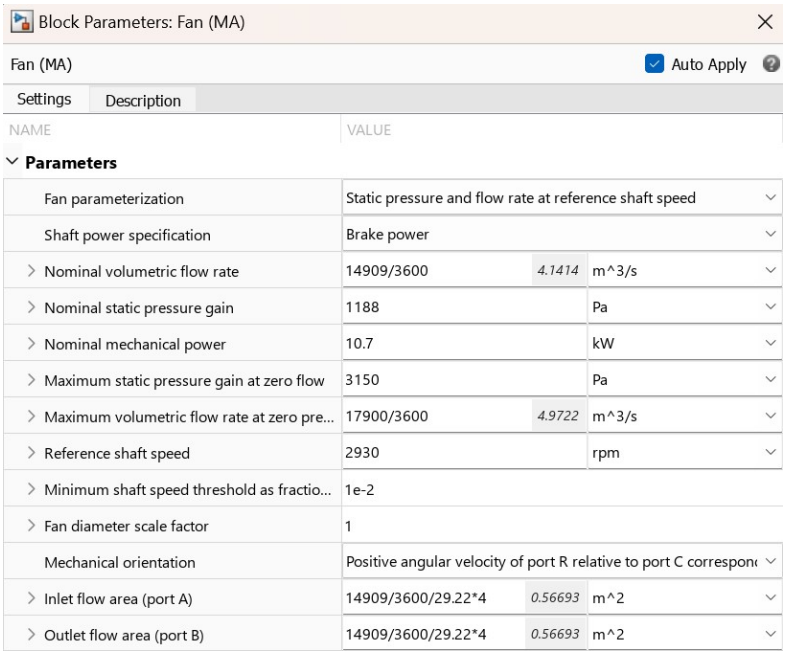


Figure 5.4: Simulink parameter dialog box for the fan configuration

In particular, this block constructs the analytical reference curve by applying a quadratic fit to three specific operational points: maximum static pressure gain at zero flow, nominal static pressure gain and maximum volumetric flow rate at zero pressure. The resulting pressure-flow characteristic is shown in Figure 5.5.

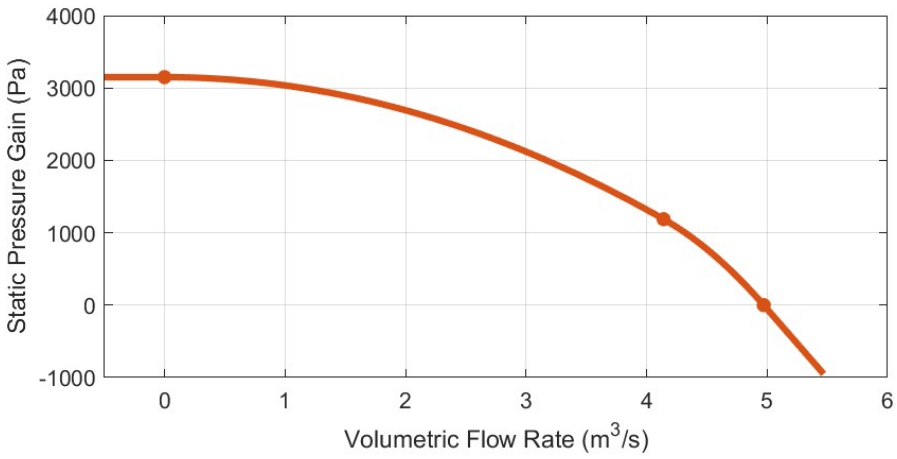


Figure 5.5: Fan characteristic curve constructed by Simulink

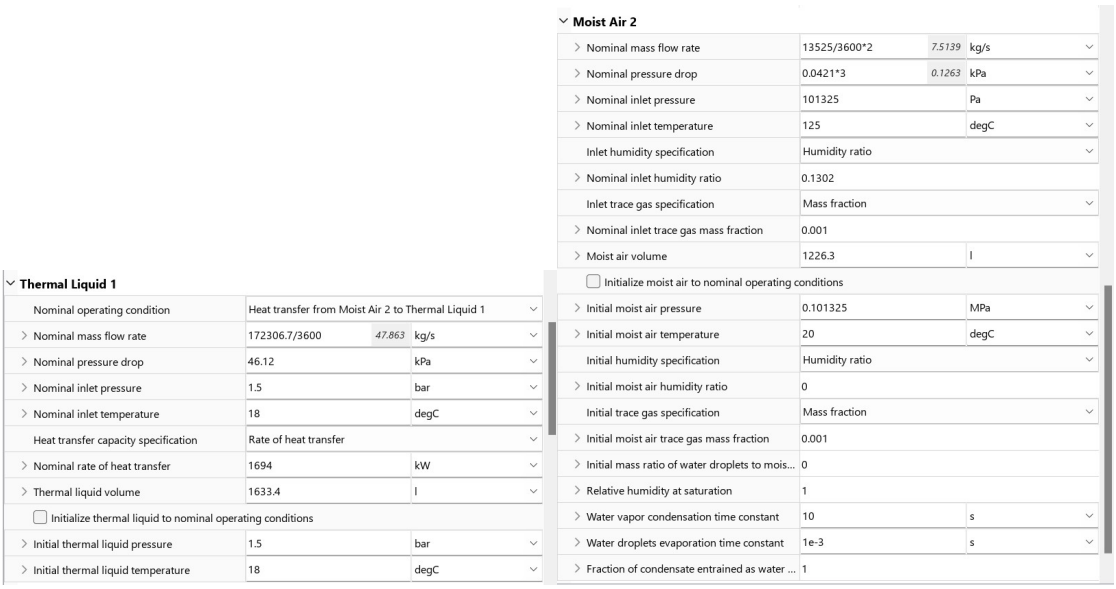
The chosen parametrization does not take into account density variation with

respect to the reference density (at nominal condition). Although a more comprehensive parametrization accounting for continuous fluid density variations is available, it was discarded after evaluating it. Keeping the solver independent of density variations was necessary to ensure numerical stability and avoid excessive computational costs, which would have significantly prolonged simulation times. At the node under examination, the average operating density is approximately 1.112 kg/m^3, presenting a -9.3% deviation from the fan's reference conditions ($\rho_{nom} = 1.226\ kg/m^3$). Therefore, the solver simulates a fluid that is heavier than the actual hot fluid, and calculates a slightly higher pressure head than the real fan would actually provide. This introduces an inherent overestimation of the volumetric flow rate, which can be estimated at around 4-5% given the quadratic dependence of pressure drops in the circuit. Consequently, the thermal power exchanged within the WHR system is also slightly overestimated. Nevertheless, this represents a perfectly acceptable engineering approximation for the scope of this system-level model.

A further limitation of the selected parametrization concerns the evaluation of the mechanical power and efficiency curves. Specifically, the Simscape block intrinsically assumes the nominal efficiency to be the peak efficiency, which can lead to inaccuracies during off-design operation. To overcome this drawback, mechanical power and static efficiency are not extracted directly from the solver. Instead, they are calculated in post-processing through a dedicated MATLAB function. This custom function relies on the manufacturer's characteristic curve (approximated via polynomial fitting) and applies affinity laws (similarity rules) starting from the nominal operating conditions. By evaluating the actual operating point, the script accurately computes the true mechanical power consumption and the actual static efficiency of the fan at each time step.

5.2.4 Heat Exchanger

The flue gas-water heat exchanger is modelled with the block "System-Level Heat Exchanger (TL-MA)" in a counter flow arrangement. It is configured with the technical data provided by the manufacturer, as shown in Section 4.1.1. According to MathWorks documentation, this block models a heat exchanger based on performance data from the heat exchanger datasheet [29]. In particular, the heat exchanger is sized to match the specified performance at the nominal operating condition at steady state. Figure 5.6 shows how the block is configured. It is important to underline that during the simulation setup, the nominal exhaust gas mass flow rate was increased to twice its nominal value to bypass a sizing failure within the Simscape solver. This modification ensures that the requested nominal heat transfer rate is thermodynamically feasible, allowing the software to properly initialize the heat exchanger geometry. In addition, the block allows to model the



(a) Thermal liquid configuration **(b)** Moist Air configuration

Figure 5.6: Simulink parameter dialog box for the heat exchanger configuration

thermal mass in order to introduce additional dynamics to the simulation during the transients. Moreover, it is possible to measure the rate of heat transfer and the total rate of water vapor condensation that is removed from the moist air through proper signal ports present in the block.

5.2.5 Minor and Major Losses: Finding the Operating Point

In order to simulate the plant resistance curve, it is necessary to increase the pressure drops simulating minor and major losses. If these losses were not modelled, the operating point (the intersection between the fan characteristic curve and the system resistance curve) would occur at an excessively low pressure drop, falling into a region where the fan operates inefficiently. To do so, three "Flow Resistance" blocks are used. These blocks model a general pressure drop proportional to the square of the mass flow rate. The density dependence is omitted in order to facilitate computational calculations. The block uses the nominal parameters to calculate the constant of proportionality between the pressure drop and the mass flow rate [30]. The positions and configurations of the three blocks are summarized in Table 5.1. The configuration of these blocks aims to obtain a plant resistance curve as close as possible to the one reported in Figure 4.2, previously shown in Section 4.1.2. The simulation is carried out with excess of flue gas produced by

Table 5.1: Flow resistance parameters for the WHR system

Flow Resistance	**Position**	ΔP_{nom} (Pa)	G_{nom} (kg/s)
1	Branch 1 before SR-01	350	1.879
2	Branch 2 before SR-02	350	1.879
3	After mixing between branch 1 and branch 2, before HE-01	220	3.757

the boilers (meaning that a certain amount of the flue gas is discharged into the environment) and with the four PID controllers active. In these conditions, the fan speed is 2737 rpm and the dry flue gas volumetric flow rate (after the condensation in HE-01) drawn by the fan is $3.91\,\mathrm{m^3\,s^{-1}}$. In Figure 5.7, the plant resistance curve and the fan characteristic curve are depicted; their intersection represents the **operating point**.

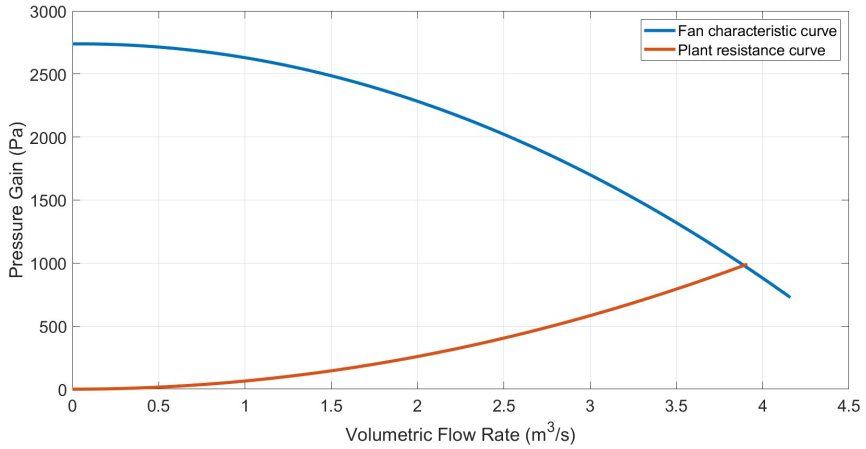
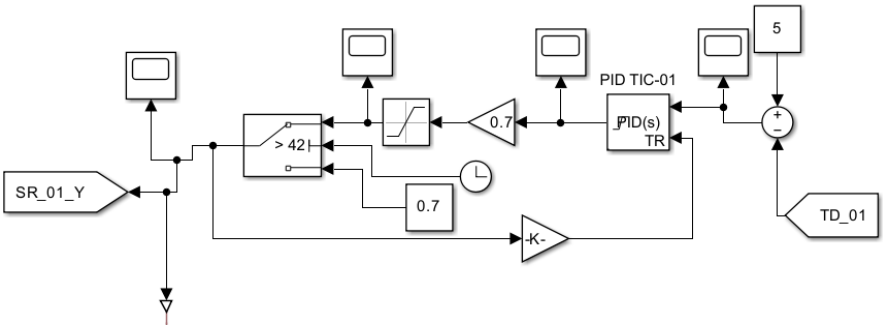


Figure 5.7: Plant resistance curve and Fan characteristic curve: Operating point

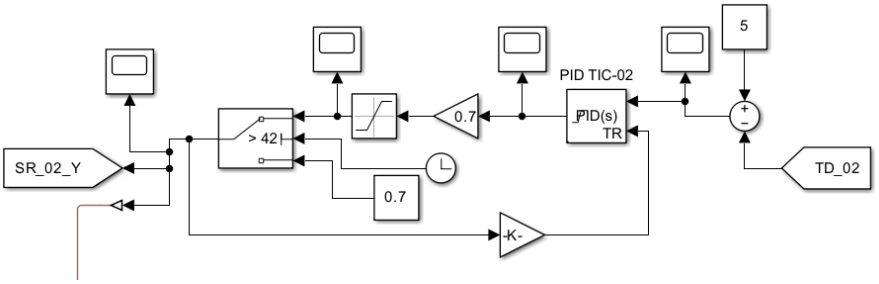
5.2.6 TIC-01 and TIC-02

The PID controllers TIC-01 and TIC-02 are designed to modulate the flow areas of damper 1 and damper 2, respectively. Within the model, these dampers are represented as "Variable Restrictions" where the manipulated variable is the restriction area (`SR-01-Y` and `SR-02-Y`). The restriction area can vary from a minimum value of $0.1\,\mathrm{m^2}$ to a maximum value of $0.7\,\mathrm{m^2}$. The control variable is the temperature

difference `TD-01` for the TIC-01 and `TD-02` for the TIC-02, continuously monitored via a temperature sensor for each respective PID control. The temperature sensor sends the feedback signal, which is compared against a fixed setpoint of 5 to generate the error signal fed into the PID controller. The implemented scheme of TIC-01 and TIC-02 is shown in Figure 5.8. The closed-loop regulation is handled by the



(a) TIC-01 Simulink scheme



(b) TIC-02 Simulink scheme

Figure 5.8: Simulink scheme for TIC-01 and TIC-02 controllers

"Discrete PID controller" block, configured in parallel mode. In this configuration, the overall controller output is the sum of the proportional, the integral and the derivative actions. According to the official MathWorks documentation, the transfer function for the parallel-form PID controller is expressed as:

$$C_{par}(s) = P + I(\frac{1}{s}) + D(\frac{Ns}{s+N}) \tag{5.7}$$

where P,I and D are the proportional, integral and derivative gains respectively, while N represents the derivative filter coefficient. This filter is essential to make the derivative term proper and to attenuate the high frequency noise. The PID output is normalized and saturated between 0 and 1, representing the fractional stroke of the actuator. To convert this normalized signal into a physical opening area, the controller's output is multiplied by a Gain block of 0.7, which corresponds

to the maximum allowable opening of the damper. The initial conditions for both the integrator and the filter are set to zero.

To ensure a stable and controlled startup, a switch logic is implemented in which during the initial transient phase the system operates in open-loop configuration. This mechanism relies on a Clock block, a Constant block and a Switch block. The Clock block tracks the simulation time and feeds it into the control port of the Switch, which is configured with a threshold of 42 s acting as follows:

- **Startup phase**: if the simulation time is below 42 s, the switch is connected to the constant value 0.7, meaning that the dampers are kept at their maximum opening to allow for the initial thermohydraulic stabilization of the system.

- **Closed-loop phase**: as soon as the simulation time exceeds 42 s, the switch toggles to its upper port and the dampers receive the dynamic output of the PID controller.

In order to apply this strategy, the Tracking Mode of the PID controllers is needed. The Tracking Mode avoids abrupt transients or jumps in the control signal and the occurrence of the windup phenomenon. In particular, the actual command signal `SR-01-Y` for the TIC-01 and `SR-02-Y` for the TIC-02 is fed back to the tracking port (TR) of the PID controller. Since the forward path scales the PID output by the maximum opening (0.7), the feedback signal is normalized by dividing it by 0.7 with a Gain block. Moreover, to prevent the integral term from accumulating excessive error when the actuator reaches its saturation limits, the clamping method was selected as internal anti-windup strategy for both the PID controllers [31].

The tuning of the PID controllers was performed using a manual trial-and-error approach. The proportional, integral and derivative gains were iteratively adjusted by observing the system's response in the Simulink environment. The tuning process was concluded once a satisfactory trade-off between settling time, overshoot and steady-state error was achieved. Table 5.2 shows the gains implemented for TIC-01 and TIC-02.

Table 5.2: Final tuned PID gains for TIC-01 and TIC-02 controllers.

Gain	**TIC-01**	**TIC-02**
P	0.100	0.100
I	0.005	0.005
D	0.000	0.000

5.2.7 TIC-03 and YIC-01

The control logic implemented in Simulink for TIC-03 and YIC-01 is designed to optimize the operation of the exhaust gas fan, aiming to minimize electrical power absorption and ensure the desired water temperature as explained in Section 4.2. The implementation of the control logic for TIC-03 and YIC-01 PID controllers is shown in Figure 5.9. Similarly to the other controllers previously explained in Section 5.2.6, also in this case "Discrete PID controller" block is used in parallel form and tracking mode.

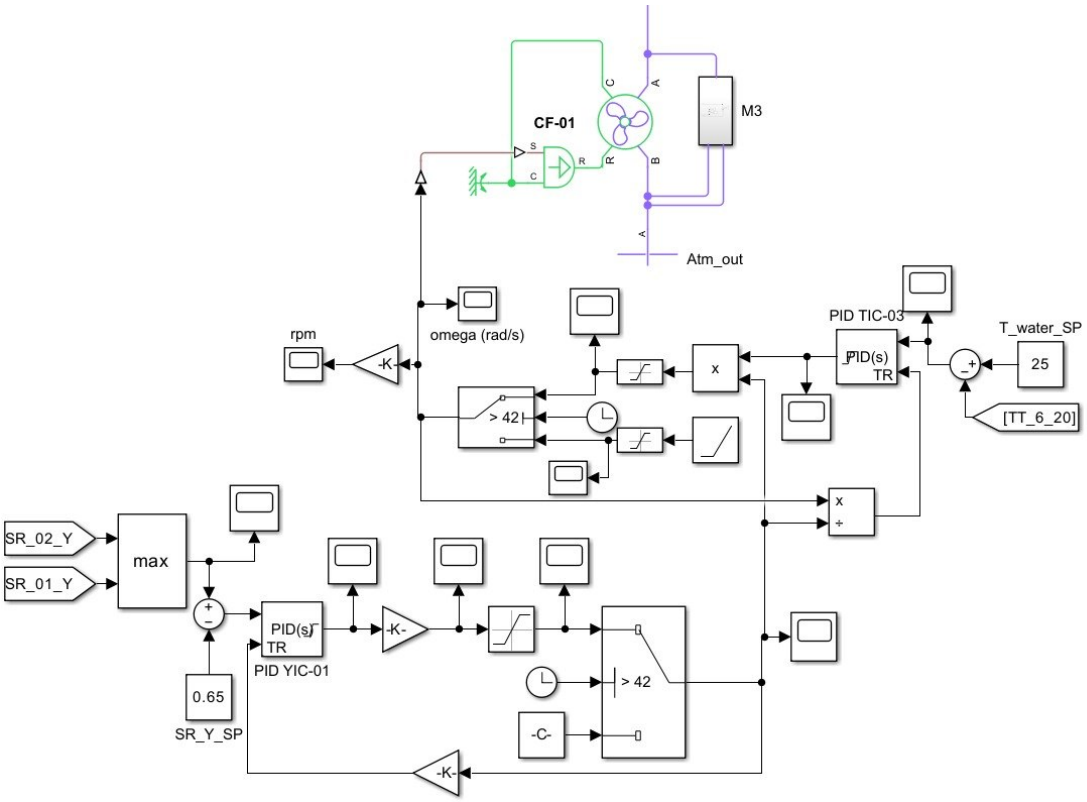


Figure 5.9: Simulink scheme for YIC-01 and TIC-03 controllers

Regarding YIC-01, the signals of the current opening of both dampers (`SR-01_Y` and `SR-02_Y`) are fed into a Max block, which calculates the maximum value that is compared against the setpoint fixed to $0.65\,\mathrm{m}^2$ (safely below the maximum physical opening of $0.70\,\mathrm{m}^2$). The output is multiplied by the nominal speed value ($n_{\mathrm{nom}} = 2930\,\mathrm{rpm}$) through a Gain block. The output of YIC-01 is normalized with respect to the saturation limits, in particular it is constrained between $\frac{1400}{2930}$ and 1. This internal lower limit is coupled with a downstream Saturation block in which the signal is limited between a lower limit $n_{\mathrm{min}} = 146.61\,\mathrm{rad\,s^{-1}} = 1400\,\mathrm{rpm}$

and a higher limit $n_{\max} = 306.83\,\mathrm{rad\,s^{-1}} = 2930\,\mathrm{rpm}$. This proportional saturation ensures that the lower internal limit of the PID corresponds exactly to the physical lower limit of 1400 rpm. The lower limit was carefully selected through operational analysis: it represents an optimal compromise that significantly reduces electrical power consumption when the thermal load is low, without forcing the fan to operate in an inefficient region of its characteristic curve, as it will show in Section 6.1.1.

As regards TIC-03 control, it regulates the water temperature (`TT-6-20`) exiting HE-01 to meet a setpoint of 25 °C. Its output is limited between 0 and 1, acting as a dimensionless modulation factor. To compute the actual commanded fan speed, this dimensionless output is fed into a Product block, where it is multiplied by the dynamic capacity limit provided by YIC-01. For safety reasons, a Saturation block is present, which limits the actual fan speed between n_{min} and n_{max}.

Like the other controllers, to manage the start-up phase, both PIDs are equipped with a tracking system managed by Switch blocks acting as follows:

- **Start-up phase**: for the first 42 s, YIC-01 is overridden by a constant manual value equal to the nominal fan speed, while TIC-03 is overridden by a ramp that peaks at the same speed.
- **Closed-loop phase**: after 42 s, the switches toggle and both the PIDs take over the automatic control.

Regarding the tracking signals, the input for YIC-01 is the manual output divided by n_{nom}, while for TIC-03 it is the manual output divided by the output of YIC-01.

For the tuning phase, a manual trial-and-error approach was conducted. In Table 5.3, the chosen gains for TIC-03 and YIC-01 are shown.

Table 5.3: Final tuned PID gains for TIC-03 and YIC-01 controllers.

Gain	TIC-03	YIC-01
P	0.250	0.500
I	0.010	0.020
D	0.000	0.000

5.2.8 Thermal Liquid Loop

In order to simulate the water loop, the Thermal Liquid domain has been used. Water is withdrawn by a Flow Rate Source from a Reservoir block set at 15 °C and 1.5 bar. The flow rate signal is provided by a Ramp block followed by a Saturation block in order to simulate the initial start-up phase. At steady state, the water mass flow rate is $172306.7\,\mathrm{kg\,h^{-1}}$. Subsequently, the water enters HE-01, where it is

heated up, and flows towards another Reservoir block set at 25 °C and 1.5 bar. This last Reservoir block does not influence the temperature reached at the outlet of HE-01. In addition, a temperature sensor located at the outlet of HE-01 measures the temperature `TT-6_20` and sends the signal to TIC-03.

5.3 Analysed Scenarios

With the aim of simulating a typical working day in which the plant works according to its production requirements, the simulation has been conducted in the following way. The simulation time is set to 8 h and four scenarios have been created in a single simulation. The scenarios are based on the amount of flue gases produced by the boilers, specifically the mass flow rates G_{B1} from Stack 1 and G_{B2} from Stack 2 can be in excess or insufficient to provide the requested heat by the user. The user demand is represented by the requirement of obtaining a water temperature of 25 °C at the outlet of the heat exchanger. Precisely, two cases can occur:

- The flue gas produced is in **excess** with respect to the user demand:
  In this case, the fan withdraws only the amount of flue gas strictly necessary to satisfy the demand, namely to obtain 25 °C at the heat exchanger outlet. The remaining amount is discharged into the atmosphere.

- The flue gas produced is **insufficient** with respect to the user demand:
  In this case, the fan withdraws the maximum available amount of flue gas, preventing ambient air from being drawn in from the top of the stacks.

These cases must be managed properly by the PID controllers. The selected four scenarios are the following:

1. $\mathbf{G_{B1}}$ and $\mathbf{G_{B2}}$ are in **excess**.
2. $\mathbf{G_{B1}}$ is in **excess** and $\mathbf{G_{B2}}$ is **insufficient**.
3. $\mathbf{G_{B2}}$ is in **excess** and $\mathbf{G_{B1}}$ is **insufficient**.
4. $\mathbf{G_{B1}}$ and $\mathbf{G_{B2}}$ are **insufficient**.

Two functions of flue gas flow rates are modelled:

1. **Piecewise linear function**: it is the easiest function to implement without stressing both the simulation calculations and the PID actions. However, it does not represent accurately the flue gas production. In Figure 5.10 the flue gas mass flow rates are shown.

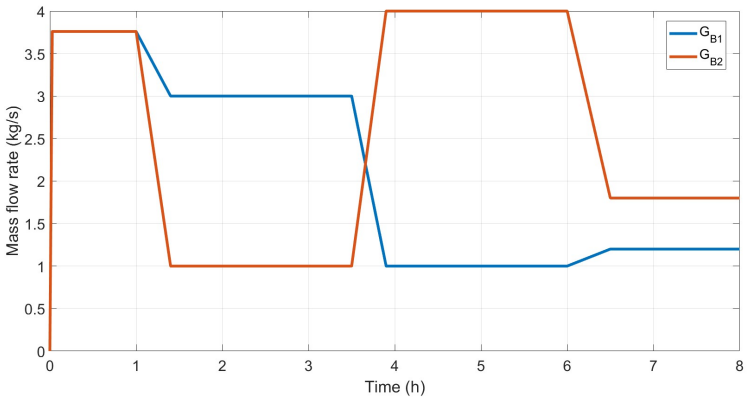


Figure 5.10: Flue gas mass flow rates represented by piecewise linear functions

2. **Fluctuating function**: it is created by adding more sinusoidal contributions to the piecewise linear function. Its purpose is to stress the PID actions in order to verify their performance and stability; additionally, it represents more accurately the flue gas production that is never exactly constant as modelled by the piecewise linear function. However, the computational cost is higher. Figure 5.11 depicts the flue gas mass flow rates with fluctuating functions.

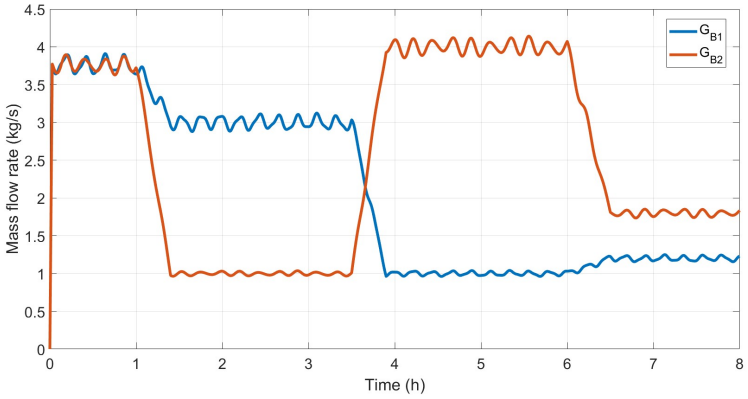


Figure 5.11: Flue gas mass flow rates represented by fluctuating functions

As can be seen, the four scenarios correspond to four distinct time intervals, delineated by the step changes in the mass flow rate values. The selection of the scenarios allows for a more comprehensive analysis of the plant's behaviour and tests the response of the four PID controllers in different conditions, as it will be discussed in Section 6.

In addition, two alternative cases are analysed. Specifically, they investigate

the influence of the lower limit of the fan capacity range in the YIC-01 controller, denoted as $n_{cap,min}$. This parameter plays a crucial role in determining the minimum fan speed and, consequently, the base electrical power absorption; therefore, its impact is important to be studied. While the upper limit is maintained constant at the nominal speed (n_{nom}), the lower limit has been varied as follows:

1. An excessively high minimum fan speed limit ($n_{\text{cap,min}} = 1900\,\text{rpm}$).
2. An optimally calibrated minimum fan speed limit ($n_{\text{cap,min}} = 1400\,\text{rpm}$).

Furthermore, two fault scenarios are investigated to analyze the system's response to the failure of crucial components. These faults are simulated during the fourth scenario (where both flue gas mass flow rates are insufficient), as it represents the most critical operating condition. Specifically, the analysis focuses on the mechanical seizure of the two dampers. When a damper gets stuck at a specific aperture area, the corresponding PID controller loses its control authority. The two cases examined are:

- **Failure of Damper 1:** The first damper (SR-01) locks in a fixed position, while all other components work correctly.
- **Failure of Damper 2:** The second damper (SR-02) locks in a fixed position, while all other components work correctly.

Evaluating these scenarios is essential to assess the system's response and to predict the consequences of component malfunctions.

Chapter 6

Simulation Results

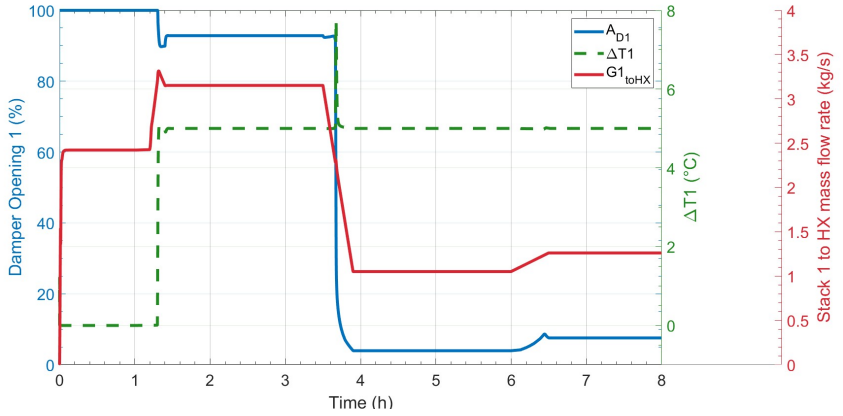
6.1 System Response to Piecewise Linear Flue Gas Profiles

The following results are obtained by maintaining the minimum fan capacity (lower limit of the YIC-01 range) at 1900 rpm and applying a piecewise linear profile of the flue gas mass flow rate emitted by the boilers. The results are shown in Figure 6.1. In particular:

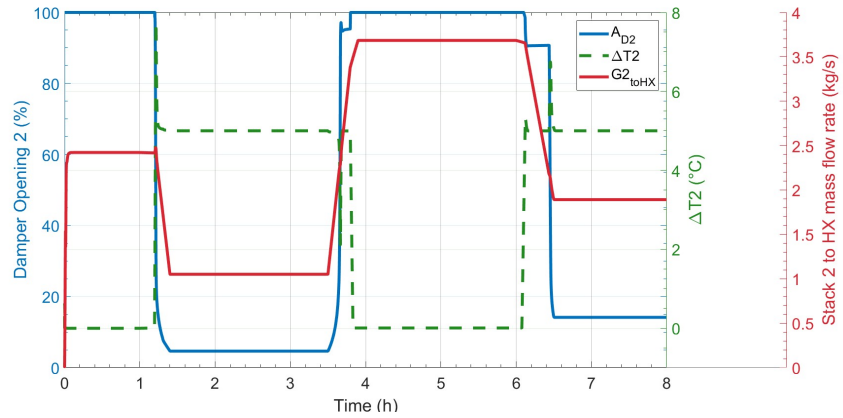
- Figure 6.1a and Figure 6.1b show the results related to the actions of TIC-01 and TIC-02. Precisely, the graphs show the variation of the damper opening percentage, the effective flue gas mass flow rate passing through the respective damper and the temperature difference which is the control variable. As can be seen, the variables strictly follow the variation of the mass flow rate produced by the boilers: when there is a deficit in flue gas mass flow rate from a boiler, the respective damper partially closes and less mass flow rate passes (and vice versa); the set-point on the temperature difference (5 °C) is always respected, meaning that the minimum temperature of the flue gas entering HE-01 is 120 °C (since the flue gas temperature at the outlet of the boilers is always constant at 125 °C).

- Figure 6.1c represents the results related to the actions of YIC-01 and TIC-03. In particular, the graph shows the variation of the fan capacity (imposed by YIC-01), the actual fan speed (calculated by TIC-03) and the water temperature at the outlet of HE-01, which is the control variable of TIC-03. As can be seen, the actual fan speed and the maximum fan capacity always coincides, except for the first scenario. This is coherent with the expected system behaviour: when the outlet water temperature is below the 25 °C setpoint, TIC-03 operates at saturation, meaning the actual fan speed is driven entirely by the maximum capacity limit set by YIC-01. It is important

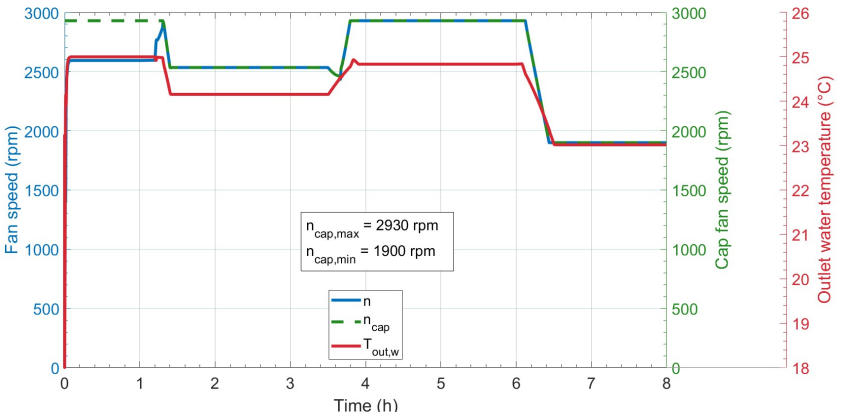
to highlight the behaviour during the fourth scenario: while both dampers are almost completely closed, the fan speed remains high (coinciding exactly with the 1900 rpm lower limit of the YIC-01 working range). This indicates that the plant is operating inefficiently. Consequently, this suggests that the lower limit of the fan capacity in YIC-01 should be decreased to prevent unnecessary electrical power consumption.



(a) TIC-01 response



(b) TIC-02 response



(c) YIC-01 and TIC-03 response

Figure 6.1: System response with piecewise linear flue gas profiles and $n_{cap,min}$=1900 rpm

6.1.1 Impact of YIC-01 Lower Limit on Electrical Power

As discussed in Section 6.1, setting the lower limit of the fan capacity to 1900 rpm leads to an improper operating condition characterized by high fan speed coupled with restricted damper openings, causing a waste of electrical power. To address this issue and optimize the YIC-01 operating range, the lower limit was decreased to 1400 rpm. The system's response to this adjustment is presented in Figure 6.3. As can be clearly seen, outside of the fourth scenario, the system behaves identically to the configuration with the 1900 rpm limit. However, during the fourth scenario, the reduced lower limit allows the actual fan speed to decrease to 1711 rpm while still maintaining the water temperature at approximately 23 °C. Simultaneously, the opening of damper 2 shifts significantly from a nearly closed state (15 %) to an almost fully open state (92.85 %). This wider damper opening, coupled with a reduced fan speed, directly leads to lower mechanical power and, consequently, reduced electrical power consumption. Figure 6.2 depicts the mechanical power consumed by the fan in both configurations. As can be seen, the mechanical power curves are always overlapped, except during the fourth scenario. In order to

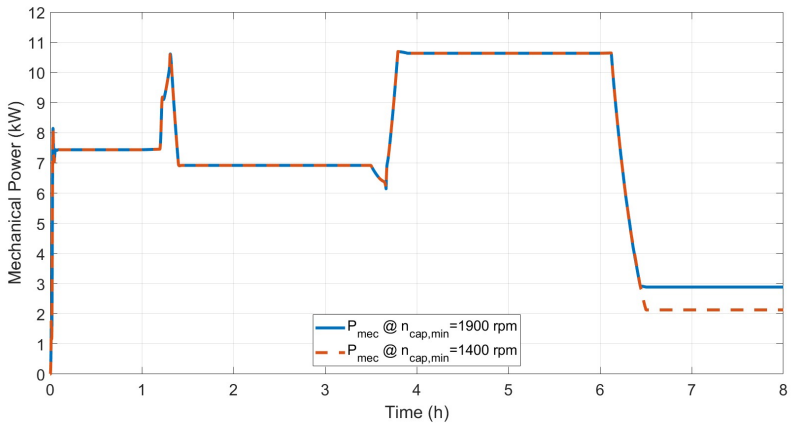


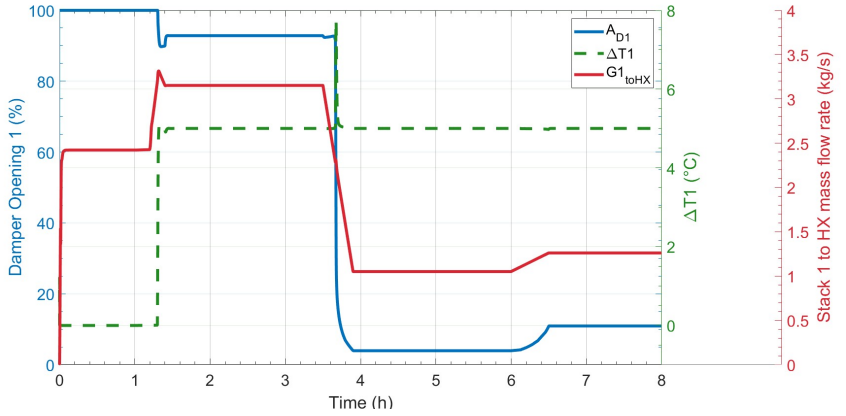
Figure 6.2: Comparison of the mechanical power absorbed in two cases with different lower limit of YIC-01 operating range

evaluate the electrical power consumed, the mechanical efficiency of the motor has to be considered. It can be extracted from the motor efficiency map (see Section 4.1.2) knowing the operating points at partial load. The electrical power evaluated in the two cases (during the fourth scenario) is:

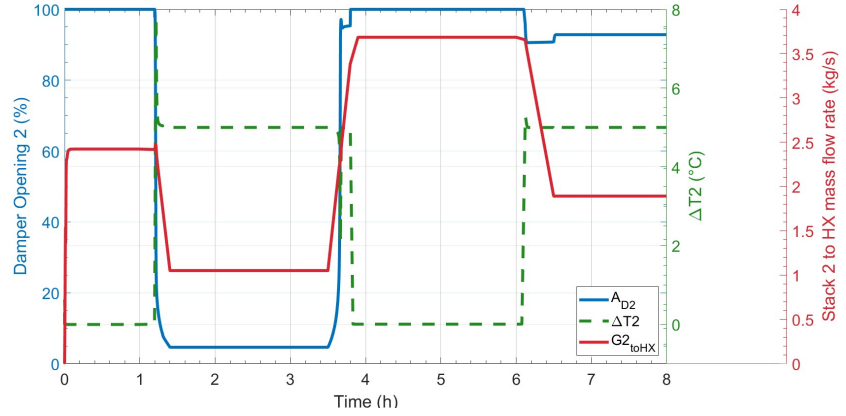
$$P_{\text{el}} = \frac{P_{\text{m}}}{\eta_{\text{m}}} = \frac{2.13}{0.89} = 2.39 \text{ kW} \quad \text{with } n_{\text{cap,min}} = 1400 \text{ rpm} \tag{6.1}$$

$$P_{\text{el}} = \frac{P_{\text{m}}}{\eta_{\text{m}}} = \frac{2.89}{0.91} = 3.18 \text{ kW} \quad \text{with } n_{\text{cap,min}} = 1900 \text{ rpm} \tag{6.2}$$

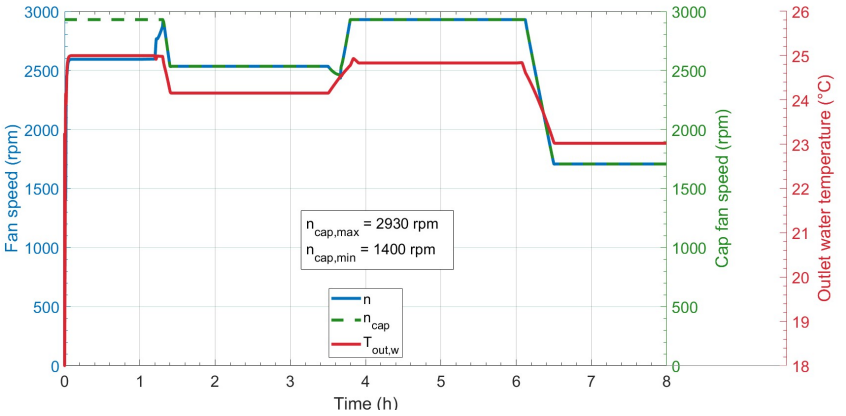
As can be seen, by adjusting the lower limit of YIC-01 operating range, it is possible to reduce the electrical power of about 24.8 %.



(a) TIC-01 response



(b) TIC-02 response

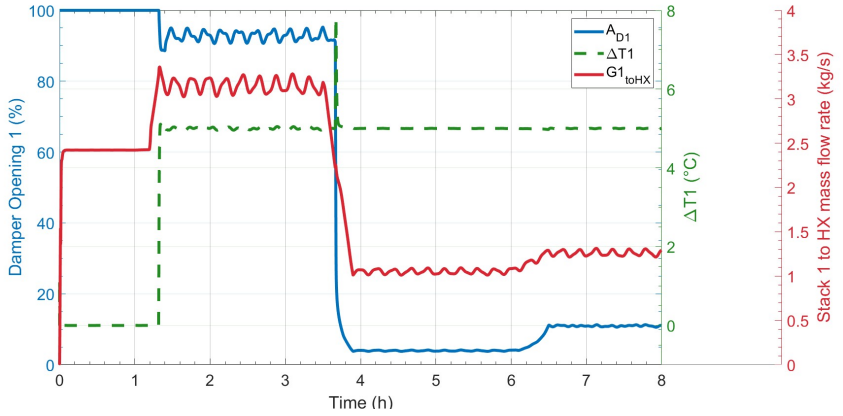


(c) YIC-01 and TIC-03 response

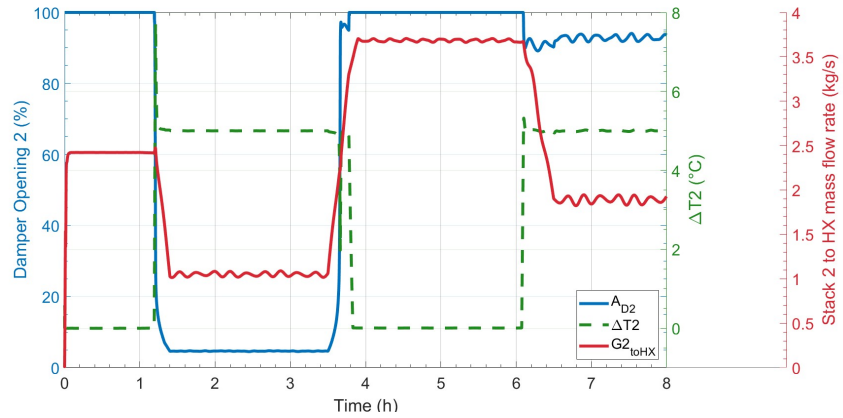
Figure 6.3: System response with piecewise linear flue gas profiles and $n_{cap,min}$=1400 rpm

6.2 System Response to Fluctuating Flue Gas Profiles

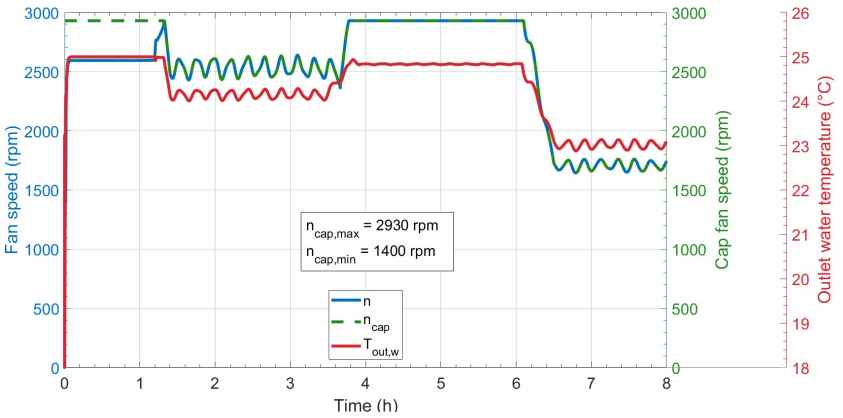
The following results are based on fluctuating profiles for the flue gas mass flow rates emitted by both boilers, maintaining $n_{\text{cap,min}} = 1400$ rpm. This case study represents a stress test for the control logic. As can be seen from the results shown in Figure 6.4, the system responds effectively and all the variables follow the fluctuations driven by the flue gas mass flow rates. This means that the PID controllers, despite the disturbances, respond effectively, proving that the system has excellent dynamic stability and well-tuned frequency response.



(a) TIC-01 response



(b) TIC-02 response



(c) YIC-01 and TIC-03 response

Figure 6.4: System response with fluctuating flue gas profiles and $n_{cap,min}$=1400 rpm

6.3 Failure Analysis

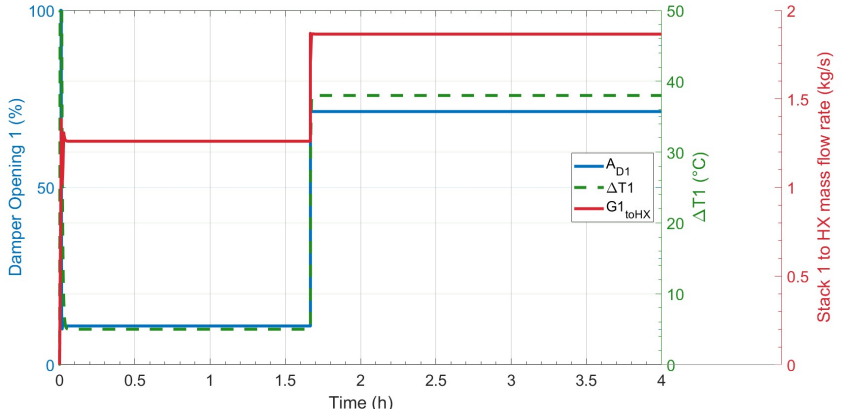
In this section, two damper failures are analysed. The simulation for both cases is performed with piecewise linear flue gas profiles during the fourth scenario (they are not sufficient to heat the water to the desired temperature). The lower limit of YIC-01 is fixed at 1400 rpm and the simulation time is set to 4 h. For both the cases, the failure occurs after 1.7 h.

6.3.1 Failure of Damper 1

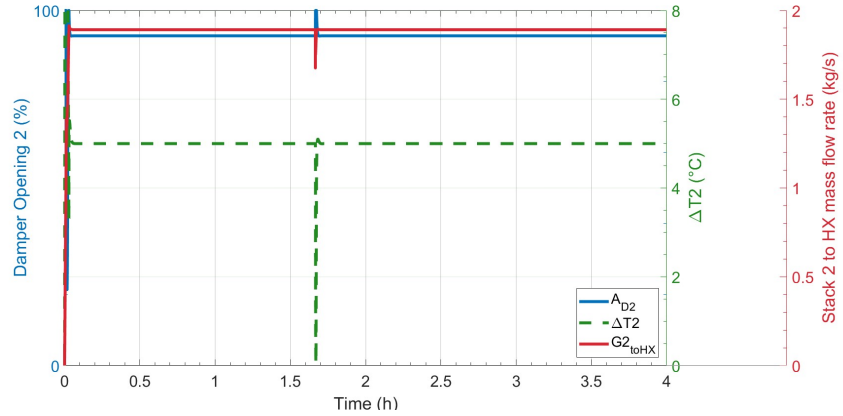
After the failure of the damper 1 mechanism, the opening increases from 10.9 % to 71.4 %. The results are shown in Figure 6.5. In this condition, due to the sudden opening of the damper 1, TIC-01 is no longer effective, and a higher flue gas mass flow rate is drawn but at a lower temperature (the temperature difference is about 38 °C), meaning that a certain amount of ambient air is drawn in. The operation of the damper 2 is not affected by the failure of the damper 1. The main consequence is a reduction in heat transfer within the heat exchanger: the lower temperature of the flue gases (104 °C) leads to a lower water temperature (22.8 °C). Regarding the fan, the speed increases to handle more mass flow rate.

6.3.2 Failure of Damper 2

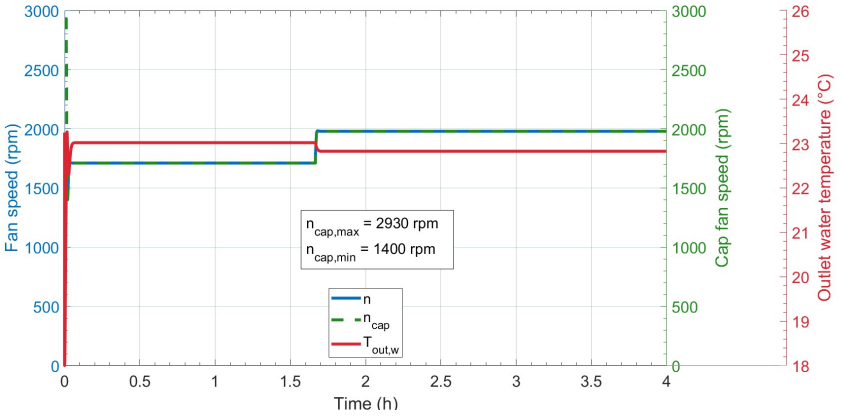
In this analysis, a failure occurs in the damper 2, where the opening decreases from 92.85 % to 60 %. As can be seen from the results depicted in Figure 6.6, a lower mass flow rate is drawn from the stack 2, but at a higher temperature (exactly 125 °C). Due to the partial closure of the damper 2, a higher pressure loss is introduced leading to a slight opening of the damper 1. The main consequence is a decrease in heat transfer within the heat exchanger, despite the high temperature of the flue gas, due to a significant lower mass flow rate. Consequently, as the damper 2 opening is decreased, YIC-01 decreases the lower limit to 1400 rpm.



(a) TIC-01 response

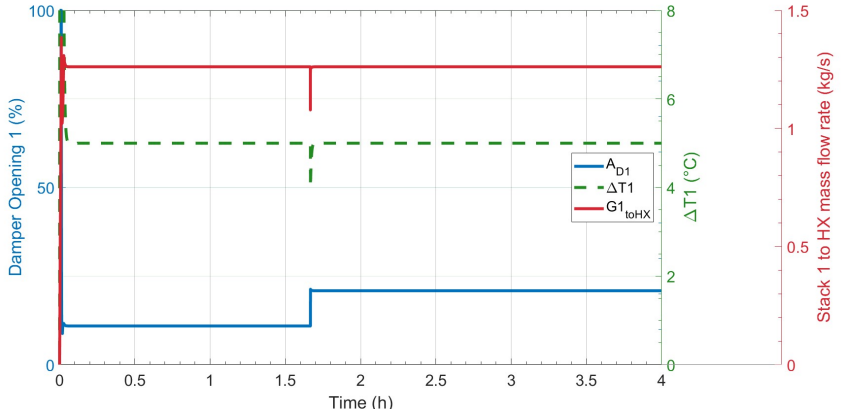


(b) TIC-02 response

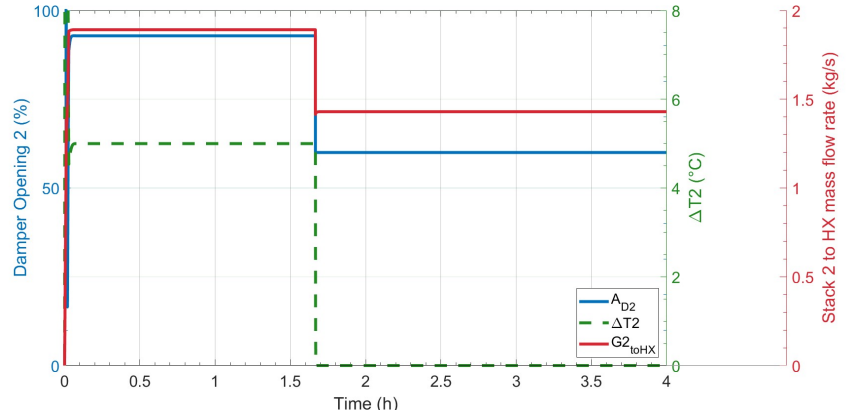


(c) YIC-01 and TIC-03 response

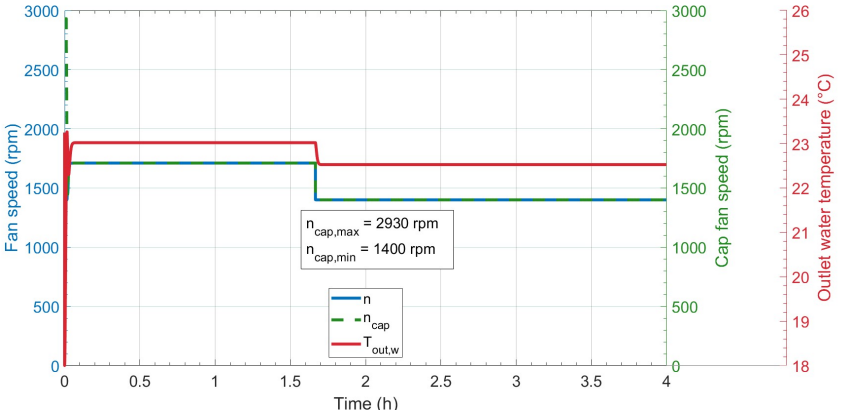
Figure 6.5: System response during a failure of damper 1.



(a) TIC-01 response



(b) TIC-02 response



(c) YIC-01 and TIC-03 response

Figure 6.6: System response during a failure of damper 2.

6.4 Energetic, Economic and Environmental Evaluation

This analysis evaluates the configuration with a minimum capacity fan speed of $n_{cap,min} = 1400\,\text{rpm}$, which yields the highest energy savings under piecewise linear flue gas profiles, using the equations introduced in Section 3.2. The results demonstrate that the designed WHR system achieves a significant reduction in primary energy consumption, as detailed in Table 6.1. Consequently, this reduction translates into significant economic and environmental advantages. Notably, during Scenario 1, where flue gases are in excess and the system reaches its maximum heat recovery amount, the economic benefit B_{eco} is nearly 33 €/h. On average, the plant yields an economic benefit of 29.26 €/h and avoids 225 kgCO_2/h of emissions. The corresponding financial savings and avoided CO_2 emissions for all simulated scenarios are illustrated in Figure 6.7.

Table 6.1: Hourly primary energy savings

Scenario	E_{saved} (kWh_p/h)
1	1066.67
2	936.97
3	1032.69
4	773.46

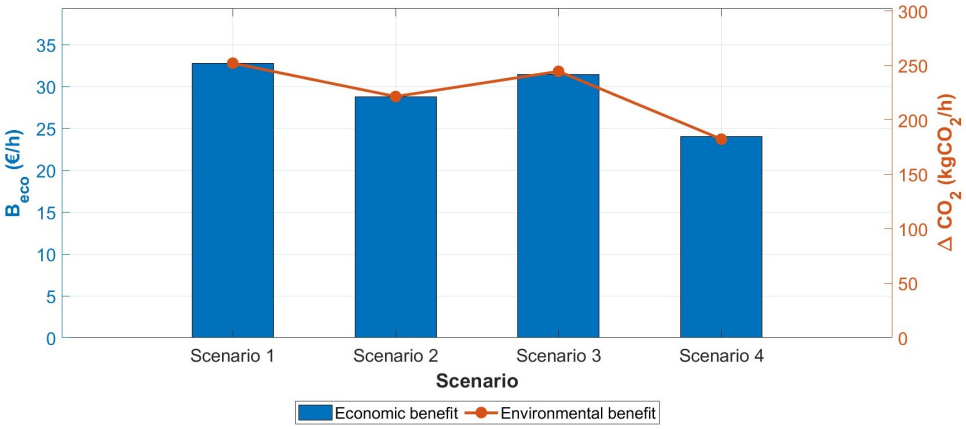


Figure 6.7: Economic and environmental benefits

Assuming a seasonal operation of 4200 h, this WHR system yields economic savings exceeding € 122,900 and avoids 945 tCO_2 of emissions per season. This

projection assumes an equal time distribution among the four operational scenarios.

6.5 Summary of Main Findings

The simulations carried out in the MATLAB-Simulink environment have shown several key insights. First of all, the control strategy designed for this WHR system from steam boiler flue gas functions effectively even in the presence of disturbances, such as fluctuations in the flue gas mass flow rate and variations in the total volume emitted by the boilers. Given the complexity of this control strategy, which relies on four mutually interacting PID controllers, having a dynamic model to simulate the system's behavior under various conditions proves highly advantageous for evaluating its performance. The analyzed scenarios cover the full operational range of the plant (flue gas in excess or not sufficient to satisfy the thermal demand); the positive outcomes obtained highlight the importance of a properly tuned PID control architecture in maintaining system stability and maximizing the overall efficiency. Specifically, the main objective of this strategy was to maximize thermal energy recovery while minimizing the electrical consumption of the fan. Through these simulations, the importance of correctly setting the lower limit of the YIC-01 controller to achieve significant energy savings was clearly demonstrated. Furthermore, the failure analysis verified that the system responds predictably and safely during fault conditions, ensuring that no unforeseen critical issues arise. To conclude, the analysed WHR systems, supported by the implemented PID control strategies, prove to be highly beneficial from both an economic and environmental perspective. Particularly, on average the plant yields an economic benefit of 29.26 €/h and avoids 225 kgCO_2/h of emissions.

Part II

Second Case Study: WHR system from Hot Rolling Mill Reheating Furnace

The second case study regards the analysis of two particular control strategies for a WHR system for a steel manufacturing facility. It specializes in the production of wire rod, a common steel product, using billets as raw material. The site operates a high-speed wire rod rolling mill, and the entire WHR system is designed to capture energy from the flue gases of that mill's reheating furnace. Specifically, the heat recovery consists of a flue gas-water heat exchanger where the flue gas transfers heat to a water circuit serving both on-site thermal users and the local district heating network. Both the control strategies rely on three PID controllers whose aim is to maximize the thermal extraction from the flue gas while maintaining the pressure in the furnace under control.

Chapter 7

WHR System Description

The system is designed to exploit the hot flue gases generated by a wire rod mill reheating furnace to heat a water circuit utilized for both on-site thermal users and the district heating network. In the existing path, the gases first pass through a combustion air pre-heater and are moved by the furnace's original extraction fans (they are two, one of which is for backup). At the outlet of the air pre-heater, a modulating damper actuated by a PID controller is used to regulate the furnace pressure. The new branch for the heat recovery is installed on the diagonal duct that connects the existing fans to the chimney stack, as can be seen in the P&ID depicted in Figure 7.1. Therefore, the new recovery branch creates a new path for the flue gases parallel to the existing stack. In the heat recovery branch, the hot flue gases pass through a shut-off damper and enter the flue gas-hot water heat exchanger, where they transfer heat to the water circuit. Then, the cooled gases are pulled by the new centrifugal fan and conveyed back into the existing stack. Two control strategies will be analysed: the first employs a variable fan speed control (described in Section 7.2.1), while the second uses a modulating damper control (described in Section 7.2.2). In both cases, a PID controller is applied to the furnace damper with the aim of maintaining a constant furnace pressure.

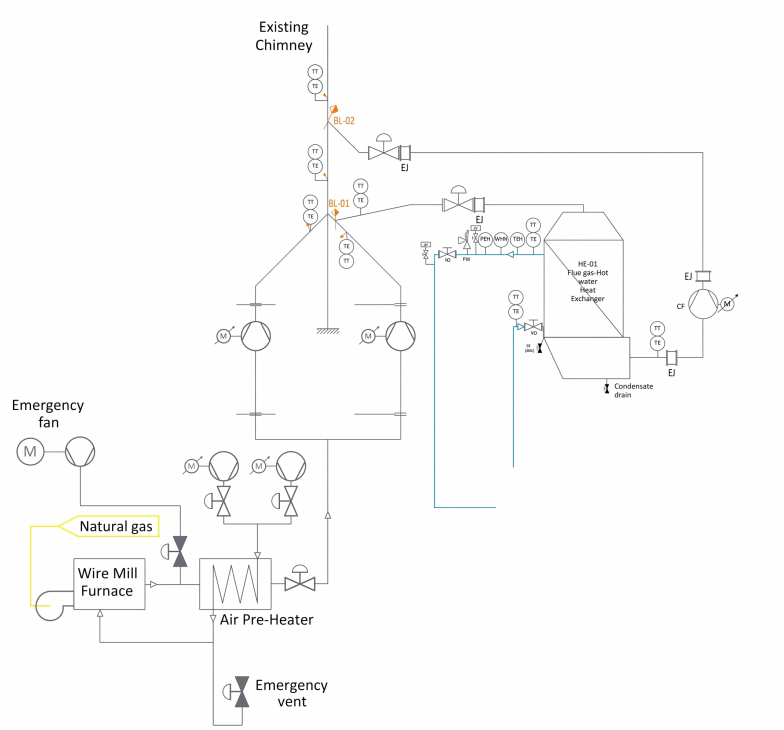


Figure 7.1: P&ID of the WHR system from hot rolling mill reheating furnace [32]

7.1 Plant Design Specifications

7.1.1 Main Exhaust Fan Specifications

The main exhaust centrifugal fan extracts the hot flue gases and conveys them towards the stack. The nominal operating conditions are the following:

- Nominal inlet temperature: $T_{in,nom} = 370\,°\mathrm{C}$
- Nominal inlet density: $\rho_{in,nom} = 0.52\,\mathrm{kg\,m^{-3}}$
- Nominal volume flow rate: $V_{nom} = 165348\,\mathrm{m^3\,h^{-1}}$
- Nominal static pressure gain: $\Delta p_{nom} = 30\,\mathrm{mmH_2O}$
- Nominal fan speed: $n_{nom} = 460\,\mathrm{rpm}$
- Nominal mechanical power: $P_{nom} = 28.3\,\mathrm{kW}$
- Nominal total efficiency: $\eta_{nom} = 56.2\,\%$

Figure 7.2 represents the fan characteristic curve and the system curve, whose intersection defines the operating point, alongside the efficiency and absorbed power curves.

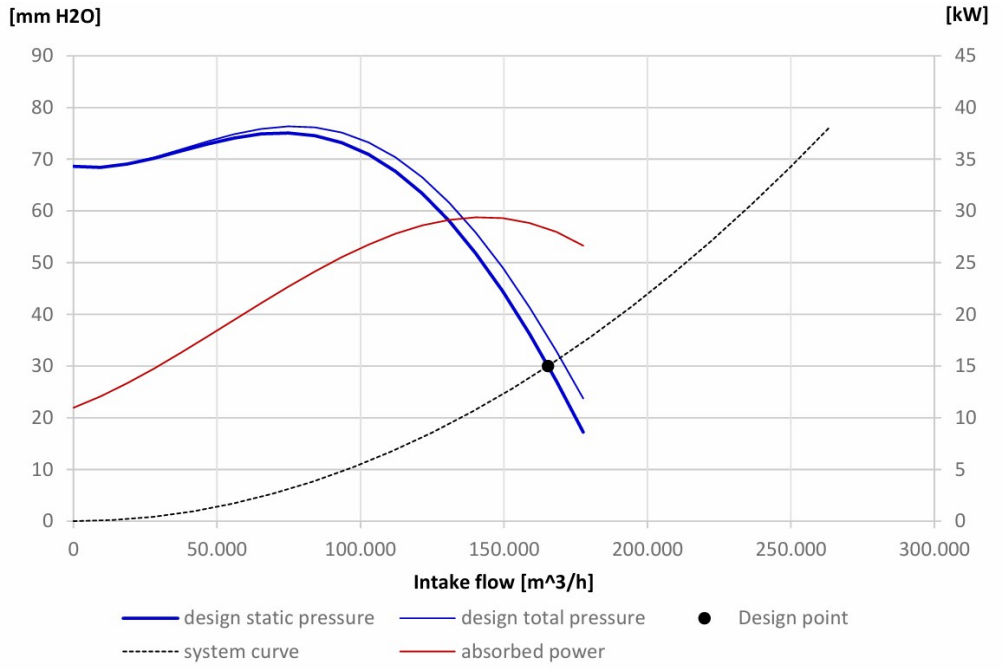


Figure 7.2: Main fan characteristic curve [33]

7.1.2 Air Pre-Heater Specifications

The air pre-heater is located downstream of the furnace and its purpose is to pre-heat the combustion air, supplied by a fan, by cooling down the hot flue gases. According to the manufacturer, the main design specifications are summarized in Table 7.1.

Table 7.1: Nominal operating parameters of the air pre-heater [34]

Parameter	**Air**	**Flue Gas**
Volume flow rate (Nm^3/h)	49700	55600
Inlet temperature (°C)	20	720
Outlet temperature (°C)	450	378
Pressure drop (Pa)	2500	196

7.1.3 Heat Exchanger Characteristics

The primary purpose of the heat exchanger located in the recovery branch is to recover thermal energy from the hot exhaust flue gases, transfering heat to a closed pressurized water circuit. Under nominal design conditions, it is designed to transfer 3526 kW of heat. It is a finned-tube (coil bundle) heat exchanger operating in a cross counter-flow pattern. The main specifications are reported in Table 7.2.

Table 7.2: Nominal operating parameters of the flue gas-water heat exchanger [35]

Parameter	**Water**	**Flue Gas**
Volume flow rate (kg/h)	100000	86128
Inlet temperature (°C)	70	315
Outlet temperature (°C)	100.2	86.7
Pressure drop (mmH_2O)	4180.8	45.3

7.1.4 Heat Recovery Fan Specifications

In the recovery branch, downstream of the heat exchanger, a centrifugal fan is located. The design conditions are the following:

- Nominal inlet temperature: $T_{in,nom} = 120\,°C$
- Nominal inlet density: $\rho_{in,nom} = 0.822\,kg\,m^{-3}$
- Nominal volume flow rate: $V_{nom} = 67900\,m^3\,h^{-1}$
- Nominal static pressure gain: $\Delta p_{nom} = 160\,mmH_2O$
- Nominal fan speed: $n_{nom} = 1055\,rpm$
- Nominal mechanical power: $P_{nom} = 40.5\,kW$
- Nominal total efficiency: $\eta_{nom} = 81.8\,\%$

Figure 7.3 shows the characteristic curve of the fan and the system curve, whose intersection defines the operating point. Additionally, the figure displays the efficiency and the absorbed power curves. The fan is driven by a robust, high-efficiency electric motor with an installed power of 45 kW and a 6-pole configuration. It operates on a 400 V, three-phase power supply at 50 Hz and achieves a premium IE4 efficiency rating. Since specific information regarding the installed motor was

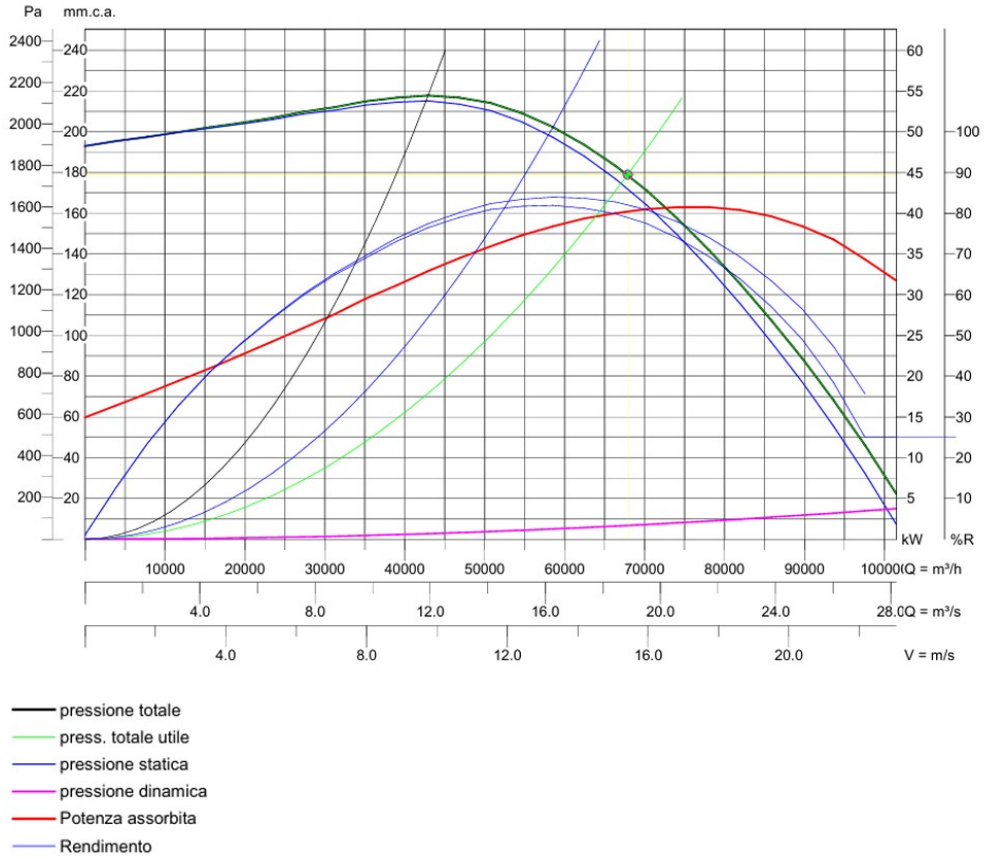


Figure 7.3: Heat recovery fan characteristic curve [36]

unavailable, the Innomotics platform was used to model a comparable unit and know the efficiency curve [19]. The evaluation of the motor efficiency at various operating points was based on the data sheet of a three-phase squirrel-cage motor (model Innomotics SD - 250 M - IM B3 - 6p). The selected motor features a nominal power of 45.0 kW, a nominal speed of 1055 rpm, and a nominal torque of 435.0 N m. Under these nominal conditions, it achieves a full-load efficiency (η) of 94.8 %. Furthermore, the motor belongs to the IE4 efficiency class and features an IP55 degree of protection. Figure 7.4 shows the efficiency map with respect to the relative torque and relative speed.

7.1.5 Flue Gas Composition and Operating Conditions

The reheating furnace is fueled by natural gas and ambient air. Measurements from an oxygen probe indicate that the oxygen content in the dry flue gas is 5.2 %. Following the steps used for the first case study in Section 4.1.3, and assuming the

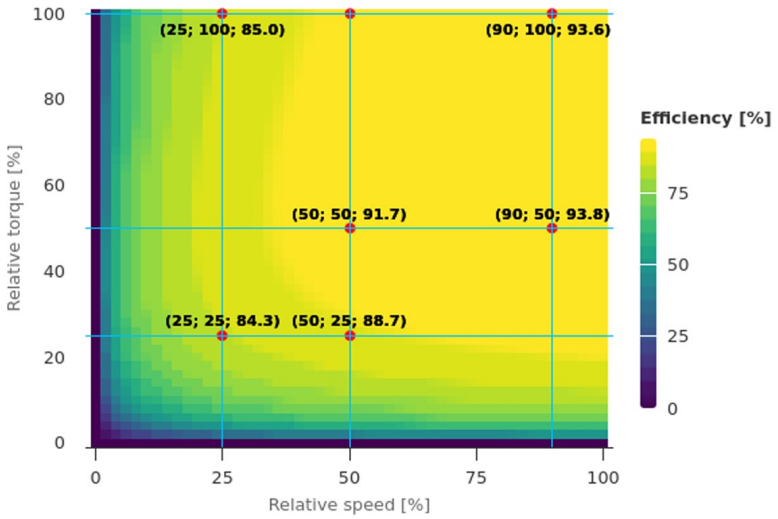


Figure 7.4: Motor efficiency map [37]

same volumetric composition of the dry combustion air, an inlet temperature of 20 °C, and a relative humidity of 60 %, the results yield an air excess of **e=29.56 %**, an absolute humidity of $\boldsymbol{x_f = 11.57\,\%}$ and a flue gas composition as reported in Table 7.3. The calculated composition was used to determine the thermophysical properties in the simulation, as will be discussed in Section 8.2.1.

Table 7.3: Flue gas composition

Property	**N_2**	**O_2**	**Ar**	**CO_2**	**H_2O**
Volumetric fraction y_i (%)	71.31	4.37	0.85	7.42	16.05
Mass fraction M_i (%)	71.67	5.01	1.22	11.72	10.37

7.1.6 Water Circuit Operating Conditions

The closed-loop pressurized water circuit operates at a mechanical design pressure of 6 bar. The water is heated in the heat exchanger, typically from 70 °C to 100 °C, and it is used to supply both the site's internal users and the local district heating network.

7.2 Control Strategy

For this application, two control strategies will be analysed: the first focuses on controlling the fan speed while using a shut-off damper (which has only two possible states: fully open or fully closed), while the other focuses on controlling the modulating damper (which replaces the shut-off damper) while keeping the fan speed constant. For both the control strategies, a PID-control is applied to the furnace damper located downstream of the furnace. Its purpose is to maintain a constant furnace pressure of 0 Pa(g) by regulating the damper aperture. Having this control is important: it prevents the outward leakage of hot, potentially hazardous exhaust gases into the surroundings, while also avoiding the infiltration of cold ambient air, which would drastically reduce the thermal efficiency of the system. Furthermore, continuous active control is necessary because the furnace pressure is highly sensitive and constantly influenced by any upstream or downstream disturbances within the plant. Additionally, this control must respond as quickly as possible to avoid any potentially dangerous peaks or drops in furnace pressure.

7.2.1 Variable Fan Speed Control

This control strategy employs two PID controllers applied to the heat recovery fan and a shut-off damper located at the inlet of the recovery branch. In particular, it consists of:

- **TIC-01**: Controls the temperature difference between the flue gas before and immediately after entering the recovery branch by modulating the extraction capacity of the recovery fan. Its purpose is to minimize the electrical power consumption of the recovery fan and prevent the recirculation of already cooled flue gases from the stack back into the recovery branch.
- **TIC-02**: Controls the water temperature at the outlet of the flue gas-water heat exchanger by modulating the actual fan speed relative to its extraction capacity. Its objective is to maintain the water temperature within the target operating range, adjusting to the thermal demand of the network.

7.2.2 Modulating Damper Control

This control strategy employs a modulating damper controlled by two PID controllers located at the inlet of the recovery branch, instead of a shut-off damper, while maintaining a constant fan speed. In particular, it consists of:

- **TIC-01**: Controls the temperature difference between the flue gas before and immediately after entering the recovery branch by modulating the maximum

opening value of the modulating damper. Its objective is to prevent the recirculation of already cooled flue gases from the stack back into the recovery branch.

- **TIC-02**: Controls the water temperature at the outlet of the flue gas-water heat exchanger by continuously adjusting the actual position of the modulating damper. Its objective is to maintain the water temperature within the target operating range.

Chapter 8

Dynamic Modelling in Simulink

8.1 Simulink Model

The system was modelled in MATLAB-Simulink using the following Simscape domains: the Gas domain (represented in violet) for both the flue gas and air circuits, the Thermal Liquid domain (in yellow) for the water circuit, and the Mechanical domain (in green) to model the mechanical components of the fans. The complete Simulink diagram in the configuration with variable fan speed and shut-off damper is depicted in Figure 8.1. To reduce computational complexity, the combustion process was not explicitly modelled. Consequently, the air and flue gas circuits operate as physically separated systems. However, the heat transfer dynamics of the real plant are fully preserved: the combustion air, drawn from an ambient reservoir and discharged into another, is heated within the air pre-heater by cooling the flue gases.

The main architectural difference compared to the real plant is the absence of fluid mixing inside the furnace. Instead, the flue gases are directly extracted from a reservoir initialized with post-combustion thermodynamic properties. A fan, positioned immediately after this reservoir, simulates the function of the real-world combustion air fan, driving the flue gas through the furnace (modelled as a constant volume chamber) and subsequently into the pre-heater. To ensure thermodynamic consistency across the heat exchanger, the air mass flow rate is proportionally linked to the flue gas mass flow rate via a fixed ratio. Downstream of the air pre-heater, the furnace damper and its associated controller (PID-SR) are implemented, followed by the main exhaust fan. The circuit then splits into two parallel paths: the main stack, which acts as a bypass, and the heat recovery branch. The latter integrates a shut-off damper or modulating damper (depending on the adopted control strategy), the flue gas-water heat exchanger and the heat recovery fan. To prevent numerical instabilities during the simulation, the junction points connecting the recovery branch to the main stack are represented using constant

volume chambers. Finally, a subsystem dedicated to simulating the stack draught is positioned immediately upstream of the atmospheric reservoir. In addition to the self-explanatory components, there are some blocks called with letter M followed by a number and they represent measuring subsystems in which variables are measured and controlled.

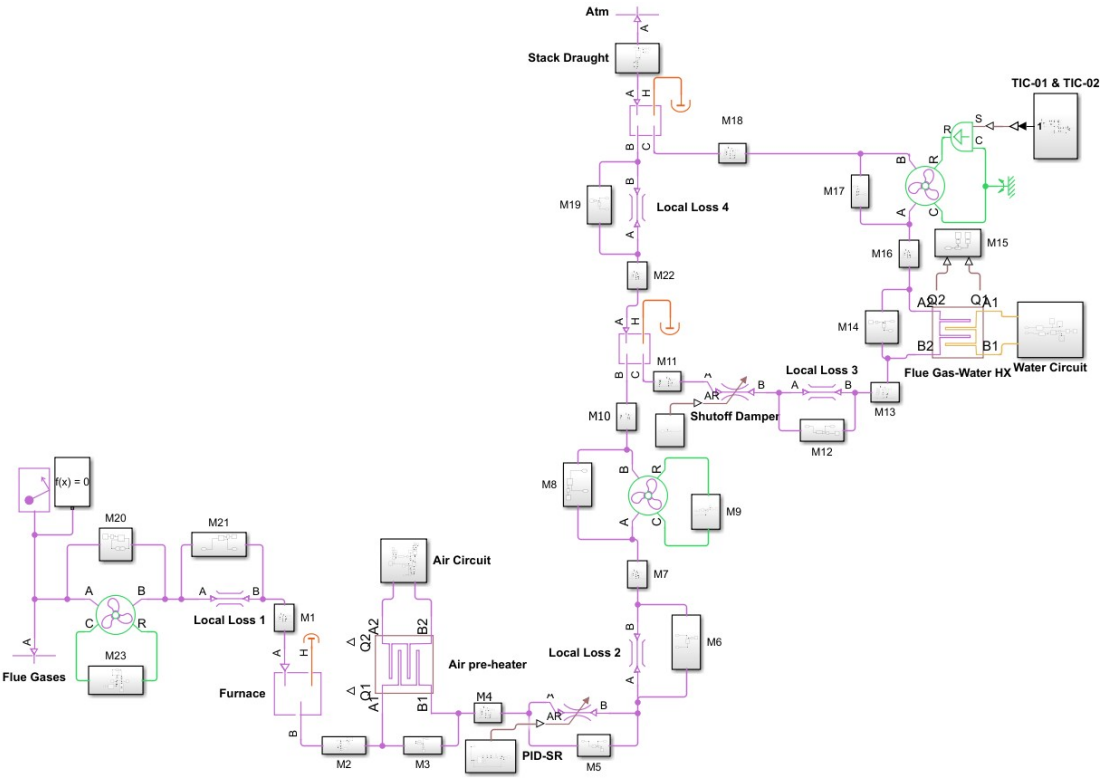


Figure 8.1: Simulink model of WHR system from hot rolling mill reheating furnace

8.2 Detailed Subsystem Modelling

8.2.1 Flue Gases Properties Configuration

The flue gases circuit is implemented in Simscape using the Gas Domain. In particular, the Gas Properties block, which defines the gas properties that act as global parameters for all the blocks connected to a circuit, has been configured in Semiperfect mode to provide a trade-off between simulation speed and accuracy. For semiperfect gas, caloric and transport properties are modeled as functions of temperature. Therefore, the thermophysical properties were first calculated for each

individual substance (CO_2,H_2O,O_2,Ar,N_2) and subsequently combined to evaluate the overall mixture properties. The implemented thermophysical properties are detailed as follows:

1. **Specific Heat**: The Aly and Lee Equation [23] was used to evaluate the specific heat of each single substance. The specific heat of the mixture was then computed using the mass fractions (y_i) of the components.

$$c_{p,i}(T) = c_1 + c_2 \left[\frac{\frac{c_3}{T}}{\sinh\left(\frac{c_3}{T}\right)}\right]^2 + c_4 \left[\frac{\frac{c_5}{T}}{\cosh\left(\frac{c_5}{T}\right)}\right]^2 \tag{8.1}$$

$$c_{p,mix}(T) = \sum_i y_i \cdot c_{p,i}(T) \tag{8.2}$$

2. **Enthalpy**: By integrating the specific heat between a reference temperature ($T_{ref} = 273.15$ K) and the fluid temperature (T), the enthalpy of each substance is obtained. The mixture enthalpy is then evaluated through a mass-weighted sum.

$$\begin{aligned} h_i(T) = c_1(T - T_{ref}) + c_2 c_3 \left[\coth\left(\frac{c_3}{T}\right) - \coth\left(\frac{c_3}{T_{ref}}\right)\right] \\ - c_4 c_5 \left[\tanh\left(\frac{c_5}{T}\right) - \tanh\left(\frac{c_5}{T_{ref}}\right)\right] \end{aligned} \tag{8.3}$$

$$h_{mix}(T) = \sum_i y_i \cdot h_i(T) \tag{8.4}$$

3. **Dynamic Viscosity**: To calculate the dynamic viscosity for each substance, the DIPPR 102 equation was used [23], while the Herning and Zipperer equation [38] was applied for the dynamic viscosity of the flue gas mixture, where x_i and M_i represent the molar fraction and the molar mass of the i-th species, respectively.

$$\mu_i(T) = \frac{c_1 \cdot T^{c_2}}{1 + \frac{c_3}{T} + \frac{c_4}{T^2}} \tag{8.5}$$

$$\mu_{mix}(T) = \frac{\sum_i x_i \cdot \mu_i(T) \cdot \sqrt{M_i}}{\sum_i x_i \cdot \sqrt{M_i}} \tag{8.6}$$

4. **Thermal Conductivity**: The thermal conductivity of each individual species was calculated using the DIPPR 102 equation [23]. For the mixture-averaged thermal conductivity, an averaging formula combining the arithmetic and harmonic means based on molar fractions (x_i) was taken from [39].

$$k_i(T) = \frac{c_1 \cdot T^{c_2}}{1 + \frac{c_3}{T} + \frac{c_4}{T^2}} \tag{8.7}$$

$$k_{mix}(T) = \frac{1}{2}\left[\sum_i (x_i \cdot k_i(T)) + \frac{1}{\sum_i \left(\frac{x_i}{k_i(T)}\right)}\right] \tag{8.8}$$

Finally, the specific gas constant of the mixture (R_{mix}) was computed by dividing the universal gas constant (R_u) by the equivalent molar mass of the mixture (M_{mix}), yielding a value of $0.2983\,\mathrm{kJ\,kg^{-1}\,K^{-1}}$.

8.2.2 Water Circuit Configuration

The water circuit is implemented using Thermal Liquid domain. However, since its default water properties are limited to a maximum temperature of 100 °C, it was necessary to extend the working temperature range to accurately simulate the system. To achieve this, the thermophysical properties of the fluid (such as density, thermal conductivity, kinematic viscosity, specific heat capacity and internal energy) were evaluated and integrated into the model using the X Steam library for MATLAB [40]. Regarding the implementation, a Flow Rate Source block draws water from a Reservoir set at 70 °C and 6 bar, and supplies it to the heat exchanger. At the outlet, the water is discharged into a second Reservoir block.

8.2.3 Equivalent Flue Gas Source

The flue gas source is represented by a Reservoir block configured at 720 °C and atmospheric pressure, followed by a fan. As described in Section 8.1, combustion is not explicitly modelled, and the fluid properties exiting the reservoir are set to post-combustion conditions. The fan extracting the flue gas from the reservoir is configured based on the main exhaust fan, appropriately scaled to account for the temperature difference, as represented in Figure 8.2. This component simulates the role of the real-world combustion air fan. Downstream, a flow resistance block is implemented to account for major and minor pressure losses.

8.2.4 Furnace

The furnace is modelled with a Constant Volume Chamber block. As described in the official MathWorks website [41], the Constant Volume Chamber block models a mass and energy storage that contains a constant volume of gas that can exchange mass and energy with the connected gas network, allowing its internal pressure and temperature to evolve over time, based on the compressibility and thermal capacity of the gas volume. The volume is set to $1000\,\mathrm{m^3}$. The furnace pressure is measured by a pressure sensor.

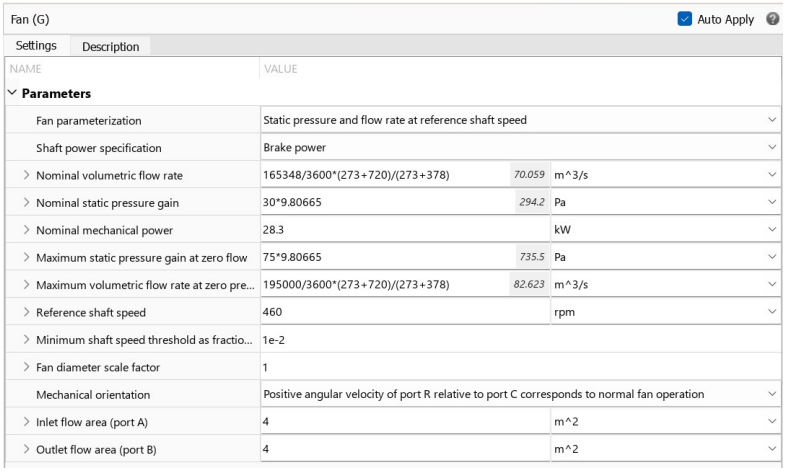


Figure 8.2: Simulink parameter dialog box for the fan configuration

8.2.5 Air Circuit

The implemented air circuit consists of a Reservoir block set to 20 °C and atmospheric pressure, from which the air is drawn by a Mass Flow Rate Source. The air mass flow rate is linked to the flue gas mass flow rate through the following relation:

$$G_a = \frac{G_{fg}}{1.05} \tag{8.9}$$

This relation ensures thermodynamic consistency and a proper coupling with the flue gas production, compensating for the absence of an explicit combustion model. Specifically, the 1.05 factor accounts for the fuel mass addition typical of natural gas combustion, reflecting an operational air-to-fuel mass ratio that includes a standard level of excess air. Finally, the air is heated in the pre-heater and subsequently discharged into another Reservoir block, as can be seen from the Figure 8.3.

8.2.6 Air Pre-Heater

The air pre-heater is modelled with a System-Level Heat Exchanger block. It is parameterized by the nominal operating condition provided in the manufacturer's data sheet, as reported in Section 7.1.2. The block sizes the heat exchanger to match the specified performance at the nominal operating condition at steady state [42]. The block configuration is shown in Figure 8.4. To obtain the mass flow rates in kg/s, the volumetric flow rates (in Nm^3/h) are multiplied by the gas density at normal conditions and divided by 3600.

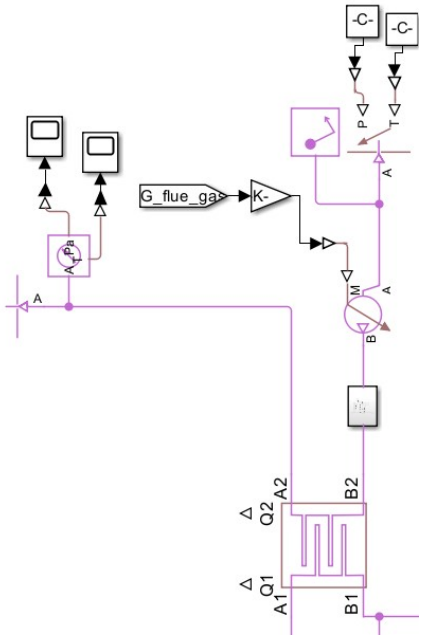


Figure 8.3: Simulink Scheme for the air circuit

Gas 1			
Nominal operating condition	Heat transfer from Gas 1 to Gas 2		
Nominal mass flow rate	55600*1.3/3600	20.078	kg/s
Nominal pressure drop	196		Pa
Nominal inlet pressure	0.101325		MPa
Nominal inlet temperature	720		degC
Heat transfer capacity specification	Outlet condition		
Nominal outlet temperature	378		degC
Gas 1 volume	25		m^3
Initialize gas 1 to nominal operating conditions			
Gas 2			
Nominal mass flow rate	49700*1.292/3600	17.837	kg/s
Nominal pressure drop	2500		Pa
Nominal inlet pressure	0.101325		MPa
Nominal inlet temperature	293.15		K
Gas 2 volume	25		m^3
Initialize gas 2 to nominal operating conditions			

Figure 8.4: Simulink parameter dialog box for the air pre-heater configuration

8.2.7 Furnace Damper Control

The furnace damper is modelled using a Local Restriction block managed by a PID controller, named PID-SR. The PID input is the error, calculated as the difference

between the furnace pressure and a setpoint of 101325 Pa. Its implementation is shown in Figure 8.5. To manage the start-up phase, a Switch block is used: the command is manual for the first 500 s, after which the PID controller takes over. To implement this strategy, the Tracking Mode of the PID controller is enabled. A Discrete PID Controller block in parallel form is used, and its output is limited between 0 and 1. To convert this normalized signal into a physical opening area, the controller's output is multiplied by a Gain block set to 3.5, which corresponds to the maximum opening area of the damper. In addition, a Rate Limiter block is used to limit the signal's rate of change, making the command more realistic. Without this block, the command signal would be excessively rapid. In the real world, there are inherent delays due to signal transmission and actuator dynamics. Since the response speed is critical in this control loop (the system is highly sensitive to pressure oscillations) the inclusion of a Rate Limiter block was essential. Moreover, to prevent the integral term from accumulating excessive error when the actuator reaches its saturation limits, the clamping method was selected as the internal anti-windup strategy. For the tuning phase, a manual trial-and-error approach was employed. The selected gains are the following: 0.004 for the proportional, 0.0015 for the integral and 0 for the derivative gain.

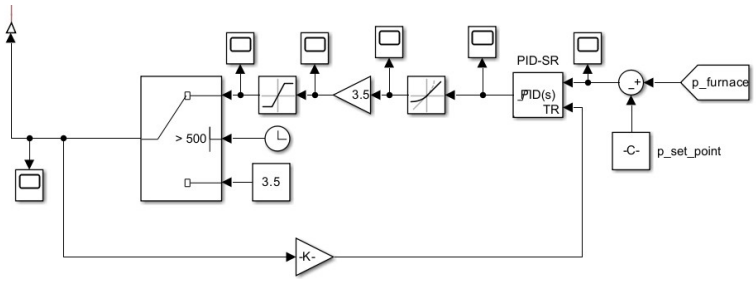


Figure 8.5: Simulink scheme for PID-SR controller

8.2.8 Main Exhaust Fan

The main exhaust fan is modelled using the Fan block configured with "Static pressure and flow rate at reference shaft speed" parametrization. The block was configured based on the nominal condition, as reported in Section 7.1.1. The scaling between the reference fan curves and the actual flow rate and pressure gain is determined from affinity laws according to the official MathWorks documentation [43]. Figure 8.6 shows the block implementation. In particular, this block constructs the analytical reference curve by applying a quadratic fit to three specific operational points: maximum static pressure gain at zero flow, nominal static pressure gain and maximum volumetric flow rate at zero pressure. The resulting pressure-flow

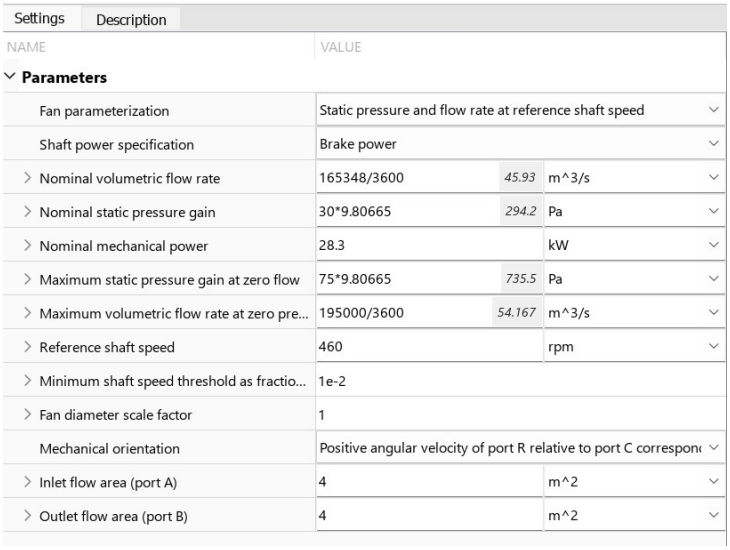


Figure 8.6: Simulink parameter dialog box for the main exhaust fan configuration

characteristic is shown in Figure 8.7. The fan speed is maintained constant at the nominal value. The same limitations and considerations regarding this block, as explained in Section 5.2.3, remain valid.

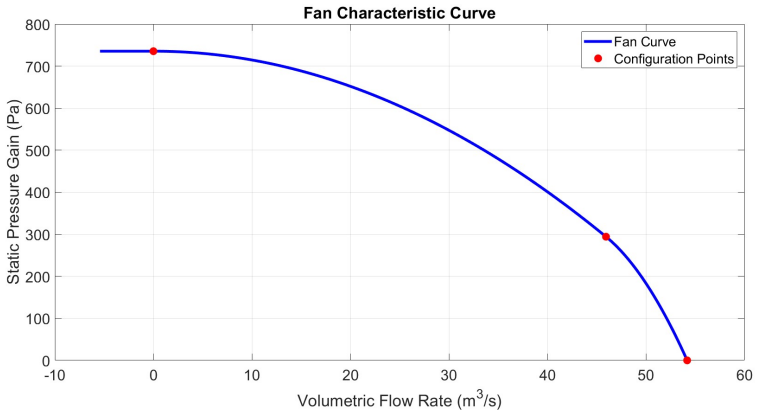


Figure 8.7: Main exhaust fan characteristic curve constructed by Simulink

8.2.9 Flue Gas-Water Heat Exchanger

To model the flue gas-water heat exchanger, the System-Level Heat Exchanger (TL-G) was used. It models a heat exchanger based on performance data, as reported in Section 7.1.3, between a thermal liquid (water) and a gas network (flue

gas). The block sizes the heat exchanger to match the specified performance at the nominal operating condition at steady state [44]. The selected flow arrangement is counter flow. Figure 8.8 shows the block configuration.

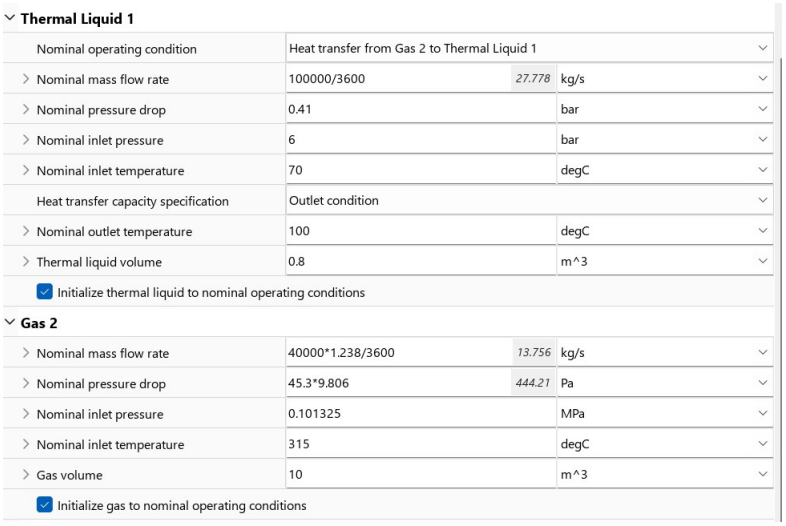


Figure 8.8: Simulink parameter dialog box for the flue gas-water heat exchanger configuration

8.2.10 Stack Draught

In this specific system, due to the high temperatures reached and the significant mass flow rates, modelling the stack draught was necessary to achieve a realistic simulation. To this end, a custom subsystem has been developed, as shown in Figure 8.9. It is implemented using a Pressure Source Flow Rate block, whose input signal is determined by the following equation:

$$\Delta P = g \cdot H \cdot (\rho_a - \rho_{fg}) \tag{8.10}$$

where g is the gravitational acceleration, H is the stack height (30 m), ρ_a is the air density ($1.225\,\mathrm{kg\,m^{-3}}$), and ρ_{fg} is the flue gas density. The latter is measured by a Thermodynamic Properties Sensor block and filtered through a Transfer Function block to avoid rapid changes in density during transients, which could lead to numerical instability. In addition, a Pipe block is used to model viscous friction losses and to account for the fluid volume. To manage the start-up phase, a 100 s ramp followed by a saturation block capped at 1 is implemented. This is necessary because, during the first few seconds, the density varies too rapidly, which would lead to numerical instabilities.

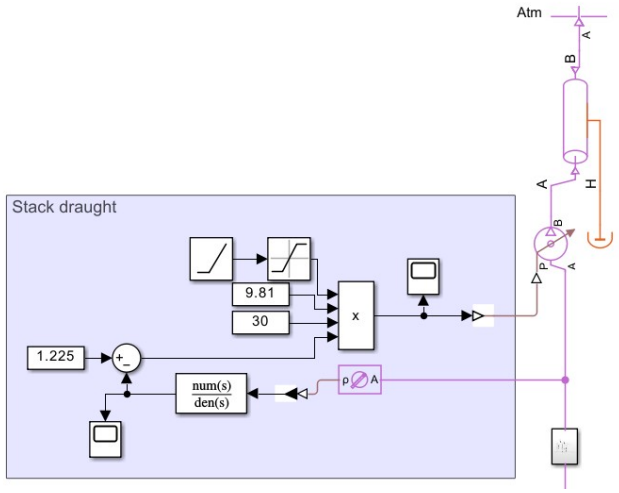


Figure 8.9: Stack draught implementation

8.2.11 Heat Recovery Fan

The heat recovery fan is located in the heat recovery branch, downstream of the heat exchanger. It is modelled using the Fan block, which is configured as explained for the main exhaust fan in Section 8.2.8, using the manufacturer data previously presented in Section 7.1.4. Figure 8.10 shows the block implementation and Figure 8.11 shows the fan curve constructed by Simulink.

NAME	VALUE		
Parameters			
Fan parameterization	Static pressure and flow rate at reference shaft speed		
Shaft power specification	Brake power		
Nominal volumetric flow rate	67900/3600	18.861	m^3/s
Nominal static pressure gain	169*9.80665	1657.3	Pa
Nominal mechanical power	40.5		kW
Maximum static pressure gain at zero flow	195*9.80665	1912.3	Pa
Maximum volumetric flow rate at zero pre...	28		m^3/s
Reference shaft speed	1055		rpm
Minimum shaft speed threshold as fractio...	1e-2		
Fan diameter scale factor	1		
Mechanical orientation	Positive angular velocity of port R relative to port C correspon		
Inlet flow area (port A)	4		m^2
Outlet flow area (port B)	4		m^2

Figure 8.10: Simulink parameter dialog box for the heat recovery fan configuration

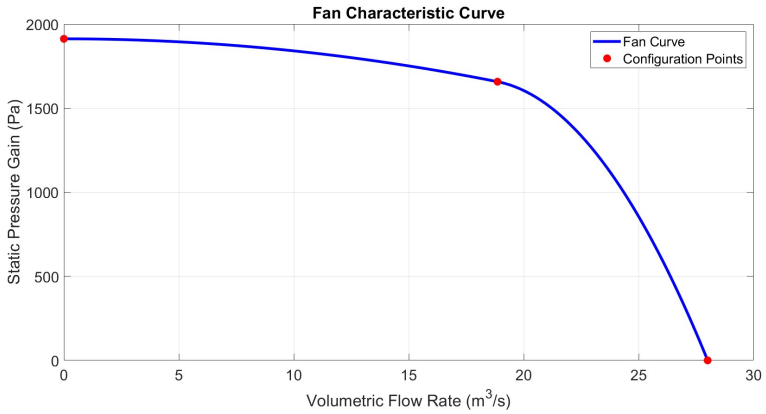


Figure 8.11: Heat recovery fan curve constructed by Simulink

8.2.12 Variable Fan Speed Control Implementation

In the variable fan speed control strategy, the fan is controlled by two PID controllers, TIC-01 and TIC-02, as previously explained in Section 7.2.1. The implementation of the control logic is shown in Figure 8.12. Each controller is implemented using a Discrete PID Controller block (configured in parallel form with clamping as the anti-windup method). The block takes the error as input, and its output (which is saturated between 0 and 1) is sent to a Gain block that converts it into a physical value (fan speed). In particular, for the TIC-01 controller, the error is calculated as $\Delta T_{SP} - \Delta T_{mix}$, where the set-point is fixed at 5 °C. The Gain block is set to the nominal fan speed (1055 rpm) to scale the normalized output, which represents n_{cap}. Regarding the TIC-02 controller, the error is calculated as $T_{SP} - T_{w,out}$ where the set-point is set to 100 °C. Its output is then multiplied by n_{cap}, which is the output of TIC-01. To manage the start-up phase, the logic involving the Switch block, manual command and TR signal is implemented in the same way as described for the previous case study in Section 5.2.6.

8.2.13 Modulating Damper Control Implementation

In this control strategy, the fan speed is maintained constant ($n = n_{nom}$) while the shut-off damper is replaced with a modulating damper controlled by two PID controllers (TIC-01 and TIC-02), as described in Section 7.2.2. The implementation of this control strategy is shown in Figure 8.13. The overall architecture (control blocks, start-up management) is similar to the one developed for the variable fan speed control strategy (Section 8.2.12). The main difference lies in the controlled variables: here, TIC-01 uses the error signal $\Delta T_{SP} - \Delta T$ (where the set-point is set to 5 °C) to output the maximum allowable damper area A_{max}, while the TIC-02

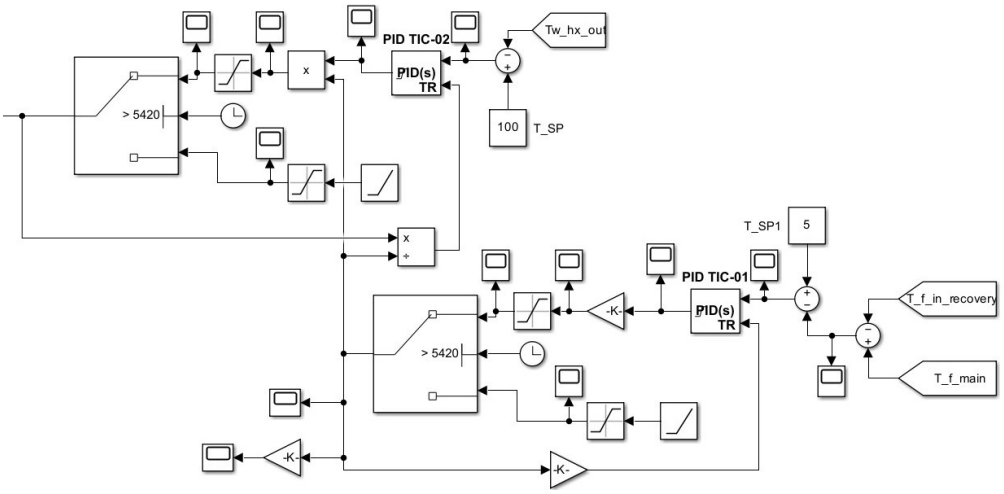


Figure 8.12: TIC-01 and TIC-02 implementation for the variable fan speed control strategy

controller uses the input $T_{SP} - T_{w,out}$ (where the set-point is fixed at 100 °C) to output the effective damper area A_D.

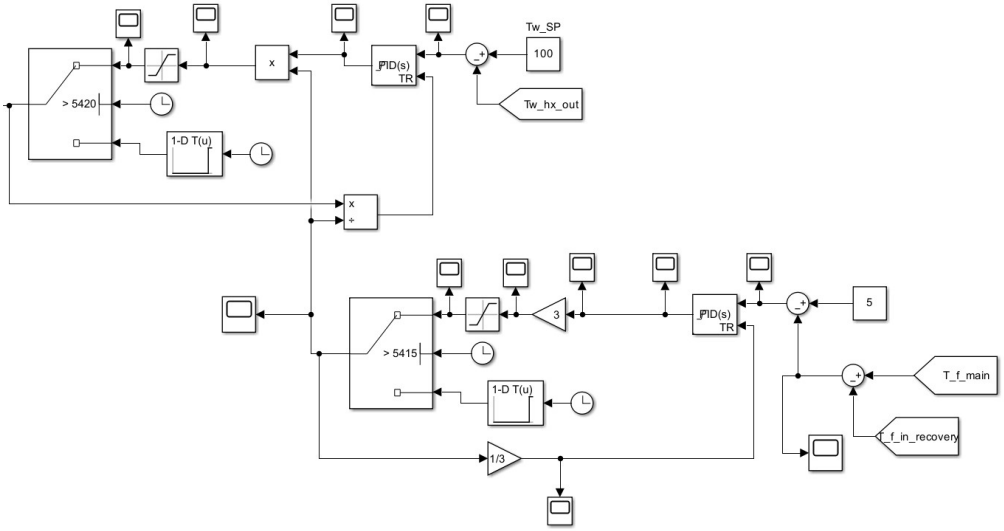


Figure 8.13: TIC-01 and TIC-02 implementation for the modulating damper control strategy

8.3 Analysed Scenario

The simulation investigates the system's response under two distinct control strategies: modulating damper control and variable fan speed control. For both configurations, the simulation time is set to 7.5 h. During the first 1.5 h the recovery branch remains closed to test the system in the absence of heat recovery, with the entire flue gas mass flow rate rejected into the environment. After this initial phase, the recovery branch is opened and the heat recovery process begins. To evaluate the plant's performance under changing operating conditions, the flue gas mass flow rate (G_{tot}) produced by the furnace was intentionally varied by adjusting the fan that draws the gases from the reservoir. This variation allowed the plant to be studied across four different scenarios characterized by either an excess or an insufficiency of flue gas compared to the thermal demand. When the flue gas is in excess, a portion of it bypasses the recovery branch (G_{byp}). Conversely, an insufficient mass flow rate prevents the system from reaching the water temperature set-point. This latter condition is critical because it introduces the risk of flue gas recirculation: the heat recovery fan may draw cold flue gases from the top of the stack, leading to increased electrical consumption and reduced heat transfer efficiency. This can be avoided thanks to a proper control strategy design.

The sequence of the four investigated scenarios is defined as follows:

- **First Scenario**: from 1.5 h to 3 h $\mathbf{G_{tot}}$ is in **excess**.
- **Second Scenario**: from 3 h to 4.5 h $\mathbf{G_{tot}}$ is **insufficient**.
- **Third Scenario**: from 4.5 h to 6 h $\mathbf{G_{tot}}$ is **insufficient**.
- **Fourth Scenario**: from 6 h to 7.5 h $\mathbf{G_{tot}}$ is in **excess**.

In addition, further simulations were performed for the variable fan speed configuration without the TIC-01 controller, in order to clearly demonstrate the effectiveness of this control loop.

Moreover, an analysis focusing on the shut-off damper full stroke time (FST) was carried out to assess its influence on the PID-SR controller, which is responsible for maintaining a constant furnace pressure.

Chapter 9

Simulation Results

9.1 Variable Fan Speed Control Configuration

The Figure 9.1 illustrates the mass flow rate balance in the stack for this configuration, detailing the total flue gas produced by the furnace G_{tot}, the bypassed flow G_{byp} and the flow entering the recovery branch G_{rec}. As can be seen, during the first 1.5 h, since the shut-off damper is fully closed, G_{byp} is null. Subsequently, the shut-off damper is fully opened. During the first and fourth scenarios, the flue gas mass flow rate produced by the furnace is in excess, resulting in a certain amount of bypass flow G_{byp}. Whereas, during the second and third scenarios, since G_{tot} is insufficient, the heat recovery fan draws as much flue gas as possible, leading to $G_{rec} > G_{tot}$, which means that the recirculation occurs. However, as will be discussed later, the TIC-01 controller limits the amount of recirculated mass flow rate.

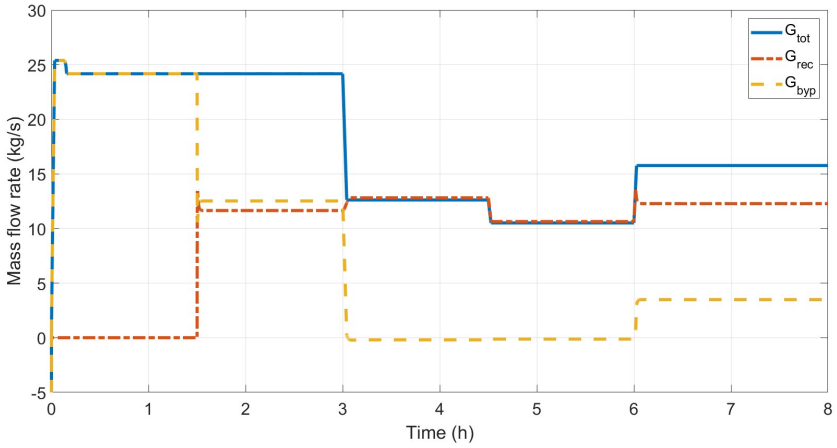


Figure 9.1: Stack mass flow rate balance

Regarding the PID-SR controller, its response is represented in Figure 9.2 where the gauge furnace pressure p_{furn} and the damper opening in percentage A_D are depicted along with the stack draught Δp_{stack}. The latter influences the furnace pressure: if the stack draught increases (due to less heat recovery), the furnace pressure tends to decrease (and vice versa). In addition, the furnace pressure is affected by changes in the flue gas mass flow rate produced by the furnace, as well as by the shut-off damper full stroke time (FST) during opening or closing, as will be discussed in Section 9.1.1. In this simulation FST=10 s. Overall, the furnace pressure is effectively maintained at the set-point value of 0 Pa.

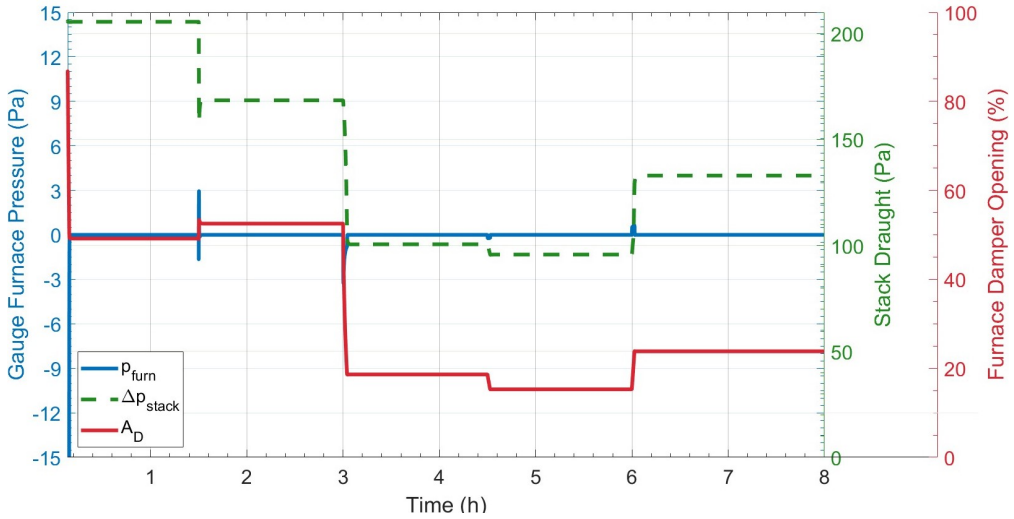


Figure 9.2: PID-SR response

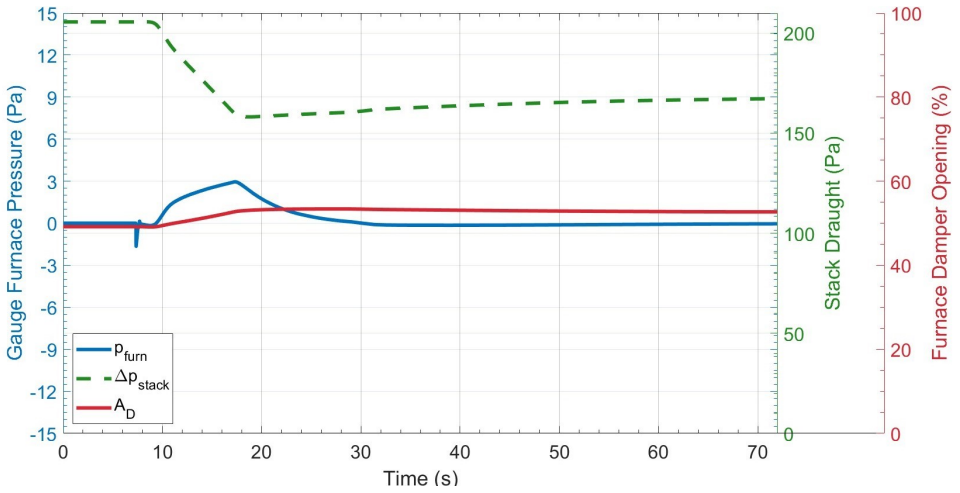
However, especially during sudden system changes, the pressure oscillates for a few seconds. To better illustrate the PID-SR response, detailed views of two critical moments are provided:

- Figure 9.3a shows the transient when the shut-off damper opens at 1.5 h. Once the shut-off damper opens, the flue gases enter the heat recovery branch and rejoin the main stack at a lower temperature; consequently, their density increases, leading to a decrease in the stack draught. As a result, the furnace pressure tends to increase, and the PID-SR gradually opens the damper to counteract this rise.

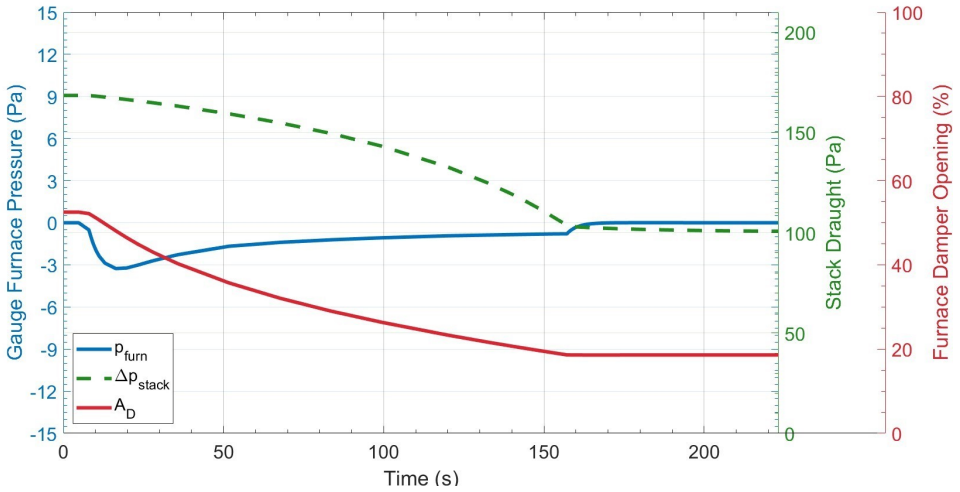
- Figure 9.3b displays the moment when the flue gas mass flow rate is reduced at 3 h. This reduction has a dual effect: first, it tends to decrease the furnace pressure since less mass enters the furnace; second, less flue gas bypasses the heat recovery branch, leading to a decrease in the stack draught. As can be

seen, the first is the predominant effect, since the furnace pressure experiences an overall decrease.

During both transients, the maximum pressure deviations are kept within acceptable limits.



(a) PID-SR response during the shut-off opening



(b) PID-SR response during a reduction of flue gas mass flow rate

Figure 9.3: PID-SR response during critical moments

As regards TIC-01 and TIC-02, their response is depicted in Figure 9.4. As can be clearly seen, when the flue gas mass flow rate is in excess (during the first and fourth scenarios), n_{cap} is at its maximum since $\Delta T_{mix} = 0$, and the actual fan speed is lower. The outlet water temperature is maintained at its set-point

(100 °C). Conversely, when the flue gas mass flow rate is insufficient (second and third scenarios), n_{cap} is reduced and coincides with the actual fan speed, ensuring that the set-point on ΔT_{mix} is respected. This means that a lower mass flow rate is drawn (due to the reduced fan speed), keeping flue gas recirculation to a minimum. As will be shown, this strategy ensures a reduction in electrical consumption while meeting the $T_{w,out}$ requirement as closely as possible.

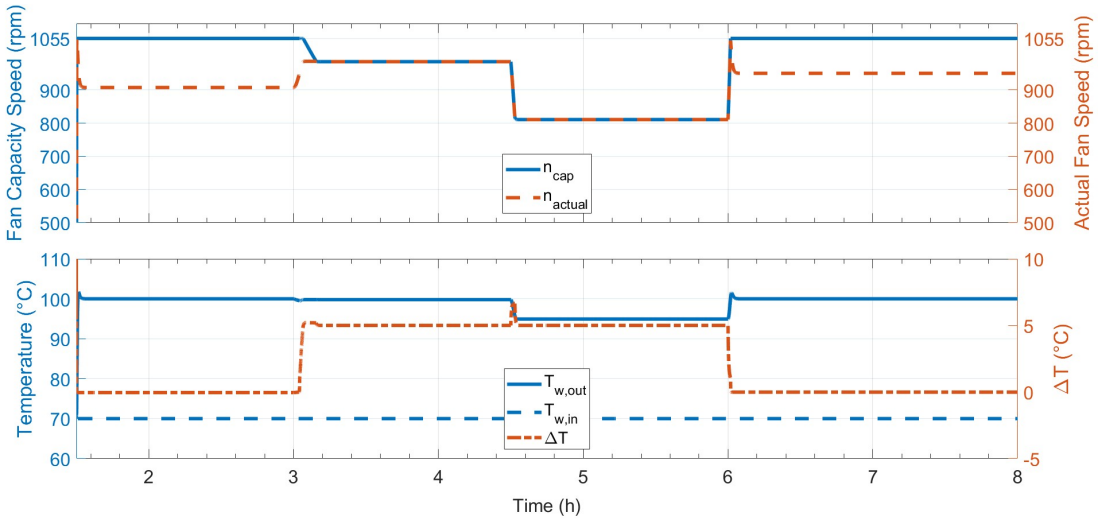
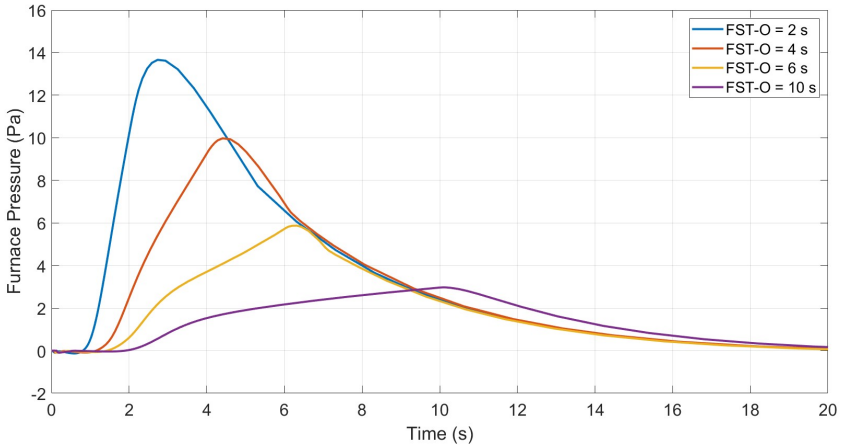


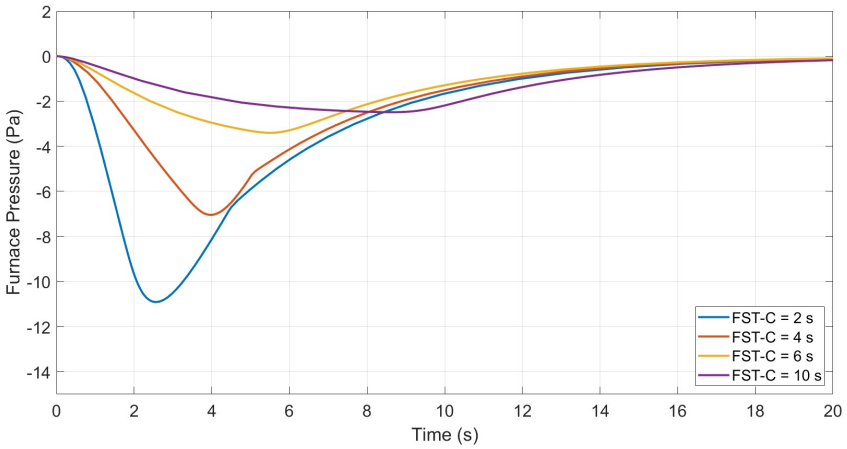
Figure 9.4: TIC-01 and TIC-02 response

9.1.1 Shut-off Damper Full Stroke Time Impact

The time required for the shut-off damper to fully open or close directly influences the furnace pressure and, consequently, the PID-SR response. This analysis was performed by testing four different Full Stroke Times (FST) for both the opening (FST-O) and closing (FST-C) phases, while recording the resulting furnace pressure. The results are depicted in Figure 9.5. As can be observed, the lower the FST, the greater the impact on the furnace pressure during both opening and closing operations. The time required to restore the pressure to the set-point (0 Pa) is approximately 20 s in all cases. This analysis suggests that rapid damper movements should be avoided to prevent the outward leakage of hot gases or the infiltration of cold ambient air.



(a) Furnace pressure response to shut-off damper FST-O



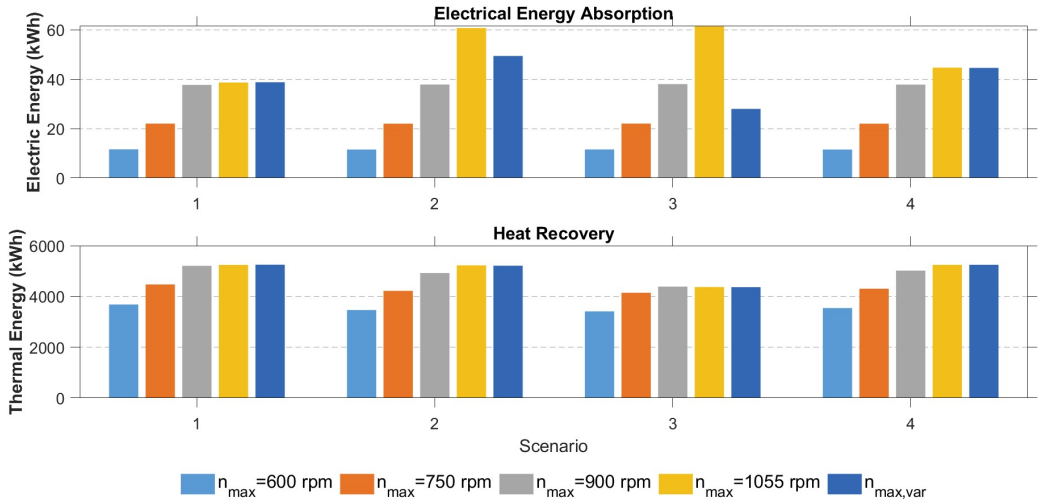
(b) Furnace pressure response to shut-off damper FST-C

Figure 9.5: Furnace pressure response to shut-off damper FST

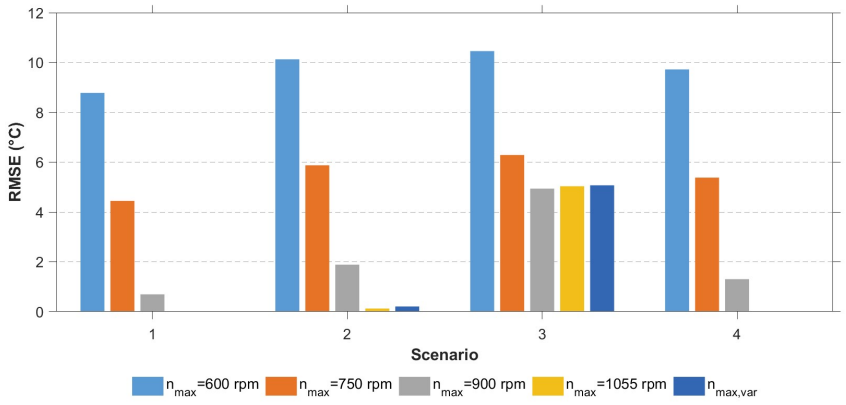
9.1.2 Impact of TIC-01 Absence on System Performance

In this analysis, the fan speed is controlled exclusively by TIC-02, meaning it is driven solely to satisfy the water temperature requirement. The study evaluates four different maximum fan speed limits (upper limit) assigned to the TIC-02 controller. The configuration incorporating the TIC-01 controller is denoted as $n_{max,var}$, whereas the configurations lacking TIC-01 (with fixed maximum capacity limits) are identified by their respective n_{max} values.

Results reveal that the $n_{max} = 600\,\text{rpm}$ and $n_{max} = 750\,\text{rpm}$ cases consistently exhibit the lowest electrical consumption, but concurrently yield the lowest heat recovery across all scenarios. With these configurations, the target water temperature is never reached. Conversely, while the $n_{max} = 1055\,\text{rpm}$ and $n_{max,var}$ configurations achieve comparable heat recovery, the implementation of the TIC-01 controller ensures significantly lower electrical consumption during the second and third scenarios. During these specific intervals, the available flue gas mass flow rate (G_{tot}) is insufficient and, without the TIC-01 controller, the TIC-02 controller forces the fan to its maximum speed, inducing cold flue gas recirculation from the stack and resulting in wasted electrical energy. Consequently, even though the outlet water temperature ($T_{w,out}$) is comparable between the $n_{max} = 1055\,\text{rpm}$ and $n_{max,var}$ cases, the latter configuration achieves electrical energy savings of 19 % during the second scenario and nearly 55 % during the third scenario. To better visualize these outcomes across the four scenarios and to highlight the operational advantages of the TIC-01 controller, the electrical consumption, heat recovery, and the root mean square error (RMSE) of $T_{w,out}$ are depicted in Figure 9.6a and Figure 9.6b. Energy values were calculated by integrating the instantaneous power over the constant time duration of each scenario.



(a) Electrical energy absorption and heat recovery comparison



(b) RMSE on $T_{w,out}$ comparison

Figure 9.6: Overall comparison of system performance

9.2 Modulating Damper Control Configuration

As explained in Section 7.2.2, in this configuration the fan speed is kept constant ($n = n_{nom}$) while the shut-off damper is replaced by a modulating damper regulated by two controllers (TIC-01 and TIC-02). The results are depicted in Figure 9.7.

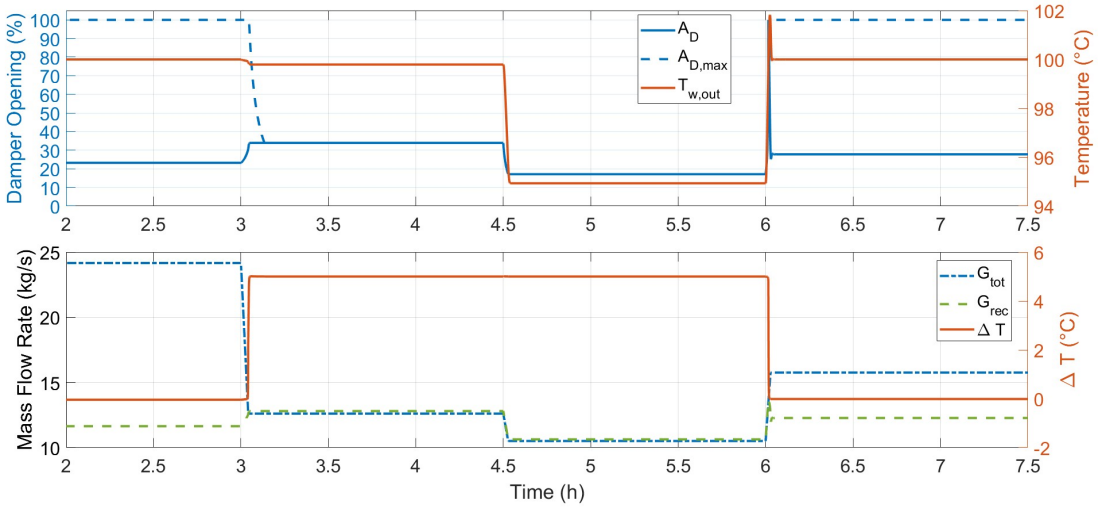


Figure 9.7: TIC-01 and TIC-02 response for the modulating damper control configuration

As observed, the behaviour is similar to the variable fan speed case: when G_{tot} is insufficient (second and third scenarios), the amount of G_{rec} is slightly higher than G_{tot} to satisfy ΔT_{mix}. As expected, the maximum area $A_{D,max}$ (which is the output of TIC-01) is 100 % during the first and fourth scenarios, since no recirculation occurs. Conversely, it is reduced during the second and third scenarios to maintain the set-point on ΔT_{mix}; during these scenarios, the actual damper area A_D coincides with $A_{D,max}$.

Regarding the PID-SR response, the results are shown in Figure 9.8. As demonstrated, the controller operates effectively, maintaining the furnace pressure at its set-point.

From an energy perspective, the heat recovery amount is comparable to the variable fan speed configuration, while the fan electrical absorption is always significantly higher, especially during the third scenario. Specifically, by keeping the fan at a constant speed ($n = n_{nom}$), the flow rate reduction required at partial loads is achieved by partially closing the damper. This alters the system curve by introducing a localized pressure drop. The fan processes a lower flow rate but must overcome a higher head, shifting its operating point toward regions of lower

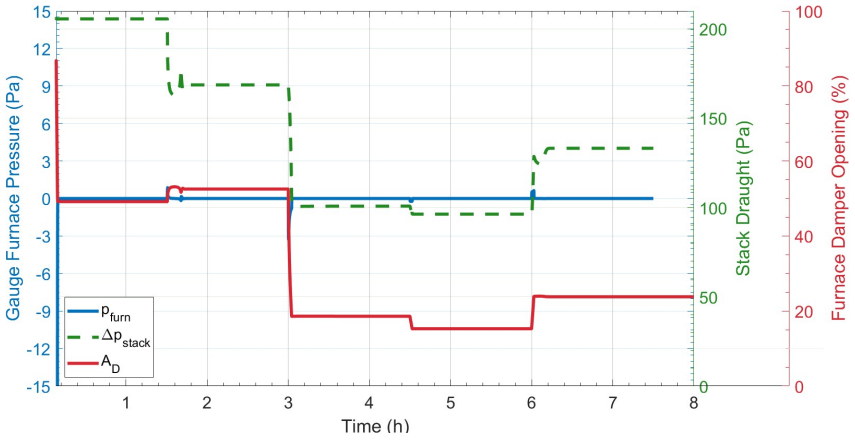


Figure 9.8: PID-SR response for the modulating damper control configuration

efficiency. Figure 9.9 represents the energy comparison between the variable fan speed control and the modulating damper control configurations.

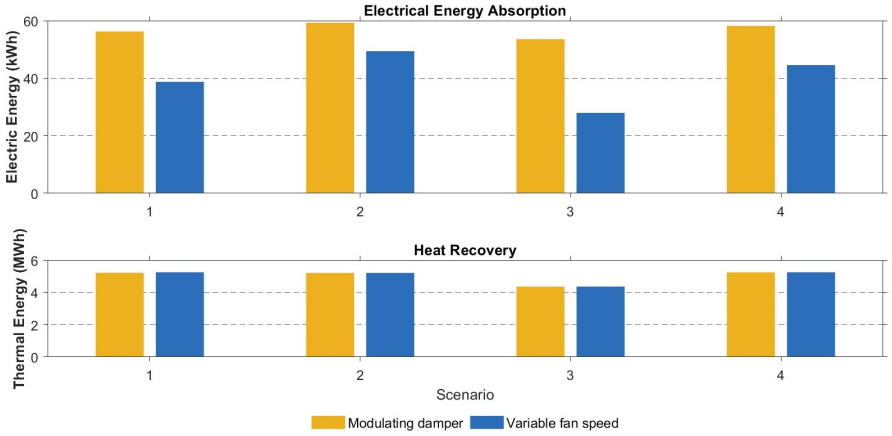


Figure 9.9: Electrical energy absorption and heat recovery comparison

9.3 Energetic, Economic and Environmental Evaluation

9.3.1 Performance of the Variable Fan Speed Configuration

In this section, the variable fan speed configuration is evaluated from an energetic, economic and environmental perspective. The results reveal that a significant

amount of hourly primary energy can be saved (Table 9.1), leading to substantial economic and environmental benefits (Figure 9.10). Specifically, this WHR

Table 9.1: Hourly primary energy savings

Scenario	E_{saved} **(kWh$_p$/h)**
1	3832.58
2	3787.57
3	3193.93
4	3822.91

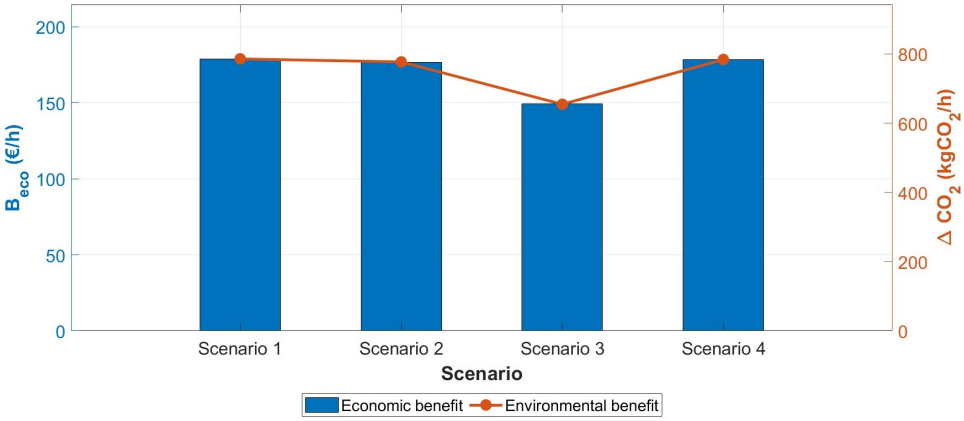


Figure 9.10: Economic and environmental benefits

configuration achieves average savings of 170.74 €/h and 750.3 kgCO_2/h across all four evaluated scenarios. Assuming an annual operating time of 8400 h per year and considering a uniform distribution of these scenarios throughout the year, the designed WHR system would generate an estimated economic benefit of approximately 1.43 million € per year and prevent the emission of around 6300 tCO_2 annually.

9.3.2 Comparative Analysis

Variable Fan Speed Configuration: Impact of TIC-01 Absence In this section, the cases with and without TIC-01 controller varying n_{max} are analysed. The results, as depicted in Figure 9.11, reveal that the configuration equipped with the TIC-01 controller ($n_{max,var}$) achieves the best values. However, the difference compared to the configuration with $n_{max} = 1055$ rpm is almost always negligible, except in Scenario 3 (where both B_{eco} and ΔCO_2 are lower due to the larger amount

of electricity consumed). Regarding the configuration with $n = 900$ rpm, the results show lower economic and environmental benefits compared to the configuration $n_{max,var}$; this is mainly due to a lower heat recovery and, consequently, lower avoided fuel costs.

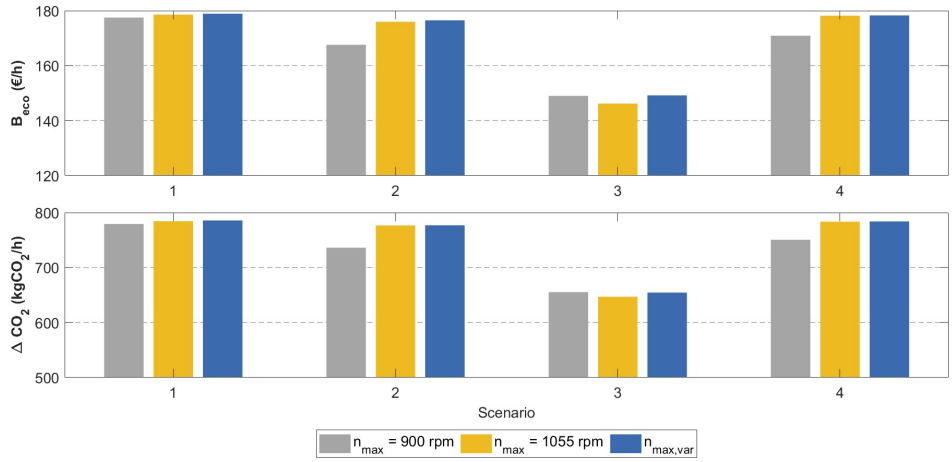


Figure 9.11: Economic and environmental benefit comparison between the configurations with and without TIC-01 controller

Comparison Between Variable Fan Speed and Modulating Damper Configurations In this section, the two control strategies are analysed. As discussed in Section 9.2, for the same heat recovery amount, the variable fan speed configuration always requires less energy than the modulating damper control strategy. Therefore, for the same fuel savings, the modulating damper configuration results in a reduced economic benefit: its average economic benefit ($B_{avg,eco}$) is 169.18 € per hour, while for the variable fan speed configuration it is 170.74 € per hour. Although the hourly difference is marginal ($\Delta B_{avg,eco} = 1.56$ €/h), it becomes significant when evaluating a long-term investment. Specifically, considering a CAPEX difference of 14000 € (the inverter present in the variable fan speed configuration leads to higher initial costs) and assuming that the OPEX difference is driven solely by the electricity cost savings ($\Delta B_{avg,eco}$), the Payback Time (PBT) in years is calculated as:

$$PBT = \frac{\Delta CAPEX}{\Delta B_{avg,eco} \cdot 8400} \tag{9.1}$$

This calculation yields approximately 1.1 years. After this period, the variable fan speed configuration provides greater economic savings than the modulating damper configuration, making the variable fan speed configuration the more profitable

long-term choice. This evaluation assumes that the plant operates 8400 h per year and that the four scenarios are equally distributed throughout the year.

9.4 Summary of Main Findings

The dynamic simulations performed in the MATLAB-Simulink environment have highlighted important aspects. Primarily, the variable fan speed control strategy represents a better long-term investment compared to the modulating damper control strategy. Specifically, the former features a higher initial investment cost due to the presence of the inverter, but yields a higher economic benefit thanks to reduced electricity absorption. Calculating the PBT demonstrates that the break-even point is slightly over one year, making the variable fan speed configuration the optimal choice.

Regarding the variable fan speed configuration, the simulations emphasize the important role of the TIC-01 controller. In particular, this control strategy effectively handles varying operational loads (fluctuating flue gas flow rates), unlike a configuration without the TIC-01 that maintains a fixed fan capacity. As demonstrated, when the flue gas production decreases (due to reduced industrial process output), the TIC-01 lowers the fan speed to prevent flue gas recirculation and save electricity. By doing so, this WHR system yields average annual primary energy savings of 30.74 GW h, leading to an economic benefit of 1.43 million € and an avoided emissions of 6302 tCO_2.

Chapter 10

Conclusions and Future Perspectives

10.1 Exploratory Study on Deep Reinforcement Learning Control[1]

Reinforcement learning (RL) is a computational framework for learning through interaction, in which an agent maps observed situations to actions with the objective of maximizing a numerical reward. The agent is not provided with explicit instructions on which action to take. Instead, during the training phase, it must autonomously discover effective behaviors by experimenting and observing the resulting rewards. Crucially, actions influence not only the immediate payoff but also future states and rewards. This dependence on trial-and-error and delayed consequences represents the defining characteristics of reinforcement learning. An RL agent must be able to perceive the state of its environment, at least partially, and to execute actions that modify that state. At the same time, it is assumed to pursue one or more goals, which are encoded through the reward signal and are related to the evolution of the environment.

Traditional RL uses lookup tables or simple functions to map states to actions. This fails in real-world systems with continuous observations and massive state spaces due to the curse of dimensionality. Deep reinforcement learning (DRL) solves this by using deep neural networks to represent policies or value functions. This allows RL to handle high-dimensional spaces, though it introduces new challenges in training stability and generalization. In DRL, the interaction framework is built around two fundamental components: the agent, which is the learner and decision-making entity, and the environment, which represents everything external to the agent and with which it interacts. The agent observes the environment, selects actions, and receives feedback as a consequence of those actions. Within this

[1]Study performed in collaboration with Andrea Franzoso.

framework, four key elements characterize most reinforcement learning systems:

1. **The policy**: it defines the agent's behavior at any given time. More precisely, it specifies a mapping from the states perceived by the agent to the actions that should be taken in those states, thereby determining how decisions are made.

2. **The reward signal**: it encodes the objective of the reinforcement learning problem. At each time step, the environment provides the agent with a scalar reward, which evaluates the immediate outcome of the chosen action. The agent's ultimate goal is to maximize the cumulative reward over time. In this sense, the reward signal identifies which events are desirable and which are undesirable from the agent's perspective.

3. **The value function**: it estimates of the agent's long-term success from a specific state.

4. **The model of the environment**: it represents the external system with which the agent interacts. In the context of this work, the environment is entirely virtual.

As a future development of the WHR plant models and PID control strategies presented in this thesis, a preliminary study on DRL was conducted. An analysis applying DRL algorithms has been performed for the first case study described in **Part I**, replacing the traditional setup that relied on four PID controllers. The specific algorithm selected for this continuous control task is DDPG (Deep Deterministic Policy Gradient). Here is how the DRL framework is configured:

- **Actions (a_i):** The control inputs commanded by the DRL agent to manage the plant's dampers and the fan speed.

- **Observations (s_i):** Inlet water temperature (T_{in}), outlet water temperature ($T_{w,out}$), temperature differences before and after the dampers (ΔT_1) and (ΔT_2), previous positions of the dampers and previous fan rotation speed.

- **Reward (r_{i+1}):** The reward function guides the agent's learning process. It is split into three objectives: minimizing the fan's energy consumption (E_{fan}), maintaining the target outlet water temperature ($T_{w,out}$) and penalizing the agent for making sudden, drastic changes to its control actions. It is calculated as:

$$r_{i+1} = E_{fan} - \alpha|25 - T_{w,out}| - \beta \sum |a_i(t) - a_i(t-1)| \tag{10.1}$$

  where α represents the weighting factor for the temperature tracking error, and β represents the penalty weight on the actuator variation, ensuring smooth control actions.

Additionally, low-pass filters are applied to two areas of the system: on the observation of temperatures (to simulate the physical behavior and dynamics of the temperature sensors) and on the application of actions (to simulate the real-world physical dynamics of the plant's hardware components like the actuation speed of the dampers and fan). The DRL framework described above is illustrated in Figure 10.1.

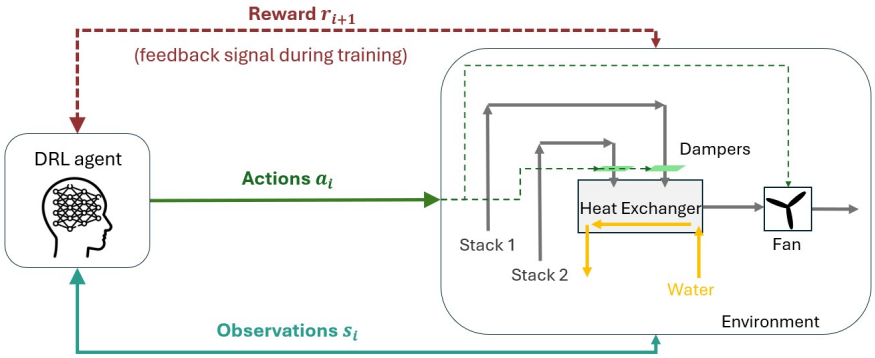


Figure 10.1: Schematic representation of the DRL framework applied for the WHR system from steam boiler flue gas

Two simulations were performed by varying the β coefficient (20 and 30), while keeping α fixed at 30. The obtained results show that the outlet water temperature deviates from the set-point more than in the PID configuration. The only exception occurs during the fourth scenario, where the configuration with $\beta = 30$ achieves the same outlet water temperature, as can be seen in Figure 10.2. Regarding energy consumption, the consequence is that the overall rebound energy required by the heat pump is higher than in the PID configuration. The rebound energy represents the extra electrical power the heat pump's compressor must draw to deliver its fixed final heating load because the colder incoming water reduced its thermodynamic efficiency. A higher rebound energy means the overall system is less efficient and consumes more electricity. Another aspect revealed by the simulations concerns the mechanical energy absorbed by the fan, which is higher in both DRL cases compared to the PID configuration. This is due to a higher fan speed and a different damper control strategy; the dampers are kept more closed than in the PID configuration, increasing the pressure drop and, consequently, the mechanical power required. To better visualize these results, Figure 10.3 compares the mechanical energy, the heat pump rebound energy, and the RMSE of $T_{w,out}$ against the PID configuration

To conclude, as this analysis constitutes a preliminary study on DRL implementation, the results highlight the need for further refinement. In particular, to improve the agent's responsiveness and overall efficiency, future work must

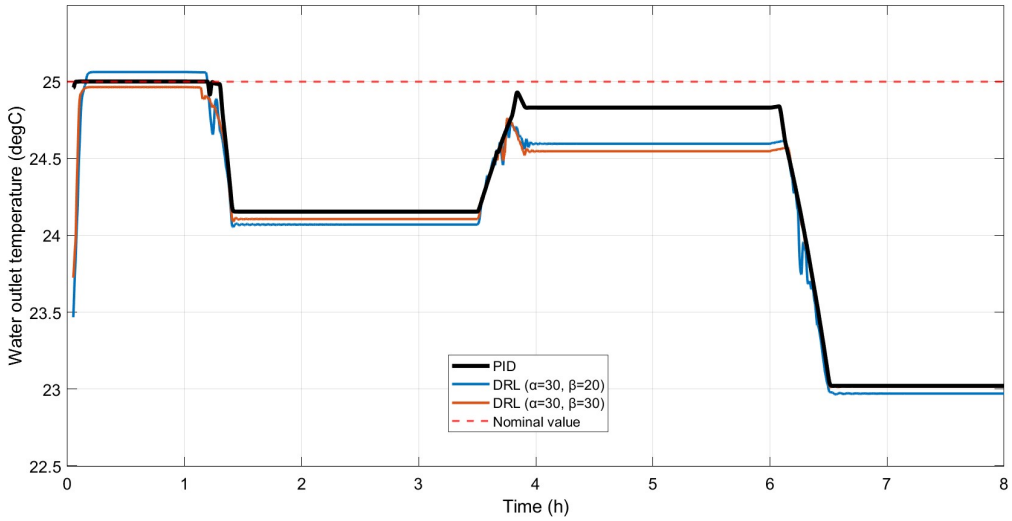


Figure 10.2: Outlet water temperature comparison between DRL and PID configurations

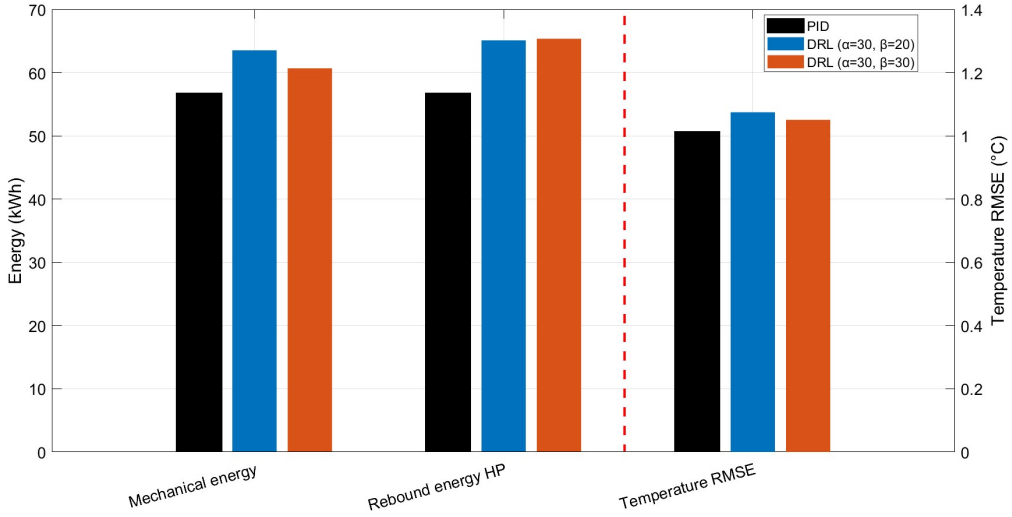


Figure 10.3: Energy and RMSE comparison between DRL and PID configurations

focus on comprehensive hyperparameter tuning and a deeper optimization of the reward function weights. Additionally, testing other RL algorithms, such as Soft Actor-Critic (SAC) or Proximal Policy Optimization (PPO), represents a necessary future perspective to help the DRL match or exceed traditional PID performance.

10.2 Conclusions

One of the main aspects that emerged from this thesis is the critical role of dual fan control. Rather than controlling the fan speed solely via a single PID controller, both systems decouple the control action into two distinct variables: the fan speed capacity (n_{cap}), which is modulated to avoid the recirculation of colder flue gas or the extraction of fresh air, and the actual fan speed (n), which is modulated within that capacity boundary to meet the thermal demand. Another key finding is the significant magnitude of the benefits, both from an economic and environmental perspective, provided by WHR systems like the two analyzed in this work.

In the first case study, the lower limit ($n_{cap,min}$) of the YIC-01 controller, which modulates n_{cap}, emerged as a critical design and operational constraint. The dynamic simulations demonstrated that setting an excessively high minimum limit (1900 rpm) forces the fan to run too fast when flue gas availability is low, causing the branch dampers to over-throttle and waste electrical energy. By optimizing this lower boundary to 1400 rpm, the dampers were allowed to operate in a wider, unthrottled position (shifting from a 16 % to a 92.85 % opening). This adjustment yielded a 24.8 % reduction in electrical power consumption during critical low-load operations without causing any deviation from the target water temperature. Regarding the overall benefits, during the winter season when the hot water feeds the heat pump, this WHR system enables average primary energy savings of 4 GW h. This translates to significant economic and environmental advantages, specifically saving 122.9 thousand € and avoiding 945 tCO_2 in emissions.

In the second case study, the analysis proved the indispensable role of a dynamically variable fan capacity (n_{cap}). In the absence of this control (operating with a fixed maximum speed), the temperature controller (TIC-02) would force the fan to run at its maximum speed during periods of low flue gas availability. This either prevents the system from reaching the target water temperature (as the fan speed is insufficient to satisfy the thermal demand) or induces massive, cold flue gas recirculation from the stack, resulting in significant electrical energy wastage. Additionally, the study demonstrated how the shut-off damper full stroke time (FST) affects the furnace pressure controller: the higher the FST, the greater the pressure oscillations. Therefore, sudden changes to the shut-off damper position should be avoided. Furthermore, the analysis highlights the inefficiency of the modulating damper control strategy. Specifically, although it allows for the same heat recovery as the variable fan speed configuration, it consumes more electrical energy. This leads to an economic benefit difference of approximately 1.56 €/h; however, since the break-even point is reached in only about one year, the variable fan speed configuration remains the optimal choice for a long-term investment. Focusing on the variable fan speed configuration, the results reveal that this system enables primary energy savings of 30.74 GW h. Assuming an equal time distribution

among the four selected operational scenarios, this leads to annual savings of 1.43 million € and the avoidance of 6302 tCO_2 emissions.

Finally, this thesis explores an innovative control approach by presenting a preliminary study on Deep Reinforcement Learning (DRL) applied to the first case study. Although this relatively unexplored field holds immense promise for managing highly non-linear systems, current results indicate that further refinement is still required for the DRL agent to outperform the traditional PID configuration.

Bibliography

[1] Clemens Forman, Ibrahim Kolawole Muritala, Robert Pardemann, and Bernd Meyer. «Estimating the global waste heat potential». In: *Renewable and Sustainable Energy Reviews* 57 (2016), pp. 1568–1579. DOI: 10.1016/j.rser.2015.12.292 (cit. on p. 1).

[2] International Energy Agency. *IEA at COP30*. International Energy Agency (IEA). 2025. URL: https://www.iea.org/events/iea-at-cop30 (visited on 07/27/2026) (cit. on p. 1).

[3] European Commission. *What is Energy Efficiency?* Directorate-General for Energy, Energy Efficient Products. Accessed: 2026-07-25. 2026. URL: https://energy-efficient-products.ec.europa.eu/faqs-0/what-energy-efficiency_en (cit. on p. 4).

[4] International Energy Agency. *Energy Efficiency 2025*. Market Report. Licence: CC BY 4.0. Paris: International Energy Agency (IEA), 2025. URL: https://www.iea.org/reports/energy-efficiency-2025 (cit. on p. 4).

[5] IPCC. *Climate Change 2023: Synthesis Report. Contribution of Working Groups I, II and III to the Sixth Assessment Report of the Intergovernmental Panel on Climate Change*. Ed. by Core Writing Team, Hoesung Lee, and José Romero. Geneva, Switzerland: Intergovernmental Panel on Climate Change (IPCC), 2023. DOI: 10.59327/IPCC/AR6-9789291691647. URL: https://www.ipcc.ch/report/ar6/syr/ (cit. on p. 4).

[6] International Energy Agency. *Energy Management for Industry*. Report. Licence: CC BY 4.0. Paris: International Energy Agency (IEA), 2025. URL: https://www.iea.org/reports/energy-management-for-industry (cit. on p. 5).

[7] Rajesh Ravi, Oumaima Douadi, Dikra Bakhchin, Mustapha Faqir, and E. Essadiqi. *Waste Heat Recovery, its Utilization and Performance Assessment: Fundamentals and Application*. Elsevier Science, 2025 (cit. on p. 6).

[8] Sarah Brückner, Selina Liu, Laia Miró, Michael Radspieler, Luisa F. Cabeza, and Eberhard Lävemann. «Industrial waste heat recovery technologies: An economic analysis of heat transformation technologies». In: *Applied Energy* 151 (2015), pp. 157–167. DOI: 10.1016/j.apenergy.2015.01.147 (cit. on pp. 6, 7).

[9] Wayne C. Turner. *Energy Management Handbook*. 4th. Lilburn, GA: The Fairmont Press, 2001. ISBN: 9780881733372 (cit. on p. 8).

[10] Nikunj Mehta, Dharmendra Chauhan, Sagar Patel, and Siddharth Mistry. «Design of HMI Based on PID Control of Temperature». In: *International Journal of Engineering Research and Technology* 6 (2017). DOI: 10.17577/IJERTV6IS050074 (cit. on p. 9).

[11] Karl Johan Åström and Tore Hägglund. *Advanced PID Control*. ISA - The Instrumentation, Systems, and Automation Society, 2006 (cit. on p. 10).

[12] Networks ARERA - Italian Regulatory Authority for Energy and Environment. *Resolution EEN 3/08: Update of the conversion factor of electrical energy into primary energy*. https://www.arera.it/atti-e-provvedimenti/dettaglio/08/003-08een. Accessed: September 5, 2026. 2008 (cit. on p. 12).

[13] Ministry of Environment and Energy Security (MASE). *Table of National Standard Parameters 2019*. Official ETS documentation. Accessed: September 7, 2026. 2019. URL: https://www.mase.gov.it/portale/documents/d/guest/fattori_standard_2019-pdf (cit. on p. 12).

[14] ISPRA - Italian Institute for Environmental Protection and Research. *CO2 emissions from the electricity sector*. https://emissioni.sina.isprambiente.it/emissioni-co2-settore-elettrico/. Accessed: September 5, 2026 (cit. on p. 12).

[15] ISPRA - Italian Institute for Environmental Protection and Research. *Emission factors for electricity production and consumption in Italy*. https://emissioni.sina.isprambiente.it/fattori-di-emissione-produzione-consumo-energia-elettrica/. Accessed: September 5, 2026 (cit. on p. 12).

[16] [Engineering Firm]. *Piping and Instrumentation Diagram (P&ID) of the Waste Heat Recovery (WHR) Plant*. Technical Drawing. Unpublished internal document. Confidential. [Engineering Firm], 2026 (cit. on p. 18).

[17] *Data Sheet: Flue Gas / Water Heat Exchanger (HE 01)*. Technical Specifications. [Private Company]. 2025 (cit. on p. 18).

[18] *Data Sheet: Flue Gas Fan (Ref. CF-01)*. Technical Specifications. [Private Company]. 2026 (cit. on p. 19).

[19] Innomotics GmbH. *Innomotics - Redefining reliable motion for a better tomorrow*. Accessed: 2026-06-10. 2026. URL: https://www.innomotics.com/hub/en/ (cit. on pp. 20, 65).

[20] Innomotics GmbH. *Efficiency Documentation for 50/60Hz Three-Phase Squirrel-Cage Motors*. Technical report generated using the Innomotics motor configuration tool for the selected motor configuration. 2026 (cit. on p. 21).

[21] Michael J. Moran and Howard N. Shapiro. *Fundamentals of Engineering Thermodynamics*. 5th. John Wiley & Sons, 2006 (cit. on p. 22).

[22] Fabio Peano and TRIGENIA S.r.l. *Control Specifications: Control Strategy for the Waste Heat Recovery (WHR) Plant*. Technical Specification. TRIGENIA S.r.l., 2026 (cit. on p. 28).

[23] Bruce E. Poling, George H. Thomson, Daniel G. Friend, Richard L. Rowley, and W. Vincent Wilding. *Perry's Chemical Engineers' Handbook*. 7th. McGraw-Hill, 2008 (cit. on pp. 30, 71).

[24] The MathWorks Inc. *Reservoir (MA) - Simscape Fluids*. 2024. URL: https://it.mathworks.com/help/simscape/ref/reservoirma.html (visited on 05/24/2024) (cit. on p. 32).

[25] The MathWorks Inc. *Flow Rate Source (MA) - Simscape*. 2026. URL: https://it.mathworks.com/help/simscape/ref/flowratesourcema.html (visited on 06/11/2026) (cit. on p. 34).

[26] The MathWorks Inc. *Constant Volume Chamber (MA) - Simscape*. 2026. URL: https://it.mathworks.com/help/simscape/ref/constantvolumechamberma.html (visited on 06/11/2026) (cit. on p. 34).

[27] The MathWorks Inc. *Local Restriction (MA) - Simscape*. 2026. URL: https://it.mathworks.com/help/simscape/ref/localrestrictionma.html (visited on 06/11/2026) (cit. on p. 34).

[28] MathWorks. *Fan (MA) - Simscape Fluids Reference*. Release R2024b. [Online]. Disponibile su: https://it.mathworks.com/help/releases/R2024b/hydro/ref/fanma.html. 2024 (cit. on p. 34).

[29] The MathWorks Inc. *System-Level Heat Exchanger (TL-MA) - R2024b Documentation*. https://it.mathworks.com/help/releases/R2024b/hydro/ref/systemlevelheatexchangertlma.html. Accessed: 14 June 2026. 2024 (cit. on p. 36).

[30] The MathWorks, Inc. *Flow Resistance (MA) - Simscape Reference*. Release R2024b. 2024. URL: https://it.mathworks.com/help/releases/R2024b/simscape/ref/flowresistancema.html (visited on 06/21/2026) (cit. on p. 37).

[31] MathWorks. *Discrete PID Controller*. The MathWorks, Inc. 2026. URL: https://it.mathworks.com/help/simulink/slref/discretepidcontroller.html (visited on 06/16/2026) (cit. on p. 40).

[32] [Engineering Firm]. *Piping and Instrumentation Diagram of the WHR Plant from hot rolling mill reheating furnace*. Technical Drawing. Unpublished internal document. Confidential. [Engineering Firm], 2026 (cit. on p. 62).

[33] *Data Sheet: Main Fan*. Technical Specifications. [Private Company]. 2026 (cit. on p. 63).

[34] *Data Sheet: Air Pre Heater*. Technical Specifications. [Private Company]. 2026 (cit. on p. 63).

[35] *Hx Performance Data Sheet & Heat Transfer Surface Summary*. Technical Specifications. [Private Company]. 2026 (cit. on p. 64).

[36] *Data Sheet: Heat Recovery Fan*. Technical Specifications. [Private Company]. 2026 (cit. on p. 65).

[37] Innomotics. *Efficiency documentation for 50/60Hz three-phase Squirrel-Cage-Motors*. Innomotics. 2026 (cit. on p. 66).

[38] Thomas A. Davidson. *A Simple and Accurate Method for Calculating Viscosity of Gaseous Mixtures*. Report of Investigations 9456. United States Department of the Interior, Bureau of Mines, 1993 (cit. on p. 71).

[39] Robert J. Kee, Michael E. Coltrin, and Peter Glarborg. *Chemically Reacting Flow: Theory and Practice*. John Wiley & Sons, 2003 (cit. on p. 71).

[40] Magnus Holmgren. *X Steam for MATLAB*. Accessed: [2026-08-02]. 2006. URL: http://www.x-eng.com (cit. on p. 72).

[41] The MathWorks Inc. *Constant Volume Chamber (G)*. Release: R2024b. Accessed: [2026-08-23]. The MathWorks Inc. Natick, MA, USA, 2024. URL: https://it.mathworks.com/help/releases/R2024b/simscape/ref/constantvolumechamberg.html (cit. on p. 72).

[42] *System-Level Heat Exchanger (G-G)*. R2024b. Release: R2024b. Accessed: [2026-08-23]. The MathWorks, Inc. 2024. URL: https://it.mathworks.com/help/releases/R2024b/hydro/ref/systemlevelheatexchangergg.html (cit. on p. 73).

[43] The MathWorks, Inc. *Fan (G) - Simscape Fluids Block Reference*. Release: R2024b. Accessed: [2026-08-23]. The MathWorks, Inc. 2024. URL: https://it.mathworks.com/help/releases/R2024b/hydro/ref/fang.html (cit. on p. 75).

[44] The MathWorks, Inc. *System-Level Heat Exchanger (TL-G) - Simscape Fluids Block Reference*. Release R2024b. The MathWorks, Inc. 2024. URL: https://it.mathworks.com/help/releases/R2024b/hydro/ref/systemlevelheatexchangertlg.html (visited on 08/26/2026) (cit. on p. 77).